INSTITUTO SUPERIOR DE ENGENHARIA DO PORTO
MESTRADO EM ENGENHARIA MECÂNICA




Evaluation of the extended finite element method for the analysis of bonded joints

VIGNESH RAMESH
outubro de 2018

POLITÉCNICO
DO PORTO

Instituto Superior de Engenharia do Porto

EVALUATION OF THE EXTENDED FINITE ELEMENT METHOD FOR THE ANALYSIS OF BONDED JOINTS

VIGNESH RAMESH

1161624

2018

ISEP – School of Engineering

Department of Mechanical Engineering

POLITÉCNICO
DO PORTO

Instituto Superior de Engenharia do Porto

EVALUATION OF THE EXTENDED FINITE ELEMENT METHOD FOR THE ANALYSIS OF BONDED JOINTS

VIGNESH RAMESH

1161624

Dissertation presented to ISEP – School of Engineering to fulfill the requirements necessary to obtain a Master's degree in Mechanical Engineering, carried out under the guidance of Professor Raul Duarte Salgueiral Gomes Campilho and Professor Francisco Jose Gomes da Silva.

2018

ISEP – School of Engineering

Department of Mechanical Engineering

POLITÉCNICO
DO PORTO

JURY

President

To define

Supervisor

Raul Duarte Salgueiral Gomes Campilho, PhD.

Adjunct Professor, Department of Mechanical Engineering.

Second supervisor

Francisco Jose Gomes da Silva, PhD.

Adjunct Professor, Department of Mechanical Engineering.

Examiner

To define

ACKNOWLEDGEMENTS

This thesis has been possible thanks to the support received by some others. I would sincerely like to thank those people who made it possible to do research in Adhesive bonding. Each of them allowed me to live a beautiful experience that goes well beyond the limits of a thesis. **Prof. Raul Duarte Salgueiral Gomes Campilho** accepted my request to do research, thus giving me this opportunity, suggested a suitable research topic. I would like to thank those, members of the technical staff, PhD students or professors, who somehow gave me a hand during the period my thesis. Thank you, Prof. Francisco J.G. Silva, for the support you have been giving me since the first time I asked you for a thesis project. Thank you for your advices, this thesis would not be the same without your contribution. Not only this, thank you Raul Duarte Salgueiral Gomes Campilho your friendliness and humanity. Last but not least, I would like to thank a colleague, a friend with whom I shared much time, who has given his personal contribution to this work with an indefatigable pursuit of the errors scattered all through the thesis

I would also wish to specially thank my grandmothers A. Gnanasoundari and G.Vanaroja, my uncles A. Gnanaseker and her wife Revathi G , A. Senthil Murugan, and her wife Mythili Senthil Murugan, my parents Ramesh Gurunathan and Sumathi Ramesh Alice, my sister Shailaja Sathish and her husband Sathish Kumar for their absolute support, and I would like to thank my uncle Naresh Babu, Vigneshmurali, and my cousin brothers Ajith kumar, Arun, Harish kumar, Abishek, Lithis menan, cousin sisters Midhu Senthilmurugan, Suganya, Saranya even when study times restricted my social interactions with them during these years.

KEYWORDS

Adhesive joints; Single-Lap joints; Double-Lap joints, Experimental tests; Structural adhesive; eXtended Finite Element Method.

ABSTRACT

The extended finite element method is an innovative approach based on finite element method. Where finite element method needs to change the mesh at every step of a crack propagation, extended finite element method does not because the mesh does not need to follow the crack anymore, that is why this method is very well suited for fracture problems. This master's thesis is the development of the 2D part of this method.

The XFEM tool in Abaqus is evaluated for two dimensional stationary cracks with a variety of parameters and features such as meshing technique, element size, symmetry and sub modeling. The purpose is to find a robust and flexible strategy to model cracks. The strategy is verified through handbook cases modeled in Abaqus, where the accuracy has been evaluated. The study was conducted through a numerical analysis by the eXtended Finite Element Method (XFEM) based on stress and strain criteria, which was validated with previously obtained experimental results. The numerical analysis allowed the study of the stress distributions, the effect of the damage initiation criterion, the effect of the propagation law and also the joints strength.

The XFEM analysis revealed that this method is fully accurate when using the QUADS initiation criterion, growth criteria and the triangular propagation law. It was shown that the SLJ and DLJ adherend's geometry and the adhesive type are the most important parameters affecting the joints strength.

PALAVRAS CHAVE

Juntas adesivas; Juntas de sobreposicao simples; Juntas de sobreposicao dupla, Ensaios experimentais; Adesivo estrutural; Método dos Elementos Finitos eXtendido.

RESUMO

O Método de Elementos Finitos eXtendido é uma abordagem inovadora baseada no Método de Elementos Finitos. Enquando o Método de Elementos Finitos precisa mudar a malha em cada etapa da propagação da fenda, o Método de Elementos Finitos eXtendido não faz mais porque a malha não precisa de seguir a fenda, e é por isso que esse método é muito adequado para problemas de fratura. Esta dissertação de mestrado é o desenvolvimento da parte 2D deste método.

A ferramenta XFEM no Abaqus é avaliada para fendas estacionárias bidimensionais com uma variedade de parâmetros e características como técnica de malha, tamanho do elemento, simetria e sub modelação. O objetivo é encontrar uma estratégia robusta e flexível para modelar fendas. A estratégia é verificada por meio de casos estudo modelados no Abaqus, cuja precisão foi avaliada. O estudo foi conduzido através de uma análise numérica pelo Método dos Elementos Finitos eXtended (XFEM) baseado nos critérios de tensão e deformação, o qual foi validado com resultados experimentais previamente obtidos. A análise numérica permitiu o estudo das distribuições de tensão, o efeito do critério de início de dano, o efeito da lei de propagação e também a resistência das juntas.

A análise XFEM revelou que este método é totalmente preciso ao usar o critério de iniciação QUADS, critérios de crescimento e a lei de propagação triangular. Foi demonstrado que a geometria do aderente SLJ e DLJ e o tipo de adesivo são os parâmetros mais importantes que afetam a resistência das juntas.

LIST OF SYMBOLS AND ABBREVIATIONS

List of abbreviations

2D	Two Dimensions
3D	Three Dimensions
ASTM	American Society for Testing and Materials
BK	Benzeggagh-Kenane
CBBM	Compliance-Based Beam Method
CBT	Corrected Beam Theory
CCM	Compliance Calibration Method
CZM	Cohesive Zone Models
DCB	Double-Cantilever Beam
DoE	Design of Experiment
ENF	End-Notched Flexure
FE	Finite Element
FEM	Finite Element Method
KM	Kriging Metamodel
LEFM	Linear Elastic Fracture Mechanics
L_o	Overlap Length
MAXE	Maximum Nominal Strain Criterion
MAXPE	Maximum Principal Strain Criterion
MAXPS	Maximum Principal Stress Criterion
MAXS	Maximum Nominal Stress Criterion
P_m	Maximum Load
QUADE	Quadratic Nominal Strain Criterion
QUADS	Quadratic nominal Stress Criterion
SAAS	Stress Analysis for Adhesive Structures
SLB	Single-Leg Bending
SLJ	Single-Lap Joint
TAST	Thick Adherend Shear Test
UV	Ultra Violet
XFEM	eXtended Finite Element Method

List of units

°C	degree Celsius
g	gram
GPa	giga Pascal
kN	kilo Newton
m	meter
min	minute
mm	millimeters
MPa	mega Pascal
N	Newton
N/mm	Newton by millimeter

List of symbols

b	Joint width
C	Curve surrounding crack tip
d_n	Damage variable in tension
d_s	Damage variable in shear
E	Young's modulus
G	Shear modulus
Gc	Fracture toughness
G_I	Strain energy release rate in pure-mode I
G_{IC}	Critical strain energy rate or fracture toughness in pure-mode I
G_{II}	Strain energy release rate in pure-mode II
G_{IIC}	Critical strain energy rate or fracture toughness in pure-mode II
G_{III}	Strain energy release rate in pure-mode III
G_{IIIC}	Critical strain energy rate or fracture toughness in pure-mode III
Gs	Strain energy release rate in pure-mode II plus pure mode III
G_T	Total strain energy release rate
J	J-integral
K	Stiffness matrix
K_{nn}, K_{ns}, K_{ss}	Stiffness parameters
L_T	Total length between gripping points
m,b	Parameters of the straight line euation
n	Element nodes
ñ	Element phantom nodes
P	Load
P_m/P_m^0	Maximum strength divided by previously predicted maximum strength
S	Arc length
t	Traction
t_a	Adhesive thickness
T_j	Traction vector
t_m^0	Cohesive strength in mixed-mode
t_n	Current tensile traction
t_n^0	Tensile cohesive strength
t_n^{und}	Current cohesive traction in tension
t_p	Adherends thickness
t_s	Current shear traction
t_s^0	Shear cohesive strength
t_s^{und}	Current cohesive traction in shear
u_j	Displacement vector

W	Energy density
x	Distance from the left edge of the adhesive layer
x_1	Coordinate system
x_2	Coordinate system
α	Parameter for the 3D criterion, power law parameter, non-dimensional parameter for the linear-exponential cohesive law
βγ	Parameter for the 3D criterion
γ_f	Shear failure strain
δ	Displacement
Δ	Percentile deviation
δ_m^0	Displacement at cohesive strength in mixed-mode
δ_m^f	Mixed-mode failure displacement
δ_n	Relative displacement in tension
δ_n^0	Displacement at peak tensile strength
δ_n^f	Failure tensile displacement
δ_n^s	Stress softening onset displacement in tension
δ_s	Relative displacement in shear
δ_s^0	Displacement at peak shear strength
δ_n^f	Failure shear displacement
δ_s^s	Stress softening onset displacement in shear
ε	Strain
ε_f	Tensile failure strain
ε_{max}	Current maximum principal strain
ε_{max}^0	Allowable maximum principal strain
ε_n	Current tensile strain
ε_n^0	Peak tensile strain
ε_s	Current shear strain
ε_s^0	Peak shear strain
η	Characteristic material parameter
ν	Poison's ratio
σ_f	Tensile failure stress
σ_{max}	Current maximum principal stress
σ_{max}^0	Allowable maximum principal stress
σ_y	Tensile yield stress, peel stress
τ_{avg}	Average shear stress
τ_f	Shear failure strength
τ_{xy}	Shear stress
τ_y	Shear yield strength

FIGURES INDEX

TABLES INDEX

INDEX

INTRODUCTION

1 INTRODUCTION

1.1 Framework

Adhesively-bonded joints are an increasing alternative to mechanical joints in several engineering applications, supplying many advantages over conventional mechanical fasteners [1]. Using adhesive bonding the integrity of the parent materials is preserved, and varied materials can be joined the realization of this work stems from the increasing use of adhesives in several areas, especially in industry. Comparatively, adhesive joints have several advantages over traditional mechanical bonding methods, namely low weight, ability to reduce stress concentration, ease of manufacture, ability to bond dissimilar materials and greater strength. However, they also present disadvantages, such as the need for a strict quality control, poor tear strength, the use of fastening tools and high cure temperatures may be needed. There are several factors that condition the behavior of an adhesive joint, and the need to devalue some of these main factors, namely the type of adhesive (fragile, ductile or a compromise between the two properties) and joint geometry, as a function of overlap length (L_0). For this work, adhesives are used commercial adhesives Araldite® AV138 (resistant but brittle adhesive), Araldite® 2015 (adhesive with moderate strength and ductility) and Sikaforce® 7752 (very ductile adhesive).

1.2 Objectives

The first purpose of this study is the experimental strength evaluation of single-lap joints (SLJ) with different values of L_0. Three different adhesives were used to bond an aluminum alloy (AW6082-T651) adherends, the brittle adhesive Araldite® AV138, the moderate ductile adhesive Araldite® 2015 and the high ductile Sikaforce® 7752. This experimental part is based on raw data extracted from earlier works executed by de Sousa [2] (joints with the adhesives Araldite® AV138 and Araldite® 2015) and by Carvalho [3] (joints with the adhesive Sikaforce® 7752). All the data analysis and later discussion from the original load-displacement (P-δ) curves from the tests were performed within the scope of this thesis. Upon the conclusion of the experimental study, begins the numerical work. The numerical conditions will be presented, either for the stress or strength analyses. Firstly, the stress analysis of the adhesive layer will be performed, allowing a better understanding of the joints' mechanical behavior, as well

as the maximum loads (P_m). Afterwards, the strength prediction by FE/CZM is carried out considering the previously mentioned conditions. This leads to the main purpose of this thesis: the evaluation of different simulation conditions in the CZM analysis for an exact strength prediction

Aim of the study to the behavior of three types of adhesives, the variation of strength according to different and evaluate the reliability of the XFEM as a strength prediction technique for adhesive joints. The numerical study includes the study of distributions of the analysis condition are damage initiation criteria and damage growth criteria and the law of strength prediction of joints.

1.3 Thesis layout

This thesis is structured in the following manner:

Section 1 presents a short contextualization of adhesive bonding, thesis objectives and layout.

Section 2, related to the bibliographic work, addresses the state-of-the-art, a brief comparative evaluation regarding other joining methods, common applications, typical loads, failure modes and joint configurations are aforementioned. The most relevant techniques for strength prediction are discussed at the end of this section.

Section 3 is divided into two main parts: subsection 3.1 related with the experimental work and subsection 3.2 addressing the numerical part of this work. Subsection 3.1 shows a detailed description of the experimental work, including all materials involved, manufacturing process, experimental tests and, finally, the experimental results were presented and discussed. Subsection 3.2 addresses the numerical work, where the numerical conditions used in the XFEM analysis are described. A stress analysis was initially performed to supply a basis for further discussions regarding the joint strength. Following, the joints' strength was predicted and compared against the experimental data. The end of this section presents and discusses the influence of different simulation conditions on the strength estimation of the bonded joints, concerning the variation of the elastic stiffness of the damage law, the decoupling of the loading modes, the evaluation of different law shape, the percentile variation of the damage parameters and the assessment of different initiation and propagation criteria.

Section 4, in this section the conclusions of this thesis as well as suggestions for future works were presented.

The last **Section, 5**, presents the bibliographic references used throughout this work.

THEORETICAL BACKGROUND

2 THEORETICAL BACKGROUND

This section addresses the main principles of adhesive bonding, common applications in several industries, typical loads, failure modes and the most popular joint configurations. Structural adhesives are also mentioned and categorized in this section, considering the different families. At the end of this section, the most relevant analytical and numerical methods for strength prediction of bonded joints are presented, with emphasis on XFEM.

2.1 Adhesive bonding

Bonding is the surface-to-surface joining of similar or dissimilar materials using a substance which usually is of a different type, and which adheres to the surfaces of the two adherends to be joined, transferring the forces from one adherend to the other. According to the DIN EN 923 standard, an adhesive is a non-metallic substance capable of joining materials by surface bonding (adhesion), and the bond having adequate internal strength (cohesion). Bonding is a material joining technique that, in the traditional sense, cannot be broken without destruction of the bond. Recently, specific bonding on-demand techniques have been develop , for example as an assembly tool without further function, or for recycling based on separation of materials, a method that today is becoming increasingly important [4].

Bonding is by far the most universal joining technique. Virtually all technically useful materials can be joined with each other, and one with another, by this surface-to-surface material-joining technique. Adhesive bonding technology offers useful design flexibility as it can be easily integrated into all available industrial sequences of single-piece work or mass production. Historically, bonding has long been recognized as a high-performance joining technique [5]. Most original natural binding materials have now been replaced by synthetically prepared adhesives. For example, phenolic resins were first introduced in the late 1920 while, during the 1940s, epoxide and polyurethane resins were developed in which have since made possible to produce synthetic adhesives.

As polymer chemistry has advanced in terms of knowledge, specific adhesives have been developed that bind very strongly to organic or inorganic materials. About adhesive strength and deformation, these adhesives meet extremely specific requirements that result from the configuration of the adhesive joint. Meanwhile, high-strength adhesive assemblies have been created with quite short curing periods. In fact, the longstanding

problem of extensive curing times necessary to obtain high strength joints has been completely resolved with the introduction of new chemical developments in the creation of adhesives. Moreover, skepticism is no longer justified as to the long-term durability of adhesive joints exposed to adverse environments, provided that the bonding is properly conceived [6].

Bonding rarely competes with other joining techniques used in industry [6]. For example, one would not consider bonding a steel bridge or a gantry, but for the lightweight construction of car bodies using steel, aluminum, glass and plastics, adhesive joining offers extremely interesting applications. Adhesive joining is particularly well suited to the joining of large-sized surfaces of dissimilar materials, such as in the construction of sandwich assemblies.

Some advantages of adhesive joints are listed as [5, 7]:

- Capacity to obtain lighter and stronger structures;
- Possibility to join dissimilar materials and materials with reduced stiffness;
- More uniform stress fields along the bonded area, enabling a more efficient load transfer;
- Good corrosion resistance;
- High fatigue strength;
- Better aesthetics (without bolts heads, rivets or welding);
- Fluid sealing;
- Reduced costs in a project, since the fabrication of bonded joints can be automated.

However, adhesive bonding also has disadvantages, such as [5, 7]:

- Joint design needs to be oriented towards the elimination of peel stresses, since adhesive joints should be primarily subjected to shear stresses;
- Low resistance to temperature and humidity;
- Requirement of a surface treatment;
- Fixing tools are needed, since adhesive curing is not instantaneous.

2.1.1 Fundaments of adhesive bonding

Adhesive bonding is a process of joining two or more solid parts with an adhesive substance. The materials of the joined parts (adherends, substrates) may be different or similar. The material of the adhesive layer is a polymer (natural or synthetic). The thickness of the adhesive layer does not usually exceed 0.02” (0.5 mm) [8].

2.1.1.1 Structure of an adhesive joint

An adhesive joint consists of two substrates with the adhesive material fill the gap between them. However, the adhesive layer is not uniform. Besides the part of the adhesive layer whose properties are not affected by the substrate, there are two boundary layers, which have been changed by impurities and products of reactions at the substrate surfaces. The boundary layer is a part of the adhesive layer adjacent to the substrate surface [9]. The principle basis of adhesive bonding is a phenomenon called adhesion.

2.1.1.1.1 Adhesion

Adhesion is a complex physicochemical process occurring at the interface of two materials brought into an intimate contact, which results in the formation of an attractive force between the two materials [10].

2.1.1.1.2 Adhesion strength

Adhesion strength is the force needed for separation of two adhered parts along the interface.

2.1.1.2 Mechanical Theory

According to mechanical theory, adhesion occurs by the penetration of adhesives into pores, cavities, and other surface irregularities of the surface of the substrate or adherend. The adhesive displaces the trapped air at the interface. Therefore, it is concluded that an adhesive penetrating into the surface roughness of two adherends can bond the two. A positive contribution to the adhesive bond strength results from the “mechanical interlocking” of the adhesive and the adherends [10].

2.1.1.3 Electrostatic (Electronic) Theory

This theory proposes that adhesion takes place due to electrostatic effects between the adhesive and adherend. An electron transfer theoretically takes place between the adhesive and the adherend, because of unlike electronic band structures. Electrostatic forces in the form of an electrical double layer are thus formed at the adhesive-adherend interface. These forces account for the resistance to separation. This theory gains support from the fact that electrical discharges have been observed when an adhesive is peeled from a substrate [11].

2.1.1.4 Diffusion Theory

This theory suggests that adhesion is developed through the inter-diffusion of molecules in and between the adhesive and adherend. The diffusion theory is primarily applicable when both the adhesive and adherend are polymers with long-chain molecules capable

of movement. The nature of materials and bonding conditions will influence if, and to what extent, diffusion takes place. The diffuse interfacial (interphase) layer typically has a thickness in the range of 10 Å–1,000 Å. Solvent cementing or heat welding of thermoplastics is a result of diffusion of molecules. Cohesive energy density [CED, Eq. (1)] can be used to interpret diffusion bonding, as defined by Eq. (2). Bond strength is maximized when solubility parameters between the adhesive and adherend are matched .

$$\boldsymbol{CED} = \frac{\boldsymbol{Ecoh}}{\boldsymbol{V}} \tag{1}$$

$$\boldsymbol{\delta} = \sqrt{\frac{\boldsymbol{Ecoh}}{\boldsymbol{V}}} \tag{2}$$

Ecoh is the amount of energy needed to separate molecules to an infinite distance, **V** is the molar volume, and **δ** is the solubility parameter.

A relevant example is adhesion of polyethylene and polypropylene to a butyl rubber. The adhesive bond is weak when two polymers are bonded at temperatures below the melting point of polyolefin. Bond strength grows sharply when the adhesion process takes place above the melting temperature of polyethylene (135°C) and polypropylene (175°C). Figure 1 illustrates the bond strength (peel strength) as a function of bonding temperature. An inference can be made that at elevated temperatures, inter - diffusion of polyolefins and butyl rubber increases, leading to higher bond strength[11].

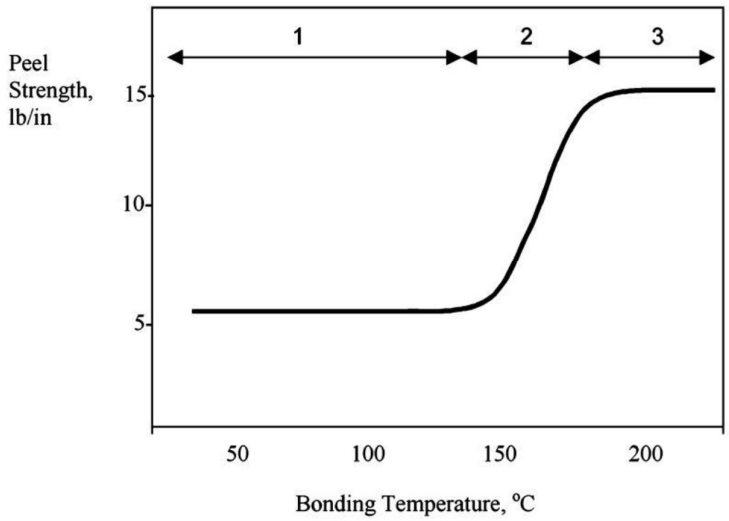

Figure 1 - Peel strength of polypropylene and butyl rubber vs a bonding temperature. 1. Adhesive failure; 2. adhesive/cohesive failure; and 3.cohesive failure [11].

2.1.1.5 Wetting Theory

This theory proposes that adhesion results from molecular contact of two materials and the surface forces that develop between them. The first step in bond formation is to

develop interfacial forces between the adhesive and the substrates. The process of setting up continuous contact between the adhesive and the adherend is called wetting. For an adhesive to wet a solid surface, the adhesive should have a lower surface tension than the critical surface tension of the solid, which is the reason for the surface treatment of plastics [12].

Figure 2 illustrates complete and incomplete wetting of an adhesive spreading over a surface. Good wetting results when the adhesive flows into the valleys and crevices on the substrate surface. Poor wetting occurs when the adhesive bridges over the valley, which results in a reduction of the actual contact area between the adhesive and adherend, and the loads to a lower overall joint strength [12]. Incomplete wetting generates interfacial defects, thereby reducing the adhesive bond strength. Complete wetting achieves the highest bond strength [8].

Most organic adhesives readily wet metal adherends. On the other hand, many solid organic substrates have surface tensions lower than those of common adhesives. The criteria for good wetting need the adhesives to have a lower surface tension than the substrate. This explains, in part, why organic adhesives such as epoxies have excellent adhesion to metals but offer weak adhesion on untreated polymeric substrates such as polyethylene, polypropylene, and fluoroplastics. Surface energy of plastic substrates is increased by various treatment techniques to allow wetting [13].

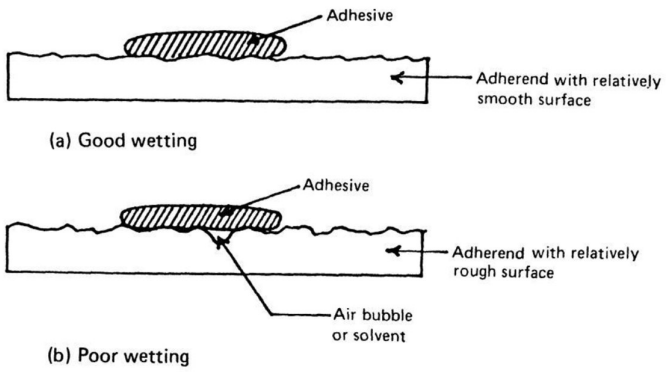

Figure 2 - Examples of good and poor wetting by an adhesive spreading across a surface. Modified after Schneberger [12]

2.1.1.6 Chemical Bonding

This mechanism attributes the formation of an adhesion bond to surface chemical forces. Hydrogen, covalent, and ionic bonds formed between the adhesive and adherends are stronger than the dispersion's attractive forces. Table 1 shows a list of these forces and their magnitudes. In general, there are four types of interactions that take place during chemical bonding: covalent bonds, hydrogen bonds, Lipsitz-van der Waals forces, and acid-base interactions. The exact nature of the interactions for a given adhesive bond depends on the chemical composition of the interface [14].

Table 1 - Forces and their magnitudes of Chemical Bonds [14]

Type	Example	E (kj/mol)
Covalent	C-C	350
Ion-Ion	$Na^+...Cl^-$	450
Ion-Dipole	$Na^+...CF_3H$	33
Dipole-Dipole	$CF_3H...CF_3H$	2
London Dispersion	$CF_4...CF_4$	2
Hydrogen Bonding	$H_2O...H_2O$	24

The definitions of intermolecular interactions are listed here [14]:

• Dipole (polar molecule): a molecule whose charge distribution is represented by a center of positive charge and a center of negative charge that do not coincide.

• Dipole-dipole forces: intermolecular forces resulting from the tendency of polar molecules to align themselves such that the positive end of one molecule is near the negative end of another.

• Hydrogen bonding: a special type of dipole-dipole interaction that occurs when a hydrogen atom, bonded to a small, highly electronegative atom (most commonly F, O, N, or S), is attracted to the lone electron pairs (most commonly on an F, O, N, or S atom) of another molecule.

• London dispersion forces (dispersion forces): intermolecular forces resulting from the small, instantaneous dipoles (induced dipoles) that result from the varying positions of the electrons during their motion around nuclei. The importance of London dispersion forces increases with atom size and number of electrons.

• Polarizability: defined as the ease with which the electron cloud of an atom or molecule is distorted. In general, polarizability increases with the size of an atom and the number of electrons in an atom.

2.1.2 Typical applications of bonded joints

Adhesively-bonded joints are nowadays present in several industries such as:

Aeronautical; the application of adhesives to the aeronautical field and planes manufacture, from several decades now the bonding technique have been especially

important for plane production. Reasons such as the high durability in terms of lifetime, the high resistance to dynamic loads, as well as fast changes and extreme temperatures handle a implementation of bonding solutions to aircrafts (Figure 3). Combining these with the reduced operating and production costs, turns the bonding process an extremely attractive and useful manufacturing method that eases the eternal quest for lightweight low-cost structures [15].

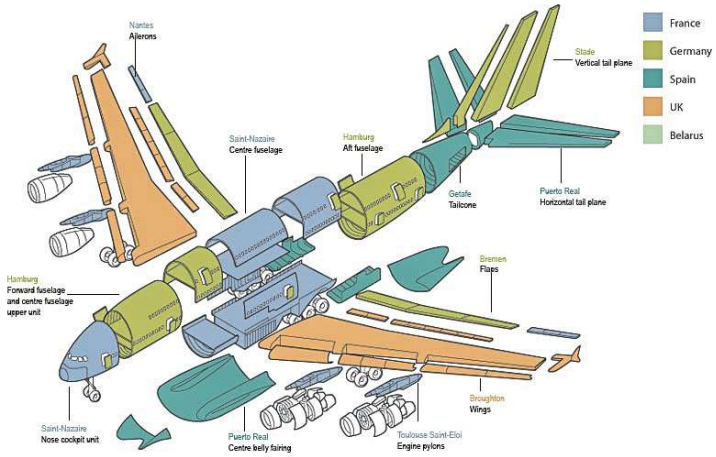

Figure 3 - Aircraft bonded parts [15]

These days, light metal alloys, CFRPs and sandwich structures have been important instruments in increasing strength and durability, while minimizing weight. The high compatibility of adhesives with the use of these kinds of materials is just another example of the several economically advantageous aspects found [15]. An example for the complex structure of the manufacturing method and it is eased by the applicability and versatility of adhesives is proven in Figure 4.

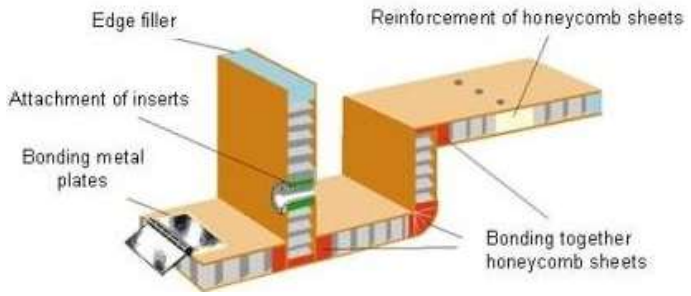

Figure 4 - Lightweight structure example produced using honeycomb sheets and adhesives [15]

Aeronautical components bonded using adhesives include airplane's engine components, airplanes rigid interior panels, filling materials for local reinforcement, and much more.

Automotive; The automotive industry is one of most active industries in the use of adhesive bonding. By joining different materials with adhesives, better performances are achieved in lightweight, durability, by overcoming fatigue issues, safety and vehicle assembly, and due to the elimination of welding access problems [7]. The use of adhesives applied to the automotive industry began decades ago with the bonding of windscreens to improve aesthetics. Afterwards, adhesives were used to fill gaps in spot-welded flanges to prevent corrosion. It was discovered that, besides corrosion resistance, adhesive bonding also enhanced the stiffness of the car body. Modern cars like the E-class and the S-class of DaimlerChrysler have more than 50 m of structural bonding. The situation is similar for other high-performance cars (Figure 5).

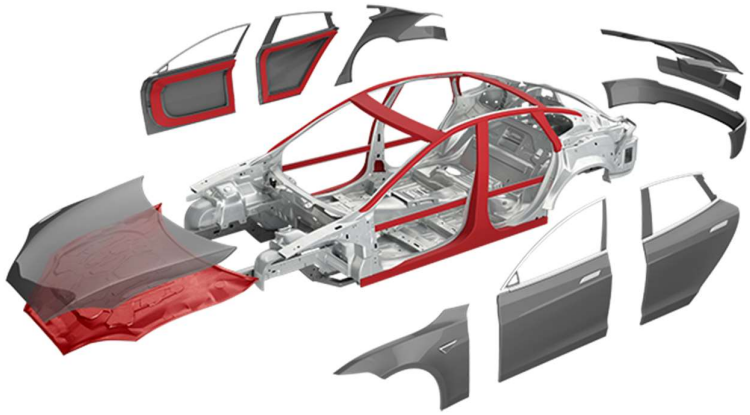

Figure 5 - Adhesive bonding in car[7]

Railway; In Figure 6 shows the train industry, adhesive bonding also became the most promising method to join multi-material structures. This technique enhances the weight advantage, improves the strength, stiffness and thermal insulation, reduces noise, and promotes the incombustibility and recyclability of trains [1].

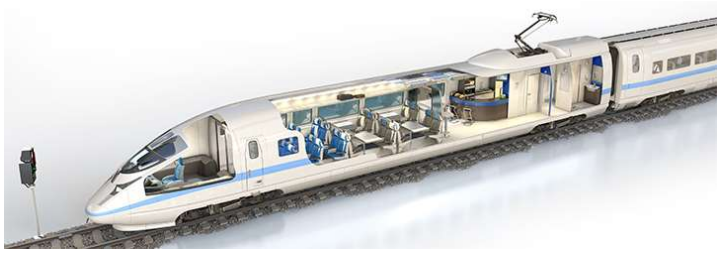

Figure 6 - Adhesive bonding used for railways

Marine; The marine industry needs a long-term durability in a seawater environment for structures. Therefore, the involved materials are mostly fiber reinforced composites, which in these industry are frequently assembled by adhesive bonding, in which surface

preparation is a vital part [16]. The marine industry covers a wide range of structures, such as small boatyards, naval shipyards, racing yachts, and bonded structures for the offshore oil and gas industries. New markets are also appearing, for example the marine energy sector, which will need adhesives to bond structures like turbine blades.
Electrical and
Civil construction.

2.1.3 Types of loads and failure modes in bonded joints

Five types of loads can be found in adhesive joints. Any combination of these loads may be met in an adhesive application. These loads are described in the next sections.

2.1.3.1 Tension

The strengths of joints loaded (Figure 7) in tension or shear are comparable. As in shear, the stress is evenly distributed over the joint area, but it is not always possible to be sure that other stresses are not present. If the applied load is offset to any degree, the advantage of an evenly distributed stress is lost, and the joint is more likely to undergo failure. The adherends should be thick with this type of joint and not likely to deflect to any appreciable degree under the applied load. Such a situation will result in non-uniform stresses. Tensile stresses develop when forces acting perpendicularly to the plane of the joint are distributed uniformly over the entire area of the bond. The types of stresses likely to result when other than completely axial loads are applied are cleavage and peel. As adhesives generally have poor resistance to cleavage and peel, joints designed to load the adhesive in tension should have physical restraints to ensure axial loading [17].

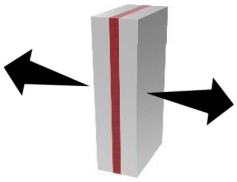

Figure 7 - Tension load (self-elaboration)

2.1.3.2 Compression

From Figure 8 shows that when loaded in pure compression, a joint is less likely to fail than when loaded in any other manner, but compression-loaded joints are limited in application. When a material is subjected to compressive loading, the relationship between stress and strain is like that obtained for a tensile loading. Up to a certain value of stress, the material behaves elastically, i.e. stress is in proportion to strain. Beyond this value, plastic flow starts, i.e. more strain starts than happening in elastic limit for any increment value of loading. It is seen that a compression test is more difficult to be

conducted than standard tensile test due to (i) the specimen must have a larger cross-sectional area to resist any buckling due to bending, (ii) the specimen undergoes strain hardening as deformation proceeds, and (iii) the cross-section of the specimen increases with deformation, thereby requiring substantial increase in the required load. The lateral instability due to buckling action can be avoided by keeping the ratio of height (h) to diameter (d) of the specimen less than 2. The compressive strength depends open 'h' to 'd' ratio. Hence, higher is 'h' to 'd' ratio, the lower is the compressive strength [7].

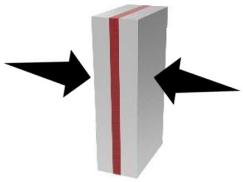

Figure 8 - Compression load (self-elaboration)

2.1.3.3 Shear

This type of loading (Figure 9)imposes an even stress across the whole bonded area, using the joint area to the best advantage and supplying an economical joint that is most resistant to joint failure. Whenever possible, most of the load should be transmitted through the joint as a shear load [17].

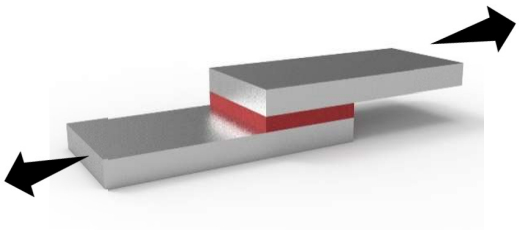

Figure 9 - Shear load (self-elaboration)

2.1.3.4 Peel

As Figure 10 shows that one or both adherends must be flexible in this type of loading. A very high stress is applied to the boundary line of the joint, and unless the joint is wide or the load is small, failure of the bond will occur [18]. This type of loading is to be avoided if possible [19].

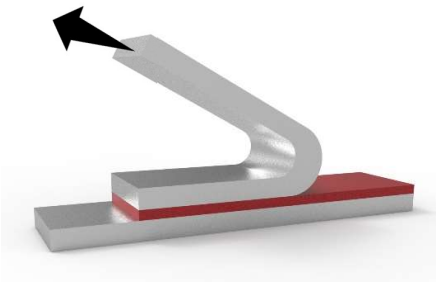

Figure 10 - Peel load (self-elaboration)

2.1.3.5 Cleavage

Cleavage is like peel and occurs when forces at one end of a rigid bonded assembly act to split the adherends apart. It may be considered as a situation in which an offset tensile force or a moment has been applied [20]. The stress is not evenly distributed (as is the case with tension) but is concentrated on one side of the joint. A sufficiently large area is needed to accommodate this stress, resulting in a costlier joint [20, 21].

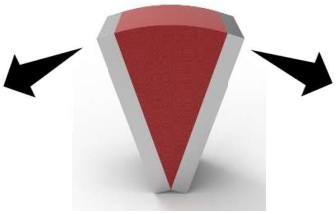

Figure 11 - Cleavage load (self-elaboration)

2.1.4 Bonded joints configurations applied in the industry

The ideal adhesive-bonded joint is one in which, under all practical loading conditions, the adhesive is stressed in the direction in which it most resists failure. Types of joints used in bonding flat adherends. These will be discussed briefly.

2.1.4.1 Butt joints

These joints are not able to withstand bending forces because, under such forces, the adhesive would undergo cleavage stress. If the adherends are too thick to design simple overlap joints, modified butt joints can be designed. Figure 12 shows that such joints reduce the cleavage effect caused by side loading. Tongue-and-groove joints are self-aligning and supply a reservoir for the adhesive. Scarf butt joints keep the axis of loading in line with the joint and require no extensive machining [22].

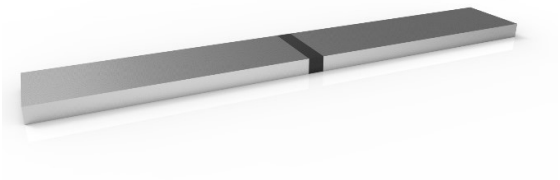

Figure 12 - Butt joint (self-elaboration)

2.1.4.2 *Single-lap joints*

Lap joints are the most commonly used adhesive joints (Figure 13). They are easy to manufacture, can be used with thin adherends and the adhesive is mostly loaded in shear. In the SLJ, the adherends are not collinear, which leads to significant peel stresses at the overlap end.

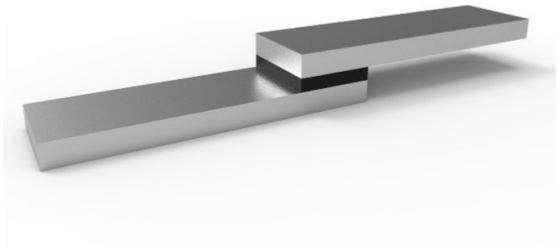

Figure 13 – Single -Lap joint (self-elaboration)

2.1.4.3 *Joggle-lap joints*

This is the easiest design for aligning loads. (Figure 14) this joint can be made by simply bending the adherends. It also supplies a surface to which it is easy to apply pressure. Taib et al. [23] analyzed a JLJ subjected to both tensile and bending loads [23]. A nonlinear beam analysis model was used for calculation of the stress profiles through the adherend thickness, while a plane stress finite element model was used for the determination of the stress field in the adhesive layer.

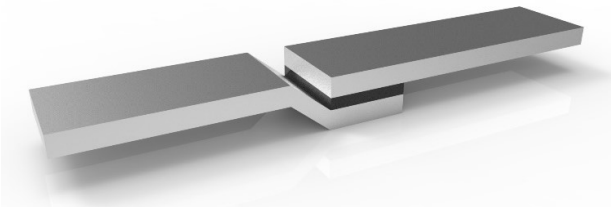

Figure 14 - Joggle Lap Joint (self-elaboration)

2.1.4.4 Double-lap joints

These joints have a balanced construction that is subjected to bending only if loads in the double side are not balanced. (Figure 15) double-lap joints have a balanced construction that decreases the bending moment. However, there are internal bending moments that cause peel stresses at the ends of the inner adherend. Recent solutions include wavy and reverse-lap joints [24].

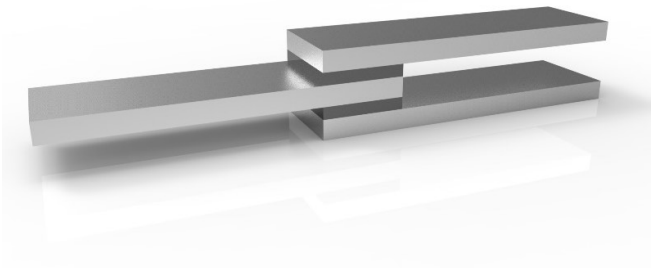

Figure 15 – Double -Lap Joint (self-elaboration)

2.1.4.5 Beveled-lap joints

These joints are also more efficient than plain lap joints. Figure 16 beveled edges allow conformance of the adherends during loading, with a resultant reduction of cleavage stress at the ends of the joint [16, 25].

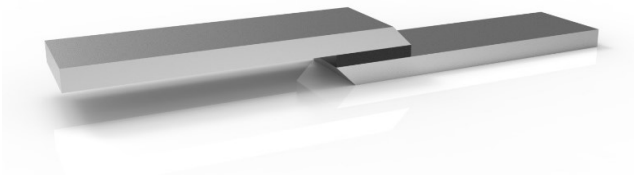

Figure 16 - Beveled Lap Joint (self-elaboration)

2.1.4.6 Strap joints

These joints keep the operating loads aligned and are used where overlap joints are impractical because of adherend thickness. As in the case of the lap joint, the single - strap joint are subjected to cleavage stresses under bending forces. The double-strap joint is superior when bending stresses are involved. Figure 17 the beveled double-strap joints and recessed double strap are the best joint designs to resist bending forces. However, both these joints require expensive machining [16].

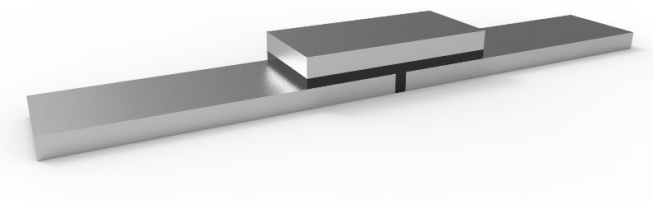

Figure 17 - Strap Joint (self-elaboration)

2.2 Strength prediction techniques

In the past, the non-existence of correct material models and suitable failure criteria led to the 'overdesign' adhesive joints, which invariably resulted on heavier and more expensive structures. With the availability of reliable design and predictive methodologies, new possibilities appeared for the efficient use of bonded joints. Two alternatives can be chosen for the analysis of adhesive joints: closed-form analyses (analytical methods) and numerical methods (i.e. finite element or FE analyses). The study of adhesive joints dates back to the 1930's with the closed-from model of Volkersen [26] that considers fully elastic materials and adhesive deformation only in shear. However, the analytical formulation of adhesive joints becomes more complex if the adhesive deforms plastically, if composite adherends are used, or if different adherend materials are employed [27]. The FE is the most popular technique for adhesive joints, and Adams and co-workers were pioneers in this technique [28]. The joint rotation, the adherends and adhesive plasticity and the influence of the spew fillet were studied in first hand by Harris and Adams [29]. The continuum mechanics approach for strength prediction of bonded joints was used in the early analysis, requiring the stress distribution and a suitable failure criterion. An FE analysis can also be used together with Fracture Mechanics criteria for strength prediction, either by the stress intensity factor or energy approaches like the Virtual Crack Closure Technique (VCCT). However, with these techniques modelling crack growth becomes cumbersome because of remeshing taking place during the analysis and respective computational cost required [30]. Major developments were made, and one of these is damage modelling by combination of FE with cohesive zone elements. This technique joins together conventional FE modelling for the regions that are not expected to undergo damage and a fracture mechanics approach via the cohesive elements to simulate crack growth. A very recent alternative to model crack propagation within materials is the eXtended Finite Element Method (XFEM), which uses enriched shape functions to represent a discontinuous displacement field.

2.2.1 Analytical techniques

Back in the initial stages of bonded structures analyses, the predictive methods consisted on analytical formulations, and the works of Volkersen [26] and Goland and Reissner [31] were precursors of a number of theoretical studies that had the advantage of simplicity to reach the stress fields in the bonded structures because of the employed simplifying assumptions in terms of the structures geometry, loading, and boundary conditions, giving efficient closed-form elasticity solutions. Thus, each bonded structure could be analyzed quickly, although with lot of embedded assumptions [32]. With these models, strains and stresses could be easily calculated, along with the distribution of the bending moment in the structure. The strength was typically predicted by stress or strain-based criteria. Up to nowadays, these studies were progressively replaced by numerical analyses, although theoretical studies were also refined over the years in terms of modelling capabilities, such as material non-linearity of the adhesive layer [33] or non-linear geometric analyses [34].

2.2.2 Numerical techniques

2.2.2.1 Continuum mechanics

In the continuum mechanics approach, the maximum values of stress, strain or strain energy, predicted by the FE analyses, are usually used in a failure criterion to estimate the assembly's strength. This is carried out when the predicted values, obtained by stress or strain-based criteria (e.g. the Maximum Normal Stress Criterion, MNSC, or the Maximum Shear Strain Criterion, MSSC), reach the strength of the structure constituents. This approach was promptly applied to general-purpose bonded joints in structural applications soon after the FE method and computer programming were made available (e.g. [29]). Advantages of this technique included the analysis of bonded structures with or without a first damage, and under an arbitrary loading. Nonetheless, these criteria hold an intrinsic limitation, since bonded structures are prone to stress singularities at the end of the overlapping regions due to sharp corners. As a result, in an FE analysis to a bonded structure, stresses at a singular region increase with the mesh refinement and convergence is not attained, giving mesh dependent predictions [32]. Over the years, improvements were introduced to this modelling technique, such as the definition of more complex stress or strain-based failure criteria for different materials and fracture mechanisms, or combination with more realistic continuum material models, but still the mesh dependency could not be solved.

2.2.2.2 Fracture mechanics

Continuum mechanics assumes that the structure and its material are continuous. Defects or two materials with re-entrant corners obviously are not consistent with such an assumption. Consequently, continuum mechanics gives no solution at these singular

points resulting in stress or strain singularities. Cracks are the most common defects in structures, for which fracture mechanics has been developed. In fracture mechanics, it is well accepted that stresses calculated by using continuum mechanics are singular (infinite) at the crack tip. With current theories on mechanics, such a singularity always exists when the crack angle is less than 180^0. This result was found by Williams [35] for stress singularities in a wedged notch. This argument is also applicable to the stress singularity in two materials bonded together with a re-entrant corner. Fracture mechanics has been successfully applied to many engineering problems in recent years. Many studies dealing with adhesive joints use the strain energy release rate, G, and respective critical value or fracture toughness, G_c [36] instead of stress intensity factors because these are not easily determinable when the crack grows at or near to an interface. However, the fracture of adhesive joints inherently takes place under mixed mode because of the varying properties between dissimilar materials and the complex stress system. Failure criteria for mixed mode fracture can be developed in a way analogous to the classical failure criteria, although the fracture surface (or envelope) concept must be introduced.

2.2.2.3 Cohesive zone models

The computer implementation of Linear Elastic Fracture Mechanics (LEFM) methods had remarkable success some decades ago, but these were limited to small-scale yielding beyond the crack tip. In addition, modern toughened adhesives develop plastic zones under load that can be larger than the adherends thickness. CZM were developed in the late 1950s / early 1960s [37] to describe damage under static loads at the cohesive process zone ahead of the apparent crack tip, giving a promising solution for more refined methods to predict damage in bonded structures. CZM were then largely tested since then to simulate crack initiation and propagation in cohesive and interfacial failure problems or composite delamination's. CZM can rely on spring or more conventionally cohesive elements [38], and they can be easily incorporated in conventional FE analyses to model the fracture behavior in various materials, including adhesively bonded joints [39]. The main concept of CZM is that one or multiple fracture interfaces/regions can be artificially introduced in structures, in which damage growth is allowed by the introduction of a discontinuity in the displacement field. This is made possible by the definition of traction-separation laws to model interfaces or finite regions. The CZM laws are enforced between paired nodes of cohesive elements, and they can connect superimposed nodes of elements being dissimilar materials or different plies in composites, or they can be applied directly between two non-contacting materials to simulate a thin strip, e.g. to simulate an adhesive bond. CZM supply a macroscopic reproduction of damage by the traction-relative displacement response between paired nodes along the crack path, which relies on large scale parameters that rule the crack growth process such as the fracture energies. The strength evolution and softening up to failure is modelled, to account for the gradual degradation of material properties. The

traction-separation laws are typically built by linear relations at each one of the loading stages [40], although one or more stages can be defined differently for a more accurate representation of the materials behavior.

2.2.2.4 Damage mechanics

This section describes Alternative to Cohesive Damage Models (ACDM) techniques, i.e., other than CZM modelling, which can be categorized within the continuum framework if modelling finite volumes of material. In these methodologies, a damage parameter is established to modify the constitutive response of materials by the depreciation of stiffness or strength, e.g. for thin adhesive bonds [41], or composite delamination's or matrix failure [42], to represent the severity of material damage during loading. This state variable can be used in a damage evolution law to model both pre-cracking damage uptake and crack growth. The damage variables can be categorized under two main groups: (1) variables that predict the amount of damage by the redefinition of the material constitutive properties but that do not directly relate to the damage mechanism, and (2) variables linked to the physical definition of a specific kind of damage, such as porosities or relative area of micro-cavities [43]. By ACDM, the growth of damage is defined as a function of the load for static modelling or the cyclic count for fatigue analyses. For bonded joints, little work is published in this field. Compared to fatigue CZM's, ACDM techniques do not provide a clear distinction between fatigue initiation and propagation phases, although they can give a basis for the predictive analysis [41]. Nonetheless, the evolution of damage prior to macro-crack growth can be simulated. On the other hand, damage modelling with fatigue CZM's is restricted to pre-defined crack paths and, on specific applications, ACDM's may be recommended if the damage is more widespread or the failure path is not known [44].

2.2.2.5 Extended Finite Element Method

The XFEM is a recent improvement of the FE method for modelling damage growth in structures. It uses damage laws for the prediction of fracture that are based on the bulk strength of the materials for the initiation of damage and strain for the assessment of failure (defined by G_n^c), rather than the values of t_n^0/t_s^0 or δ_n^0/δ_s^0 used for the CZM's. XFEM gains an advantage over CZM modelling as it does not need the crack to follow a predefined path. Actually, cracks are allowed to grow freely within a bulk region of a material without the requirement of the mesh to match the geometry of the discontinuities neither remeshing near the crack [45]. This method is an extension to FE modelling, whose fundamental features were firstly presented in the late 90's by [46]. The XFEM relies on the concept of partition of unity and it can be implemented in the traditional FE by the introduction of local enrichment functions for the nodal displacements near the crack to allow its growth and separation between the crack faces [47]. Due to crack growth, the crack tip continuously changes its position and orientation

depending on the loading conditions and structure geometry, simultaneously to the creation of the necessary enrichment functions for the nodal points of the finite elements around the crack path/tip.

2.2.2.5.1 Theoretical fundaments of the method

Although a few static implementations of the XFEM were developed in recent years for scenarios other than bonded joints, the generic Abaqus® embedded formulation will be described in this Section [48] The XFEM considers a first linear elastic behavior of the materials, which is represented by an elastic constitutive matrix that relates stresses with the normal and shear separations of the cracked elements. Damage and failure are simulated in XFEM by suitable damage initiation criteria and damage laws between the real and phantom nodes of a cracked element (to be detailed further in this Section). The damage initiation criteria can rely on stresses or strains, while the traction-separation laws that simulate material degradation up to failure can be linear or exponential. Abaqus® starts and propagates damage during the simulation at regions experiencing stresses and/or strains higher than the corresponding limiting values. Six crack initiation criteria are available in Abaqus®. The MAXPS (maximum principal stress) and MAXPE (maximum principal strain) criteria are based on the introduction of the following functions (by the respective order)

$$f = \left\{ \frac{\langle \sigma_{\max} \rangle}{\sigma^{o}_{\max}} \right\} \quad \text{or} \quad f = \left\{ \frac{\langle \varepsilon_{\max} \rangle}{\varepsilon^{o}_{\max}} \right\} \tag{3}$$

σ_{max} and σ^{o}_{max} represent the current and allowable maximum principal stress. The Macaulay brackets indicate that a purely compressive stress state does not induce damage. ε_{max} and ε^{o}_{max} represent the current and allowable maximum principal strain. The MAXS (maximum nominal stress) and MAXE (maximum nominal strain) criteria are represented by the following functions, respectively

$$f = \max\left\{ \frac{\langle t_n \rangle}{t^{o}_{n}}, \frac{t_s}{t^{o}_{s}} \right\} \quad \text{or} \quad f = \max\left\{ \frac{\langle \varepsilon_n \rangle}{\varepsilon^{o}_{n}}, \frac{\varepsilon_s}{\varepsilon^{o}_{s}} \right\} \tag{4}$$

t_n and t_s are the current normal and shear traction components. t_n^0 and t_s^0 represent the respective limiting values. The strain parameters have identical significance. The quadratic nominal stress (QUADS) and quadratic nominal strain (QUADE) criteria are based on the introduction of the following functions, respectively

$$f = \left\{ \frac{\langle t_n \rangle}{t^{o}_{n}} \right\}^2 + \left\{ \frac{t_s}{t^{o}_{s}} \right\}^2 \quad \text{or} \quad f = \left\{ \frac{\langle \varepsilon_n \rangle}{\varepsilon^{o}_{n}} \right\}^2 + \left\{ \frac{\varepsilon_s}{\varepsilon^{o}_{s}} \right\}^2 \tag{5}$$

All criteria are fulfilled, and damage initiates, when *f* reaches unity. For damage growth, the fundamental expression of the displacement vector **u**, including the displacements enrichment, is written as [48].

$$\mathbf{u} = \sum_{i=1}^{N} N_i(x)\left[\mathbf{u}_i + H(x)\mathbf{a}_i + \sum_{\alpha=1}^{4} F_\alpha(x)\mathbf{b}_i^{\alpha}\right]. \quad (6)$$

$N_i(x)$ and $\mathbf{u}_i$ relate to the conventional FEM technique, corresponding to the nodal shape functions and nodal displacement vector linked to the continuous part of the formulation, respectively. The second term between brackets, $H(x)\mathbf{a}_i$, is only active in the nodes for which any relating shape function is cut by the crack and can be expressed by the product of the nodal enriched degree of freedom vector including the mentioned nodes, $\mathbf{a}_i$, with the associated discontinuous shape function, $H(x)$, across the crack surfaces [48].

$$H(x) = \begin{cases} 1 & \text{if} \quad (\mathbf{x} - \mathbf{x}^*).\mathbf{n} \geq 0 \\ -1 & \text{otherwise} \end{cases}. \quad (7)$$

x is a sample Gauss integration point, **x*** is the point of the crack closest to **x**, and **n** is the unit vector normal to the crack at **x*** (Figure 18). Finally, the third term is only to be considered in nodes whose shape function support is cut by the crack tip and is given by the product of the nodal enriched degree of freedom vector of this set of nodes, $\mathbf{b}_i^{\alpha}$, and the associated elastic asymptotic crack-tip functions, $F_\alpha(x)$ [49]. $F_\alpha(x)$ are only used in Abaqus® for stationary cracks, which is not the current case.

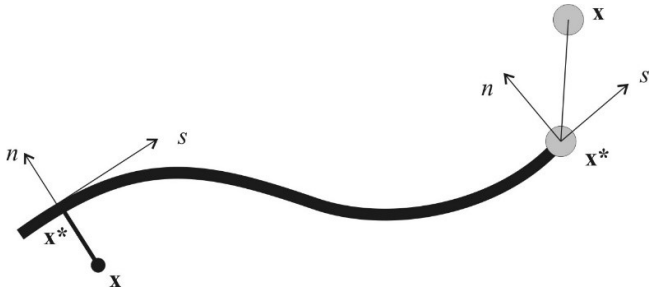

Figure 18 - Representation of normal and tangential coordinates for an arbitrary crack [50].

In the presence of damage propagation, a different approach is undertaken, based on the establishment of phantom nodes that subdivide elements cut by a crack and simulate separation between the newly created sub elements. By this approach, the asymptotic functions are discarded, and only the displacement jump is included in the formulation. Propagation of a crack along an arbitrary path is made possible using phantom nodes that initially have the exact same coordinates than the real nodes and that are completely constrained to the real nodes up to damage initiation.

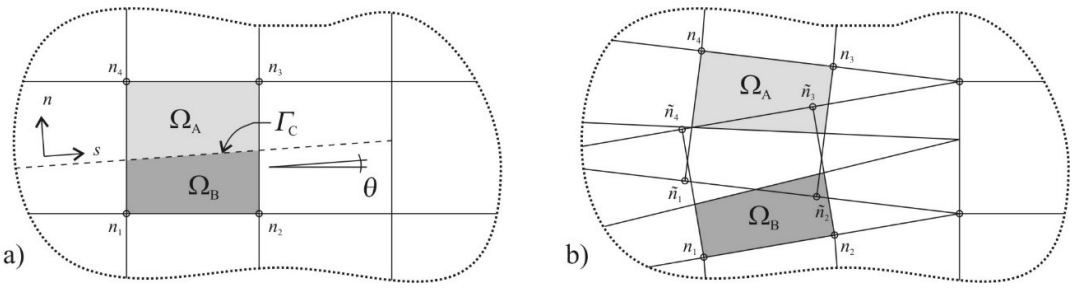

Figure 19 - Damage propagation in XFEM using the phantom nodes concept: before (a) and after partitioning (b) of a cracked element into sub elements [50].

In Figure 19, the highlighted element has nodes n_1 to n_4. After being crossed by a crack at Γ_C, the element is partitioned in two sub-domains, Ω_A and Ω_B. The discontinuity in the displacements is made possible by adding phantom nodes ($\tilde{n}_1$ to $\tilde{n}_4$) superimposed to the original nodes. When an element cracks, each one of the two sub elements will be formed by real nodes (the ones corresponding to the cracked part) and phantom nodes (the ones that no longer belong to the respective part of the original element). These two elements that have fully independent displacement fields replace the original one, constituted by the nodes $\tilde{n}_1$, $\tilde{n}_2$, n_3 and n_4 (Ω_A) and n_1, n_2, $\tilde{n}_3$ and $\tilde{n}_4$ (Ω_B). From this point, each pair of real/phantom node of the cracked element can separate according to a suitable cohesive law up to failure. At this stage, the real and phantom nodes are free to move unconstrained, simulating crack growth. In terms of damage initiation, Abaqus® allows the user to define initial cracks, but this is not mandatory. Regardless the choice taken, Abaqus® starts and propagates damage during the simulation at regions experiencing principal stresses and/or strains greater than the corresponding limiting values specified in the traction-separation laws. Crack initiation/propagation will always take place orthogonally to the maximum principal stresses or strains.

2.2.2.5.2 Application to bonded joints

The XFEM is not yet widely applied and studied for the strength prediction of bonded joints. Nonetheless, few research works are available that address this topic. The work of Stuparu et al. [51]. Experiments have shown that the fracture energy can depend on mode mixite. The damage models were later extended to the mode II fracture process, in which the tangential traction and separation are considered instead [51]. As Högberg mentions in, experimental observations show distinctive characteristics of the micromechanical failure mechanisms in peel and shear fracture, thus the damage behavior is expected to be mode dependent.

The recently developed extended finite element method is an extension of the FEM, and its fundamental features were described by Belytschko and Black [46] , based on the idea of partition of unity presented in [52], which consists on local enrichment functions for the nodal displacements to model crack growth and separation between crack faces.

With this technique, discontinuities such as cracks are simulated as enriched features, by allowing discontinuities to grow through the enrichment of the degrees of freedom of the nearby nodes with special displacement functions. As the crack tip changes its position and path due to loading conditions [53], the XFEM algorithm creates the necessary enrichment functions for the nodal points of the finite elements around the crack path/tip. The XFEM excels in simulating crack onset and growth along an arbitrary path without the requirement of the mesh to match the geometry of the discontinuities neither remeshing near the crack. This can be an advantage to CZM modelling for the simulation of bonded engineering plastics or polymer-\matrix composites, where adherend cracking may occur after initiation criteria of the adhesive.

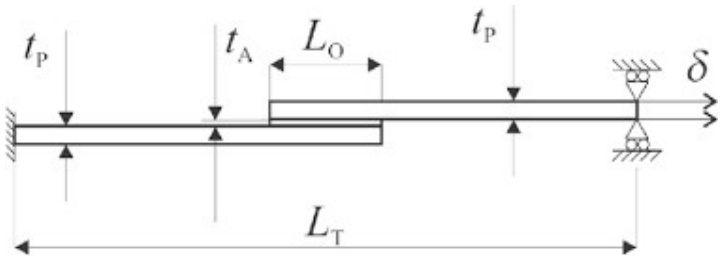

Figure 20 - Single lap joint geometry with initial delamination used for the numerical model [51].

This does not occur with the XFEM, as crack propagation is allowed anywhere within the models. This is a limitation in the specific case of thin adhesive layers since their behavior is not consistent with that of the corresponding bulk adhesives, because of the constraints on deformations imposed by the adherends and respective discrepancies in the stress fields near the crack tip [51, 54].

Stuparu et al. [51] underlined that the current implementation of XFEM and CZM in Abaqus® showed that there is a potential discontinuity in the crack path as at the interface the crack cannot continue in the adherend. Therefore, a layer of cohesive elements in the adhesive layer was used to simulate cohesive failure at the experimentally observed site of failure. As an experimental-numerical methodology for identification of mode I failure parameters of unidirectional fiber reinforced composites for which crack propagation is controlled by a bi-linear cohesive law. XFEM always propagates cracks orthogonally to the maximum principal stresses/strains, which in some cases may not correspond to the real behavior of materials and give inaccurate predictions. In these situations, the XFEM still predicts with accuracy the location of damage initiation by the stress or strain criteria. Concerning the mesh dependency of the XFEM for the strength predictions, it behaves in an identical manner to CZM, since it is almost mesh independent for the simulation of fracture propagation. This is because the strain energy is averaged over a finite area while crack growth is taking place. Despite this fact, given that the prediction of crack initiation is carried out by the value of t_0 n, this feature is mesh dependent, as stresses/strains at concentration regions are mesh dependent as well. A first delamination of same length is induced at one end of

the adhesive as a starter for crack extension. Thus, crack initiation/propagation will always take place orthogonally to the maximum principal strains. The thickness of the adhesive and the position of a first delamination are modified as to study the crack trajectory through the adhesive with XFEM and the delamination process at the interface with CZM. Observations on the joint use of the two methods are done and conclusions on the feasibility of such an approach are drawn. It is shown that the crack trajectory is influenced by the local state of stress and even if by XFEM it reaches or not the lower interface a main crack is formed by CZM at the upper interface [51].

The following values were used for this work: adherend thickness 5 mm, adhesive thickness 1, 3, and 5 mm, overlap length being 20 mm, and specimen width 25 mm. A first delamination of 5 mm length is induced at the left end of the adhesive. The interface has been modelled using zero thickness layers of cohesive elements. To optimize the solving time required for analysis, the adherends have been meshed using Abaqus® bias capability, with elements size of 0.5-1 mm. The 0.5 mm elements were used near the interface with the adhesive. For the adhesive region, elements with constant size of 0.2 mm were considered. Table 2 summarizes the mechanical properties used in the simulation, for the aluminum adherends and the Araldite® AV138 adhesive. Only a linear elastic response of the adherend and the adhesive was considered, as this adhesive has a very brittle behavior, and differences between a linear and non-linear analysis were not found to be significant.

As general description, the delamination process is simulated using cohesive zone modelling by a linear softening traction-displacement law after damage initiation ε0 n is produced. The crack is propagated by using the critical strain energy release rate. In the first analyses we used three values of strain for damage initiation: 0.1% - in the elastic region, 0.75% - representing the maximum elastic strain of the adhesive and 1.21% - value of the strain for which the adhesive fails. Taking into account that failure is adhesive in the cohesive elements at the interface, and cohesive, but the propagated crack by using XFEM is small in size, we can conclude that the strain at initiation has quite a small influence over the global behavior; therefore we chose for further analyses this value as being 0.75 % as mentioned also in Table 2.

The model under discussion has the following geometrical characteristics: 1 mm adhesive thickness with 20 mm overlap. A first delamination of 5 mm length is positioned in the middle of the adhesive layer. Hereby the behavior of the adhesive and the adherends is linear elastic. Crack initiation - in the adhesive the damage initiation strain is reached and crack initiates in the first element. The status of the enriched element in XFEM is 1.0 if the element is completely cracked, and 0 if the element has not failed. Complete crack propagation by XFEM through the adhesive till the interface - it is to be noticed that meanwhile the CZM started to be effective: a delamination of about 1 mm is produced at the lower interface. From this moment on the delamination starts to propagate at both interfaces between the adhesive and the adherends. The

crack remains at the interface and does not move back to the adhesive, nor into the adherend. An inconsistency may appear in coupling XFEM with CZM in the last element of the adhesive near the interface. For the same adhesive thickness of 1 mm the size of the elements was refined by reaching squares of 0.05 mm for the adhesive and 0.2 mm for the adherend. It was noticed that the crack propagates with XFEM through the last element of the adhesive only if the interface starts already to open with CZM. It is also possible to use as a damage initiation criterion a shear criterion - which is a phenomenological model for predicting the onset of damage due to shear band localization. When considering the effective response of the adhesive AV138 as being perfectly plastic beyond the onset of damage, with a critical shear failure strain of 7.8 %. Such a criterion may be used only if the adhesive is loaded in pure shear. Crack propagates through the adhesive only between the two interfaces, but never in any of the interfaces.

For all the analyzed thicknesses three positions of the initial delamination's, measured from the bottom interface, were analyzed: at quarter of the thickness, in the middle, and at three quarters.

Table 2 - Properties of materials [55, 56]

	Araldite® AV138	Aluminum
E(GPa)	4.89	70.07
G(GPa)	1.56	26.34
$\varepsilon_n^0(\%)$	0.75	21.70
G_0^c	0.2	15
G_s^c	0.38	15

In all cases the crack propagates by XFEM toward the lower interface. Fig.12(a) and 12(b) the lower interface starts eventually to open through CZM. For the case presented in Fig.12(c) the crack propagates toward the lower interface and within it, but meanwhile the upper interface opens significantly and takes over the failure process. After reaching the interface with the adherend XFEM crack propagation is taken over by CZM and a new crack forms in the upper interface and increasing its length leads to failure. When the initial delamination is closer to the interface and the adhesive is less constrained by the stiffer adherends and the crack propagates by XFEM toward the lower interface looking for symmetry and then stops. A major crack forms as before at the upper interface and this one leads to failure. It is to be underlined that for all considered thicknesses of the adhesive, although the state of stress is different, the crack generated by XFEM remains at the interface, may propagates along it, but does not, ever, penetrate

the adherend. The XFEM propagating crack will never turn back into the adhesive if the interface is reached. Damage growth remains at the interface and is governed by CZM.

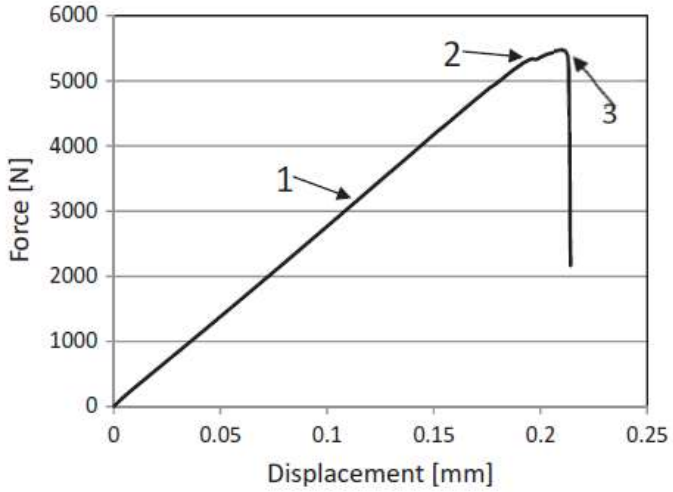

Figure 21 - Force–displacement curve for the given geometry [45]

.

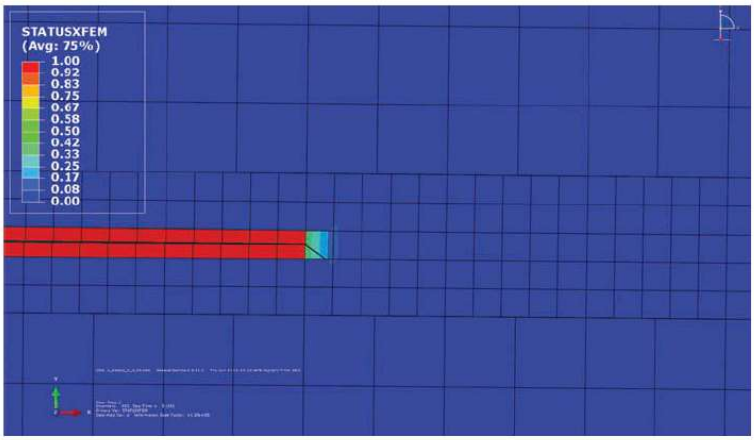

Figure 22 - Crack initiation in the first adhesive element by XFEM [51].

The main objective of this work is to evaluate the capabilities and limitations of using the current implementations of cohesive zone modelling or extended finite element modelling available in Abaqus® to simulate the behavior and strength of a single lap adhesively bonded joint. An initial delamination of same length is induced in the adhesive of three different thicknesses as to initiate crack propagation through XFEM. Depending on the initial position of the delamination, the crack trajectory is influenced by the local state of stress and may be linear or slightly turning following the principle

of local symmetry and reaching or not the lower interface. This situation is in conjunction with the formation by CZM of another delamination at one or both interfaces between the adhesive and the adherends. The crack formed at the upper interface propagates and thus the single lap joint fails. The use of the combined methods of simulation in Abaqus® proved to be successful if they are used simultaneously. The use of XFEM is nicely completed with CZM by propagating cracks along the interface, but an interface cohesive crack cannot turn back into the adhesive by using XFEM.

Article -2

The Cohesive Zone Modelling (CZM) and eXtended Finite Element Modelling (XFEM) is not yet widely applied and studied for the Cohesive and XFEM evaluation of adhesive failure for dissimilar single-lap joints. The work of Stuparu et al. [57] Nonetheless, few research works are available that address this topic. Experiments have shown that fracture energy can depend on mode mixite, as shown by Cao and Evans, Wang and Suo, Liechti and Chai. They concluded that there is no general agreement about the test suitability for mixed-mode fracture assessment of adhesive joints [57].

Before the physical crack is formed, these two surfaces are held together by traction within a cohesive zone. A cohesive law is also denoted a traction-separation law. The cohesive zone modelling approach has emerged as a powerful analytical tool for nonlinear fracture processes. Cohesive zone models have particularly been used to analyze composite delamination problems. Most damage models, such as the Progressive Damage Model for Composites provided in Abaqus® and typical cohesive elements as presented by Camanho et al [57].

The recently developed eXtended Finite Element Method is an extension of the FEM, and its fundamental features were described by Belytschko and Black, based on the idea of partition of unity presented by Melenk and Babuska, which consists on local enrichment functions for the nodal displacements to model crack growth and separation between crack faces. As the crack tip changes its position and path due to loading conditions, the XFEM algorithm creates the necessary enrichment functions for the nodal points of the finite elements around the crack path/tip. XFEM excels in simulating crack onset and growth along an arbitrary path without the requirement of the mesh to match the geometry of the discontinuities neither remeshing near the crack as done by Campilho et al. CZM has a strong intrinsic limitation since cohesive elements to simulate damage growth must be placed at the growth lines where damage is supposed to occur [57].

The digital image correlation method has inspired several researchers for CZM identification and to analyze the strength of lap-joints. When dealing with classical CZM based on DIC techniques, researches are limited to an identification of the cohesive parameters when the cohesive law is a priori fully or partly given, and/or for predefined crack paths or pre-cracked samples. Only as examples, Valoroso and Fedele identified the mode I parameters of a cohesive zone model for the analysis of adhesive joints and

Shen and Paulino provided a full-field DIC algorithm to compute the smooth and continuous displacement field, which is then used as input to a finite element model for inverse analysis through an optimization procedure to compute the cohesive properties of a ductile adhesive. Proposed a CZM evaluation based on DIC full field measurements [57].

As boundary conditions, one adherend was fixed at one end and on the other adherend a displacement was imposed horizontally at the opposite end. The two-dimensional meshing of the adhesive was done by using COH2D4 and CPE4 for adherends four-node linear plane strain elements. The adhesive layer was modelled with cohesive elements of 0.5 x 0.5 mm; same size of the elements was used for the adherends. The variation of stresses can be represented over the length of the adhesive overlap as a function of a normalized coordinate , having values from 0 to 1 [57]. Two moments were important: the initiation of damage in the first cohesive element and the moment of propagation of damage, considered as crack propagation. Fracture at bonded interfaces was modelled by defining a tie constraint between the adherend and the adhesive material. Only the initial stiffness value used for the cohesive elements at the interface was changed. The zero-thickness cohesive layer damage takes place according to the quadratic nominal stress criterion and the crack propagates using power low mixed mode fracture energy behavior. The active overlap length is L = 20 mm as before and at both ends symmetric 5 mm length delamination's were introduced in the middle of the adhesive layer of 1 mm thickness.

Table 3 - Some mechanical properties of the adhesive and the aluminum adherend used in simulations [57].

	Araldite® 2015	Aluminum
E(MPa)	1850	70000
G(MPa)	560	26340
$\varepsilon_n^0(\%)$	21.6	230
G_0^c	0.43	15
G_s^c	4.70	15

The adherends and adhesive were modelled with XFEM by using the plane strain element CPE4 of size 0.2x0.2 mm. For optimizing the calculations the adherends were modelled with the same elements by using the bias function from Abaqus® which enables the increase of the size of the elements from 0.2x0.2 mm to 0.2x1 mm as to be noticed in Figure 23, Hereby the behavior of the adhesive and the adherends is linear elastic. Zero-thickness cohesive elements are considered at the interface between the adhesive and the adherend. Failure in the cohesive elements at the interface through

delamination. After propagation the crack remains at the interface and doesn't move back to the adhesive, nor into the adherend [57]. Cohesive elements of zero thickness take over the increase of the delamination up to the failure of the joint.

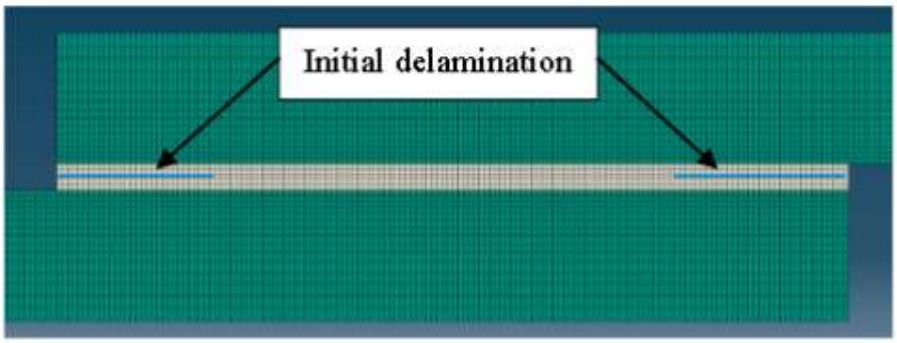

Figure 23 - XFEM-cohesive FE model [57]

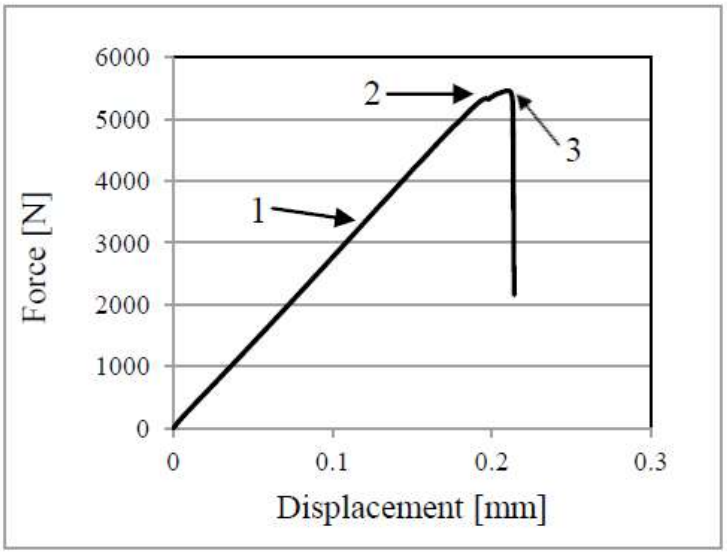

Figure 24 - Force-displacement curve for the given geometry [57].

The single-lap joint prepared for DIC measurements is shown in Figure 25. On the left side it is better noticed the uneven surface due to the wax of constant 0.5 mm thickness which filled the overlap for 5 mm on each side as to control the adhesive thickness. The relative displacements between the adherends were monitored in the overlap region and both peeling and shearing deformations were measured by using DIC. For each configuration out of the five performed tests only the representative one was chosen for further comparisons. The lateral surface of the single-lap joint was analyzed by using DIC. The ARAMIS 2M system was used to measure the deformations of the adhesive.

The relative displacements of the adherends are measured along the x axis as to investigate the peeling deformation and the corresponding strain, and along the y axis to monitor the shearing displacement of the adherends and the shearing strain.

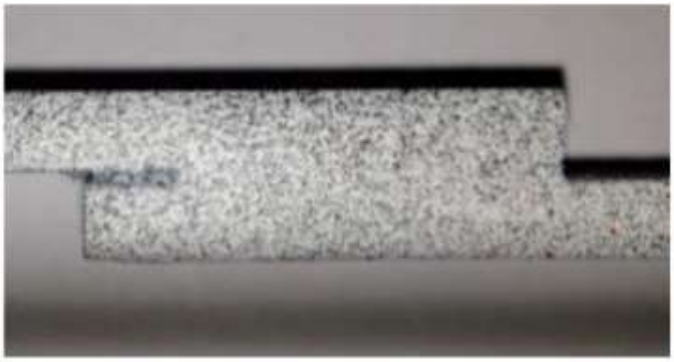

Figure 25 - Surface of a single-lap joint prepared for DIC measurements [57].

A maximum strain of about 9% was obtained at the lower extremity of the adhesive shortly before the failure of the joint. As getting towards the middle region of the overlap compression is produced in the adhesive, thus indicating the bending of the adherends. If the interface strength is assumed to be constant regardless the thickness of the carbon adherends it results that a lower stiffness will lead to a higher peeling force as the thickness of the adherend is decreased. During experiments the pull-out of the carbon fibers due to the interlaminar failure of the adherend was evident [57].

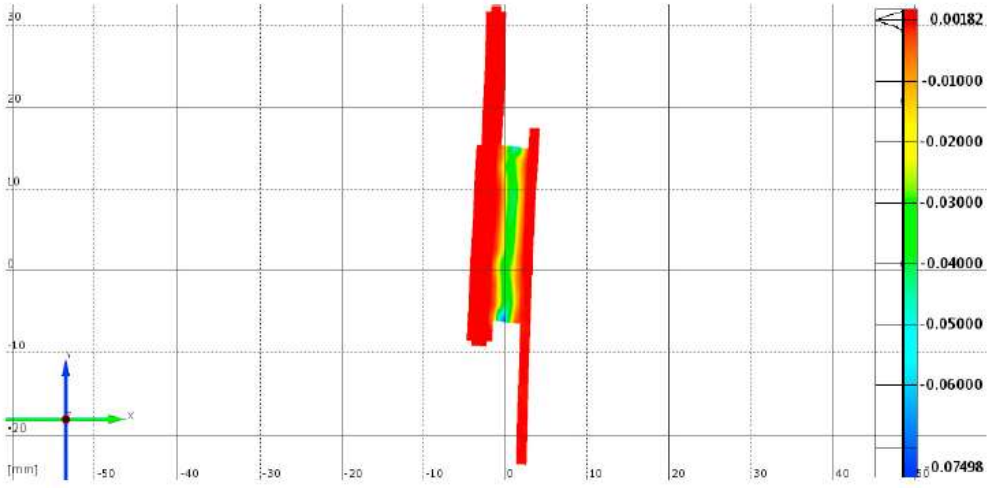

Figure 26 - Shearing strains in the adhesive for an aluminum-carbon joint [57].

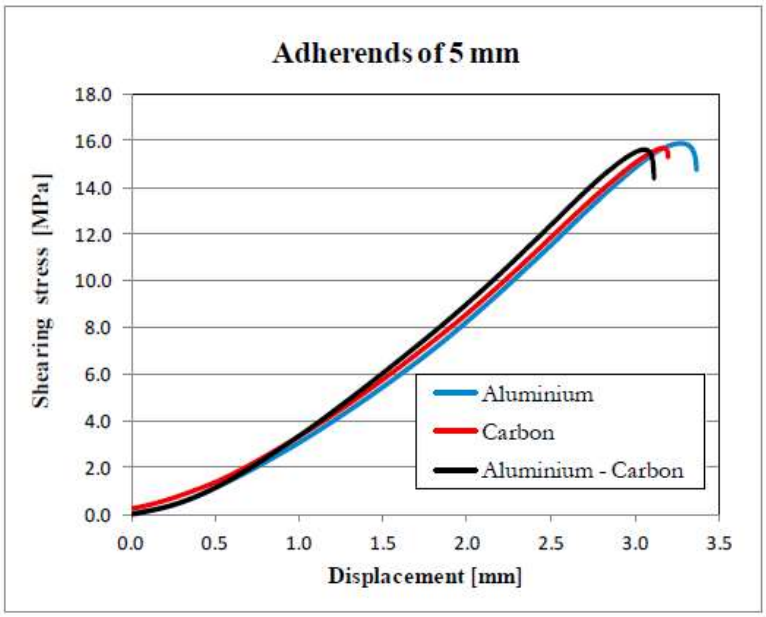

Figure 27 - Influence of material combinations for 5 mm adherend thickness [57].

Following the forces and displacements indicated by the testing machine the corresponding curves are shown in Figure 27. A slightly maximum displacement until failure is obtained for the aluminum-lap joint, as it has a more ductile behavior. The global values of the displacements of the single-lap joint measured by the displacement of the grips of the testing machine is at failure about 3 mm for the 5 mm adherends, and about the same value or less for the 3 mm adherends. Only the local relative displacements are reflecting the correct behavior of the adhesive. Local vertical displacements are measured with DIC over a virtual gage length of 50 mm which was emulated symmetrically with respect to the overlap length. The behavior of the joint obtained through numerical simulations indicates a stiffer assembly which fails sooner at about 9000 N. The experimental tests give a more ductile behavior of the dissimilar joint able to withstand a maximum force of about 8000 N with displacements at failure in between 0.35-0.55 mm. The maximum force keeps around 8000 N, but the displacements at failure are below 0.4 mm for all tests [57].

The dissimilar aluminum-carbon and carbon-carbon joints are of special interest as the numerical analyses of their strength overestimate the experimental evidence given by DIC. Digital image correlation measurements done in the immediate vicinity of the adhesive layer can provide correct information about the shearing and peeling deformations [57]. Dissimilar aluminum-carbon joints succeed to maintain the stiffness of the assembly as compared to the aluminum joints, but their strength is diminished by the pull-out and delamination of carbon fibers. For carbon-carbon single-lap joints both strength and stiffness are diminished as significant additional interlaminar damage compromises the integrity of the joint and leads to premature failure of the assembly.

Article – 3

The eXtended Finite Element Modelling (XFEM) is not yet widely applied and studied for the Numerical modelling of adhesively-bonded double-lap joints by the eXtended Finite Element method. The work of Santos and Campilho [58]Nonetheless, few research works are available that address this topic. Adhesive joints have been used in various application fields. The use of adhesive joints in industrial applications has been increasing in recent years because of the significant advantages offered compared to traditional joining methods such as welding, fastening and riveting [27]. The most common bonded joints are single and double-lap, and scarf joints. In single-lap joint the poor performance is caused by the joint eccentricity and respective deflection under load at the bonded region, which reflects on high through-thickness normal peak stresses at the overlap edges [59, 60].

Kinloch compared τxy stresses of single and double-lap, and scarf joints, between aluminum adherends. Two alternatives can be chosen for the analysis of adhesive joints: closed-form analyses and numerical methods [61]. The XFEM is also emerging as a method to predict the joints' behavior, although this has not yet been adequately studied for the application to adhesive joints [62]. Compared the CZM and XFEM models available in Abaqus® in which regards the strength prediction of single and double-lap bonded joints with aluminum adherends and a brittle adhesive, considering LO values between 5 and 20 mm. CZM were used to simulate damage propagation in the adhesive layer of single-lap joints. Which considered a hybrid CZM/XFEM approach to simulate single-lap joints between aluminum adherends.

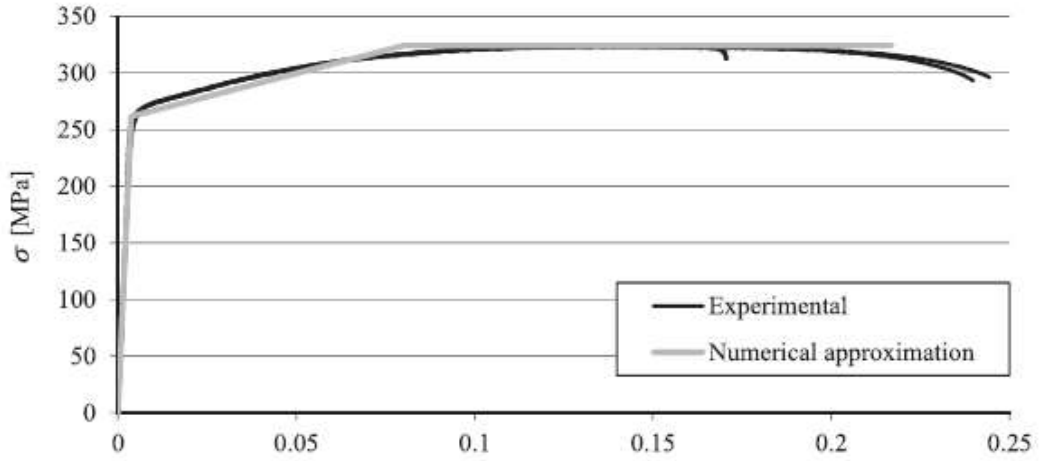

Figure 28 - Experimental and numerical σ-ε curves of the aluminum.

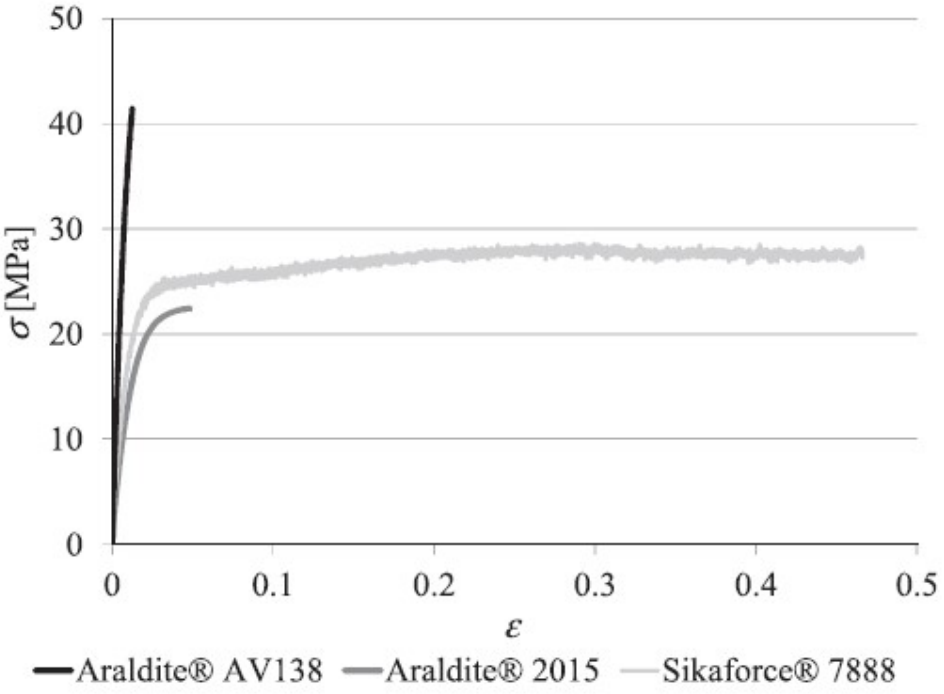

Figure 29 - Representative σ-ε curves of the three adhesives considered.

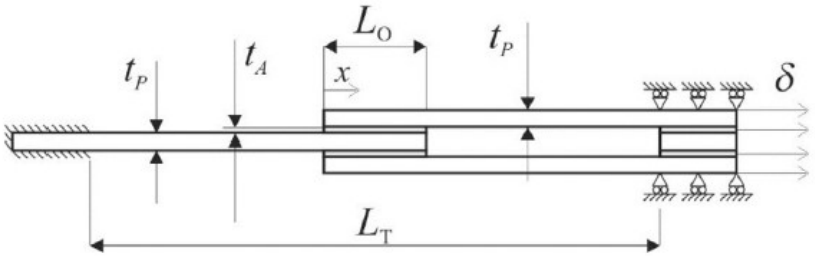

Figure 30 - Geometry and dimensions of the double-lap joints.

Bulk specimens were tested in a servo-hydraulic machine to obtain E, σy, σf and εf. The DCB test was selected to obtain GIC and the End-Notched Flexure test was used for the shear fracture toughness [63]. A dummy spacer was also bonded in-between the adherends at the specimen's side with double adherends, to facilitate alignment and gripping in the testing machine [64]. A total of 60 double-lap joint specimens were tested. All tests were carried out in a Shimadzu AG-X 100 electro-mechanical testing machine with a 100 kN load cell. Figure 31(a) shows the experimental setup with a L_O=25 mm specimen ready for testing, while Figure 31(b) details the dummy spacer at the double-ended side, to promote the alignment in the testing machine.

Table 4 - Properties of the adhesives Araldite® AV138, Araldite® 2015 and Sikaforce® 7888

Properties	Araldite® 2015	2015	7888
Young's modulus, E [GPa]	4.89 ± 0.81	1.85 ± 0.21	1.89 ± 0.81
Poisson's ratio, ν	0.35[a]	0.33[a]	0.33[a]
Tensile yield strength, σy [MPa]	36.49 ± 2.47	12.63 ± 0.61	13.20 ± 4.83
Tensile failure strength, σf [MPa]	39.45 ± 3.18	21.63 ± 1.61	28.60 ± 2.0
Tensile failure strain, εf [%]	1.21 ± 0.10	4.77 ± 0.15	43.0 ± 0.6
Shear modulus, G [GPa]	1.56 ± 0.01	0.56 ± 0.21	0.71b
Shear yield strength, τy [MPa]	25.1 ± 0.33	14.6 ± 1.3	-
Shear failure strength, τf [MPa]	30.2 ± 0.40	17.9 ± 1.8	20[a]
Shear failure strain, γf [%]	7.8 ± 0.7	43.9 ± 3.4	100[a]
Toughness in tension, GIC [N/mm]	0.20[c]	0.43 ± 0.02	1.18 ± 0.22
Toughness in shear, GIIC [N/mm]	0.38[c]	4.70 ± 0.34	8.72 ± 1.22

*a Manufacturer's data.
*b Estimated from Hooke's law.
*c Estimated in reference [20].

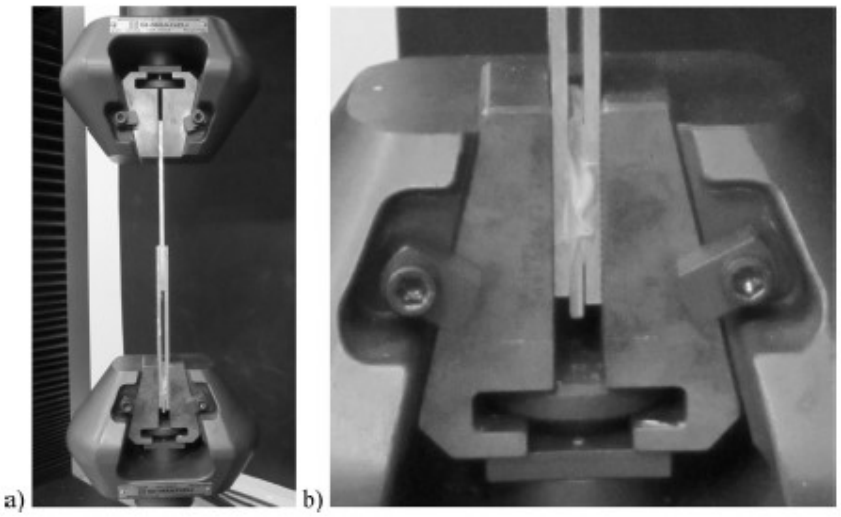

Figure 31 - Experimental double-lap joint testing setup (a) at gripping detail at the double-ended side, showing the dummy spacer (b).

These functions allow modelling the displacement jump between crack faces that occur during the propagation of a crack. Six crack initiation criteria are available in ABAQUS®. Crack growth for the MAXPS and MAXPE criteria is software defined as orthogonal to the maximum principal stress/strain direction. For the MAXS, MAXE, QUADS and QUADE

criteria the user can select between horizontal or vertical crack growth. The second term between brackets, H(x)ai, is only active in the nodes for which any relating shape function is cut by the crack and can be expressed by the product of the nodal enriched degree of freedom vector including the mentioned nodes, ai, with the associated discontinuous shape function, H(x), across the crack surfaces.

The method is based on the establishment of phantom nodes that subdivide elements cut by a crack and simulate separation between the newly created sub-elements. Propagation of a crack along an arbitrary path is made possible using these phantom nodes that initially have the same coordinates than the real nodes and that are completely constrained to the real nodes up to damage initiation. After being crossed by a crack, the element is partitioned in two subdomains. Thus, the crack size increment for a given crack orientation is equal to the distance between the cracked element's edges.

Inspection to the failed specimens after testing revealed that most joint configurations suffered cohesive failures in the adhesive layer. The bonded joints with the Araldite® 2015 and L_O=25 mm failed by cohesive failure of the adhesive induced by extensive adherend plasticization. Stress distributions along the adhesive layer highly influence Pm of bonded joints, especially when using brittle adhesives. In which regards the geometry, the ideal solution to promote flat stress distributions along the bond line is to use scarf joints, whose tapering effect of the adherends at the bonded region minimizes the differential deformation effect, largely visible in single or double-lap joints, for example. The joint materials also affect stress distributions by a significant amount.

The stress plots concern the joints bonded with the Araldite® 2015, although generically they are valid for all three adhesives. Double-lap joints cut the transverse adherend flexure of single-lap joints arising due to the asymmetric transmission of loads between adherends, since the loads applied to double-lap joints are symmetric. According to Shishesaz and Bavi , normalized σy peel peak stresses for the double-lap joint are smaller than for equivalent single-lap joints for all L_O values because of the significant reduction in the joint deflection. τxy stresses show the typical evolution for bonded joints, consisting of a lightly stress inner portion with growth towards the overlap ends. In double-lap joints, the stress profiles are not symmetric and are higher at the outer overlap end than at the opposite one.

These two features resulted in the behavior depicted in for the joints bonded with the Araldite® AV138, i.e., reduced Pm improvement with L_O, since the adhesive was not able to deal with the maximum peak stresses because of the absence of plasticization of the adhesive layer. The joints bonded with the Sikaforce® 7888 showed significantly better results than the other two adhesives for L_O=12.

Figure 32 - Detail at the overlap edge showing failure initiation with the MAXS, MAXE, QUADS and QUADE criteria (a) and MAXPS and MAXPE criteria (b).

Figure 32 - gives representative examples of failure initiation with the MAXS, MAXE, QUADS and QUADE criteria, which occurred and propagated along the adhesive length, and MAXPS and MAXPE criteria, whose cracks propagated orthogonally to the maximum principal stresses/strains due to the intrinsic formulation of these criteria, resulting in damage growth towards the adherends. The inadequacy of these criteria is related to damage and failure in the adhesive layer being governed by the limit stresses of the adhesive layer instead of its deformations. For the MAXPS and MAXPE criteria, crack propagation along the adhesive layer was not possible to accomplish because of the crack growth direction being governed by the maximum principal stress, which resulted in crack growth towards the adherends soon after cracking initiated in the adhesive layer. As a result, Pm was reached, as an approximation, when crack initiates in the adhesive layer, which clearly under predicted the results. In conclusion, irrespectively of the adhesive's ductility, the MAXS and QUADS initiation criteria provided results close to the experiments, while the other criteria were not adequate for application to bonded joints: the QUADE and MAXE criteria over predict the results, the MAXPS criterion under predicts the results, and the MAXPE criterion, depending on the adhesive's ductility, ranges from under to over predictions.

The numerical stress analysis was valuable in understanding the differences in behavior between adhesives. The XFEM analysis revealed that it is possible to accurately predict the joints' strength using the MAXS and QUADS damage initiation criteria, with a maximum deviation of −15.0% for the adhesive Sikaforce® 7888 and L_O=12. For the adhesive Araldite® AV138, the MAXE and QUADE criteria largely overestimated the

experimental values of Pm, reaching a difference of 50.2% and 45.1%. These criteria also showed a maximum deviation of approximately 100% and 55.8% for the adhesives Araldite® 2015 and Sikaforce® 7888, respectively. For ductile adhesives, the influence of diminishes up to having virtually no influence on Pm for the most ductile adhesive.

THESIS DEVELOPMENT

3 THESIS DEVELOPMENT

3.1 Experimental work

This section addresses the experimental part of the thesis, where all material properties, joint geometry, manufacturing process, results and comments are presented. The experimental work described in this thesis was previously executed by de Sousa [2] (joints with the adhesives Araldite® AV138 and Araldite® 2015) and by Carvalho [65] (joints with the adhesive Sikaforce®7752). The work carried out in this section consisted of the raw data analysis from the tests, respective treatment and analysis for later comparison with the numerical results.

3.1.1 Materials

The next subsections concern the materials used to perform the experimental work, and their most relevant mechanical properties useful for the experimental and numerical analyses.

3.1.1.1 Adherends

The material used as adherend in all joints was the high strength and ductile aluminum alloy AW6082-T651. This alloy is obtained through artificial ageing at 180°C [66], and it was selected not only because of its good mechanical properties, but also due to the vast structural applications under different extruded or rolled shapes. This aluminum alloy was characterized in the work of Campilho et al. [55], where the most relevant mechanical properties presented in Table 5 were defined.

The aluminum σ-ε curves presented in Figure 33 were experimentally obtained according to the ASTM-E8M-04 standard [55]. The numerical approximation used in the numerical simulations is also represented.

Table 5 - Relevant mechanical properties of the aluminum alloy AW6082-T651 [55]

Properties	Aluminum 6082-T651
Tensile failure stress, σf [MPa]	324.00±0.16
Young´s modulus, E [GPa]	70.07±0.83
Tensile yield stress, σy [MPa]	261.67±7.65
Tensile Failure strain, εf [%]	21.70±4.24
Poisson´s ratio, ν	0.3*

* Manufacturer´s value

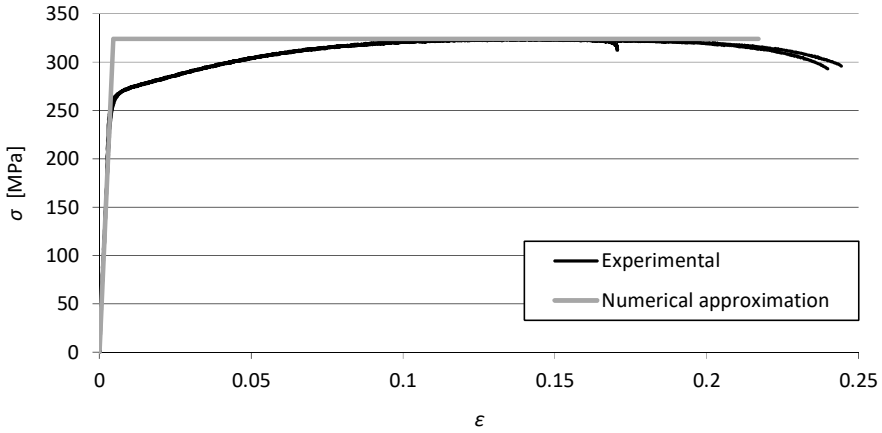

Figure 33 – Aluminum *σ-ε* curves and numerical approximation [55]

3.1.1.2 Adhesives

The three adhesives tested were all two part (resin + hardener), two epoxy (Araldite® AV138 and Araldite® 2015) and one polyurethane (Sikaforce®7752). They all present a low viscosity, which promotes an easier application on the adherends.

3.1.1.2.1 Araldite® AV138

The structural epoxy adhesive Araldite® AV138 is manufactured by HUNTSMAN ADVANCED MATERIALS. It has a brittle behavior but high strength (Figure 34), and it is suitable to join miscellaneous materials like metals, composites, polymers [67].

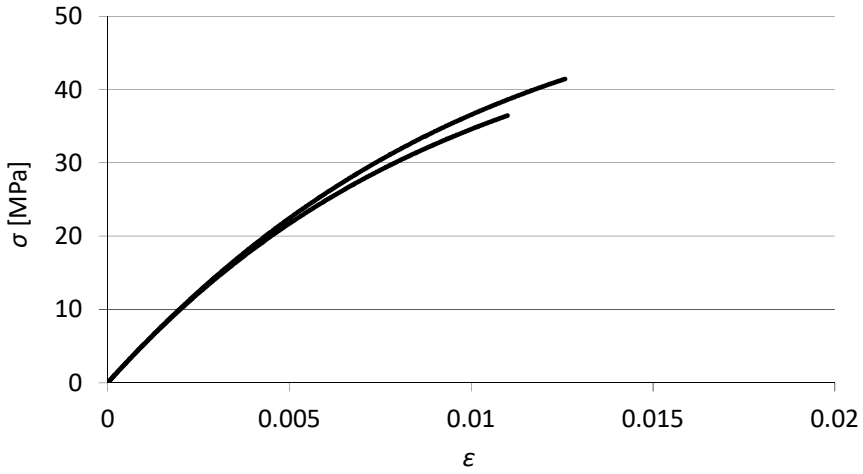

Figure 34 –*σ-ε* curves estimated by the bulk specimens of the Adhesive Araldite® AV138 [55]

This adhesive is provided in two recipients (Figure 35), one with a thermoset resin AV138 and other with the hardener HV998, and the mixture is performed manually after weighting in the correct proportion. The mixture proportion is 100 g of resin for 40 g of hardener, with an accuracy of ±5%. This adhesive is a thixotropic gap filling paste with low out gassing and volatile loss, and it cures at temperatures down to 5°C.

Figure 35 - Adhesive Araldite® AV138 [2]

Table 6 - Properties of the Araldite® AV138 [68]

Properties	Araldite® AV138
Young´s modulus, E [GPa]	4.89±0.81
Poisson´s ratio, ν	0.35*
Tensile yield stress, σy [MPa]	36.49±2.47
Tensile failure stress, σf [MPa]	39.45±3.18
Tensile failure strain, εf [%]	1.21±0.10
Shear modulus, G [GPa]	1.56±0.01
Shear yield strength, τy [MPa]	25.10±0.33
Shear failure strength, τf [MPa]	30.20±0.40
Shear failure strain, γf [%]	7.80±0.70
Toughness in tension, GIc [N/mm]	0.20**
Toughness in shear GIIc [N/mm]	0.38**

* - Manufacturer´s value

** - Estimated in reference [55].

3.1.1.2.2 Araldite® 2015

The adhesive Araldite® 2015 is also manufactured by HUNTSMAN ADVANCED MATERIALS, and it is equally a two-part structural epoxy adhesive. It shows a smaller ultimate strength than the earlier adhesive and has intermediate ductility, allowing large plastic flow prior to failure. A redistribution of stresses occurs at stress concentrated regions which usually take place in the edges of the overlap ends of bonded joints. Figure 36 shows the cartridges incorporating mixers for application of the adhesive.

Figure 36 – Adhesive Araldite® 2015 [2]

The bond strength and durability of joints with this adhesive are dependent on an adequate surface treatment. At least, surfaces to be bonded should be clean with solvent wiping (acetone). However, surface preparation may also include a combination of mechanical abrading, chemical cleaning and acid etching [20].

The analysis of Figure 37 and, which present the σ-ε curves and mechanical properties, respectively, shows that the shear failure strain is six times higher than that of the earlier adhesive. However, the tensile and shear failure strength of the Araldite® AV138 is twice the value of the Araldite® 2015. Thus, this ductile adhesive allow stress distribution at the stress concentration area, typically at the edges of the overlap due to joint asymmetry and to the adherends' differential deformation [69].

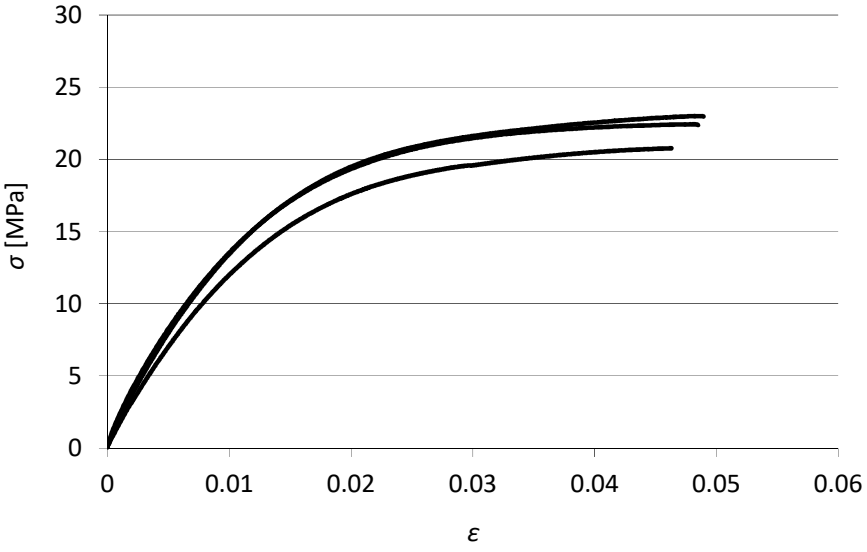

Figure 37 – σ-ε curves estimated by the bulk specimens of the Araldite® 2015 [6]

Table 7 - Properties of the Araldite® 2015 [6]

Properties	Araldite® 2015
Young´s modulus, E [GPa]	1.85±0.21
Poisson´s ratio, v	0.33*
Tensile yield strength, σ_y [MPa]	12.63±0.61
Tensile failure strength, σ_f [MPa]	21.63±1.61
Tensile failure strain, ε_f [%]	4.77±0.15
Shear modulus, G [GPa]	0.56±0.21
Shear yield strength, τ_y [MPa]	14.60±1.3
Shear failure strength, τ_f [MPa]	17.9±1.8
Shear failure strain, γ_f [%]	43.9±3.4
Toughness in tension, G_{Ic} [N/mm]	0.43±0.02
Toughness in shear G_{IIc} [N/mm]	4.70±0.34

* - Manufacturer´s value

3.1.1.2.3 Sikaforce® 7752

The structural polyurethane adhesive Sikaforce®7752 is manufactured by Sika® and it is provided in two parts (Figure 38). The mixing proportion is 100 g of resin for 20 g of hardener.

Figure 38 - Adhesive Sikaforce®7752 [65]

It is the most ductile of the three adhesives, as depicted in the σ-ε curves of Figure 39. Analyzing the mechanical properties presented in Table 8, the adhesive Sikaforce®7752 has the lowest tensile and shear tensile strength. However, it has high ductility, which allows large plastic flow prior to failure, resulting in a higher joint strength [70].

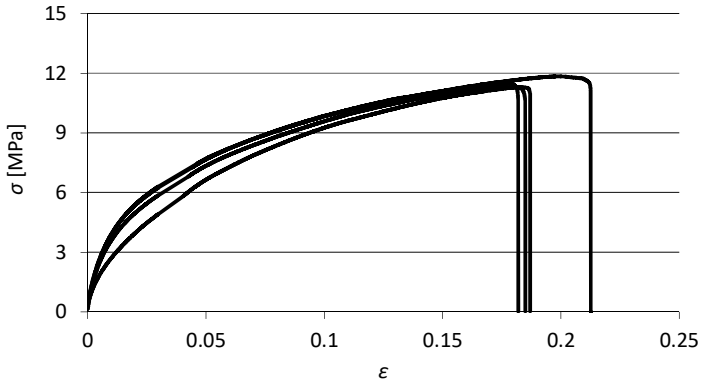

Figure 39 - σ-ε curves estimated by the bulk specimens of the Sikaforce®7752 [70]

Table 8 - Properties of the Sikaforce®7752 [70]

Properties	Sikaforce® 7752
Young´s modulus, E [GPa]	0.49±0.09
Poisson´s ratio, ν	0.30*
Tensile yield strength, σ_y [MPa]	3.24±0.48
Tensile failure strength, σ_f [MPa]	11.48±0.25
Tensile failure strain, ε_f [%]	19.18±1.40
Shear modulus, G [GPa]	0.19±0.01
Shear yield strength, τ_y [MPa]	5.16±1.14
Shear failure strength, τ_f [MPa]	10.17±0.64
Shear failure strain, γ_f [%]	54.82±6.38
Toughness in tension, G_{Ic} [N/mm]	2.36±0.17
Toughness in shear G_{IIc} [N/mm]	5.41±0.47

* - Manufacturer´s value

3.1.2 Joint geometry

The SLJ & DLJ geometry and characteristic dimensions are presented in Figure 40 and Table 9. All the specimens have the same geometric configuration varying only the L_O.

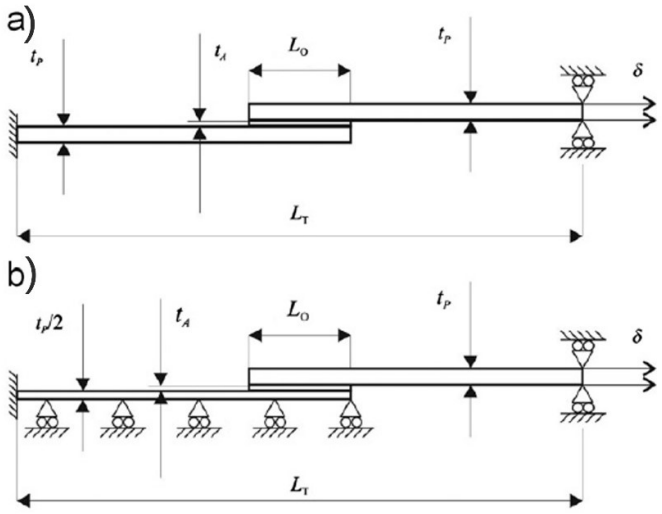

Figure 40 Geometry and dimensions of the single-lap joint (a) and double-lap joint (b).

Table 9 - Specimen dimensions of SLJ and DLJ (mm)

Designation	Dimension
Length between grips (L_T)	170
Overlap length (L_o)	12.5/25/37.5/50
Adherend thickness (t_P)	3
Adhesive thickness (t_A)	0.2
Specimen width (b)	25

3.1.3 Adhesive joint fabrication

The adherends were already provided in their final dimensions. Sixty adherends were necessary to obtain 5 specimens per joint configuration. The first step (Figure 41) consists of roughening, by manual abrasion, the surfaces to bond and cleaning it with acetone to supply oxide removal and improve the bonding process.

a) b)

Figure 41 - Surface preparation (a) and acetone cleaning (b) [2]

The surface preparation removed from the adherends' surface foreign materials such as dirt, oil, moisture and weak oxide layers. Otherwise, the adhesive will bond to these weak boundary layers rather than the adherend.

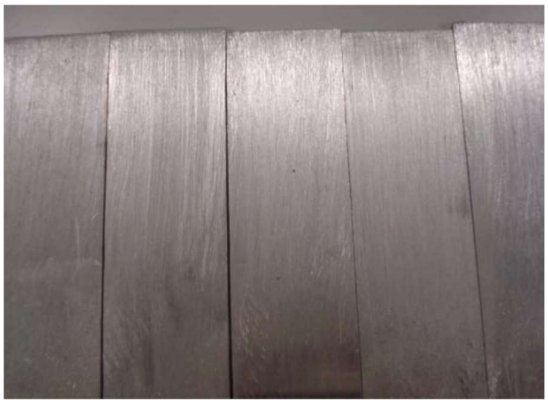

Figure 42 – Adherends' appearance after surface cleaning [2]

The next step consisted of the preparation to apply the adhesive and assemble the joints. With this purpose, the adherends were fixed in an apparatus for the correct alignment (Figure 43), using a calibrated fishing line with 0.2 mm placed under the upper adherend to ensure a constant adhesive thickness (t_A), as presented in Figure 44.

Figure 43 – Adherends fixing and alignment [2]

Figure 44 - Adherend with calibrated fishing line [2]

Following, the adhesive was applied on the bonding surfaces. The curing process was accomplished using pressure grips to guarantee the adherends' alignment (Figure 45). Tabs were glued at the specimens' edges to ensure a correct alignment in the testing machine.

Figure 45 - Grip fixing [2]

The joints were left to cure at room temperature for one week to assure complete curing. To supply square edges at the overlap region, the excess adhesive was removed using a grindstone in a vertical drill (Figure 46). This is important because the adhesive excess influences the joint strength, which theoretically and in numerical models does not exist.

Figure 46 - Adhesive excess removal [65]

3.1.4 Experimental testing

To perform the experimental tests, a Shimadzu® AG-X 100 (Figure 47) testing machine with a 100 kN load cell was used, considering a distance between grips of 170 mm and room temperature. The displacement rate was 1 mm/min.

a) b)

Figure 47 - Shimadzu testing machine (a) and adherend fixation (b) [2]

3.1.5 Results

In this section the P-δ curves obtained from the experimental tests, the failure modes and the P_m are presented. A brief analysis of the joint strength is discussed about the three adhesives

3.1.5.1 P-δ curves

The experimental results of few joints were markedly different from the average behavior and, therefore, those results were excluded from the analysis.

3.1.5.1.1 Single Lap joints

In Figure 48, Figure 49, Figure 50, the curves P-δ for various SLJ overlap lengths are shown for the Araldite® AV138, Araldite® 2015 and Sikaforce® 7752 adhesives, respectively. n these graphs, it is possible to check the linear behavior of the adhesive joints up to the breaking for the three selected adhesives, and the displacement to the joint of the Araldite® AV138 is smaller, because this adhesive is a fragile adhesive. In the case of Araldite® 2015, given the its higher ductility allows plasticization, thus it is possible to reach higher δ values.

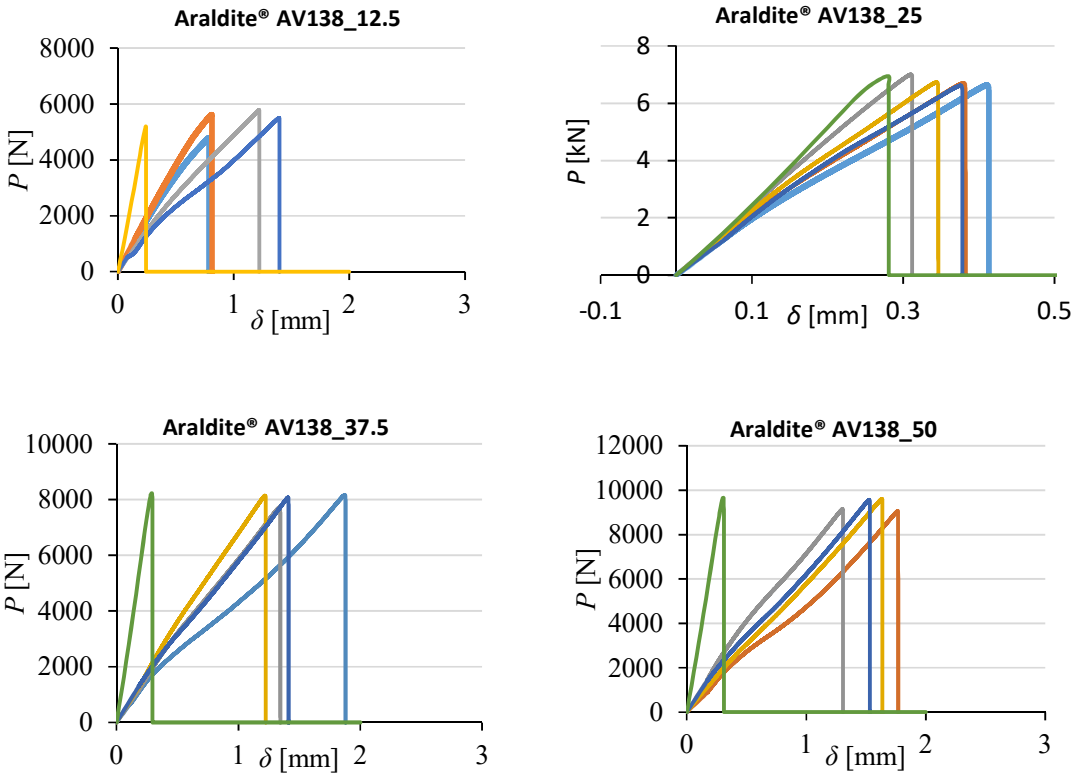

Figure 48 - P-δ curves for the single-lap joints bonded with the Araldite® AV138 and L_O=12.5, L_O= 25, L_O= 37.5, L_O= 50.

The following tables (Table 10, Table 11, Table 12) show the average P_m for each adhesive and L_O, respective standard deviation, and the percentile P_m increase between a joint with a given L_O and the earlier one.

Table 10 - Pm and deviation for the single-lap joints bonded with the Araldite® AV138

L_O (mm)	12.5	25	37.5	50
P_m average (N)	5421.66	6738.18	8016.33	9342.21
Standard deviation	439.37	155.4	206.3	278.5
P_m increase (%)	-	24.3	19.0	16.5

Table 10 shows that P_m increases with L_O, but not steadily, since the P_m improvement is not too significant between L_O=25 and 50 mm. P_m overall increases by only 59.08% from L_O=12.5 to 50 mm. due to the brittleness of the adhesive. This characteristic does not allow the adhesive's plastification and, therefore, failure occurs when the tensile peak is reached [71].

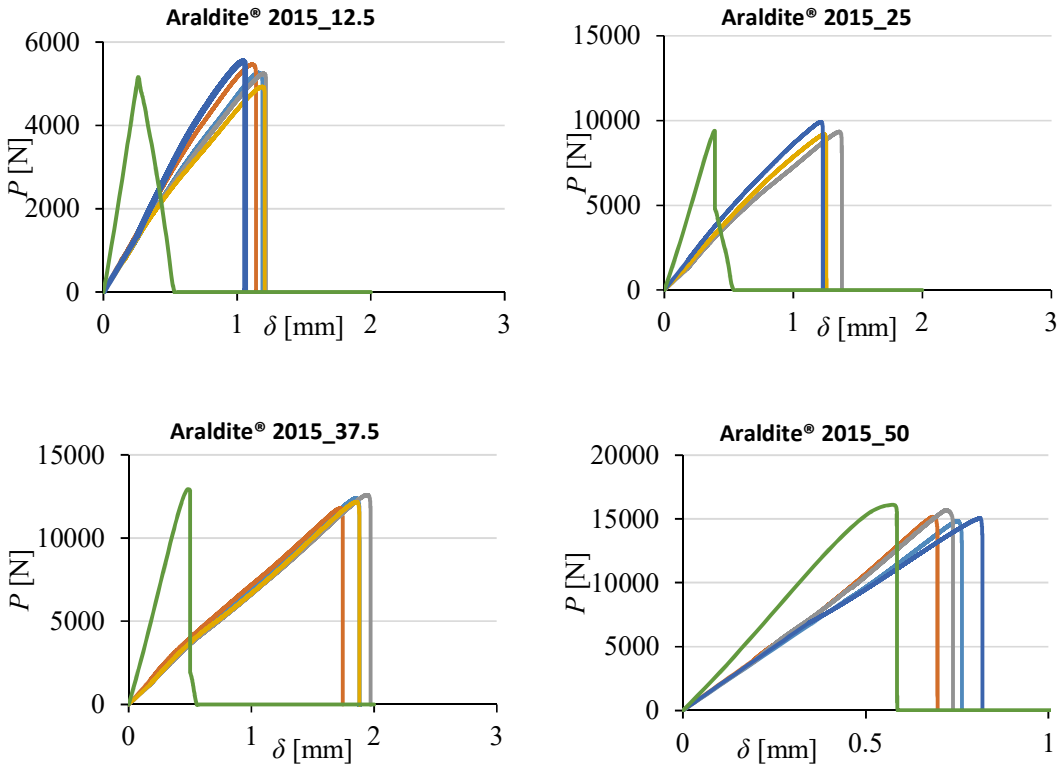

Figure 49 - P-δ curves for the single-lap joints bonded with the Araldite® 2015 and L_O=12.5, L_O= 25, L_O= 37.5, L_O= 50.

The *P-δ* curves of the adhesive Araldite® 2015 depicted in Figure 49 present a linear behavior up to failure, as the earlier adhesive, but with smaller fluctuations on the displacement at P_m. There is also a good reproducibility regarding P_m.

Regarding Table 11for the adhesive Araldite® 2015, P_m substantially increases with L_O. The overall increase is 142.29% from L_O=12.5 to 50 mm. The reason of such difference between this and the previous adhesive is the plasticity that the Araldite® 2015 possesses, enabling stress redistribution before P_m is reached [71, 72].

Table 11 - Pm and deviation for the single-lap joints bonded with the adhesive Araldite® 2015

L_O (mm)	12.5	25	37.5	50
P_m average (N)	5287.83	9480.68	12235.22	15182.21
Standard deviation	237.21	386.6	343.9	370.4
P_m increase (%)	-	79.3	29.1	24.1

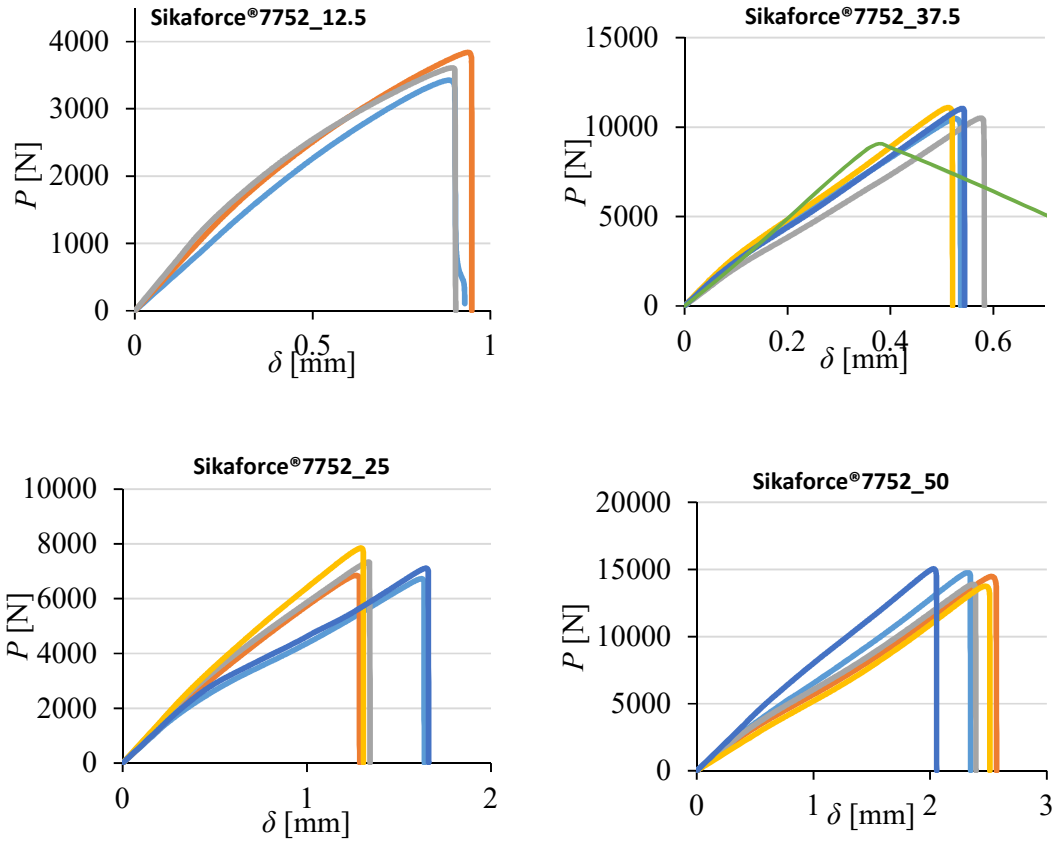

Figure 50 - P-δ curves for the single-lap joints bonded with the Sikaforce® 7752 and L_O=12.5, L_O= 25, L_O= 37.5, L_O= 50.

Figure 50 shows the *P-δ* curves of the adhesive Sikaforce® 7752, which present a nonlinear behavior before reaching P_m, due to the high adhesive´s plasticity. Deviations on the plastic stiffness in the beginning of experimentation can be observed. However, the plots present good reproducibility regarding the stiffness and P_m.

Table 12 - Pm and deviation for the single-lap joints bonded with the adhesive Sikaforce® 7752

L_O (mm)	12.5	25	37.5	50
P_m average (N)	3625.55	7175.51	10774.10	14383.65
Standard deviation	206.8	445.5	334.1	553.6
P_m increase (%)	-	97.9	50.2	33.5

The P_m evolution with L_O is the highest of the three adhesives (Table 12). This is since the Sikaforce® 7752 is the most ductile of all three adhesives, which results in failure under global yielding conditions [73]. The overall P_m increase is 263.99% from L_O=12.5 to 50 mm.

3.1.5.1.2 Double Lap joints

In Figure 51, Figure 52 and Figure 53, examples of P-δ curves for various DLJ overlap lengths are shown for the Araldite® AV138, Araldite®2015 and Sikaforce®7752 adhesives respectively. For joints with Araldite®AV138 and Sikaforce®7752 adhesives, they keep a linear behavior until rupture. In addition to the joint with Araldite® 2015 (L_0 = 37.5 mm), it shows a non-linear behavior due to the adhesiveness of the adhesive, which supports higher loads, and so, causing the substrates to be classified. Table 13 shows the Pm and deviation for the double-lap joints bonded with the Araldite® AV138.

Table 13 - Pm and deviation for the double-lap joints bonded with the Araldite® AV138

L_O (mm)	12.5	25	37.5	50
P_m average (N)	3625.55	7175.51	10774.10	14383.65
Standard deviation	206.8	445.5	334.1	553.6
P_m increase (%)	-	97.9	50.2	33.5

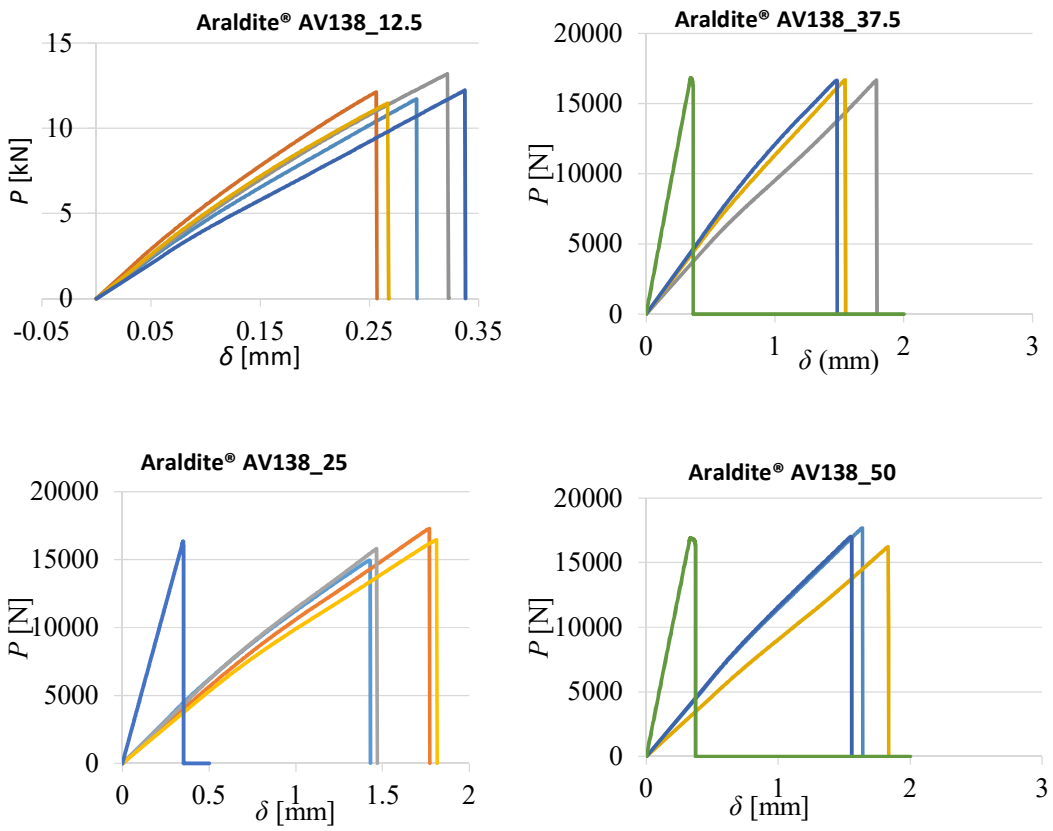

Figure 51 - P-δ curves for the double-lap joints bonded with the Araldite® AV138 and L_O=12.5, L_O= 25, L_O= 37.5, L_O= 50.

Table 14 - Pm and deviation for the single-lap joints bonded with the Araldite® 2015

L_O (mm)	12.5	25	37.5	50
P_m average (N)	3625.55	7175.51	10774.10	14383.65
Standard deviation	206.8	445.5	334.1	553.6
P_m increase (%)	-	97.9	50.2	33.5

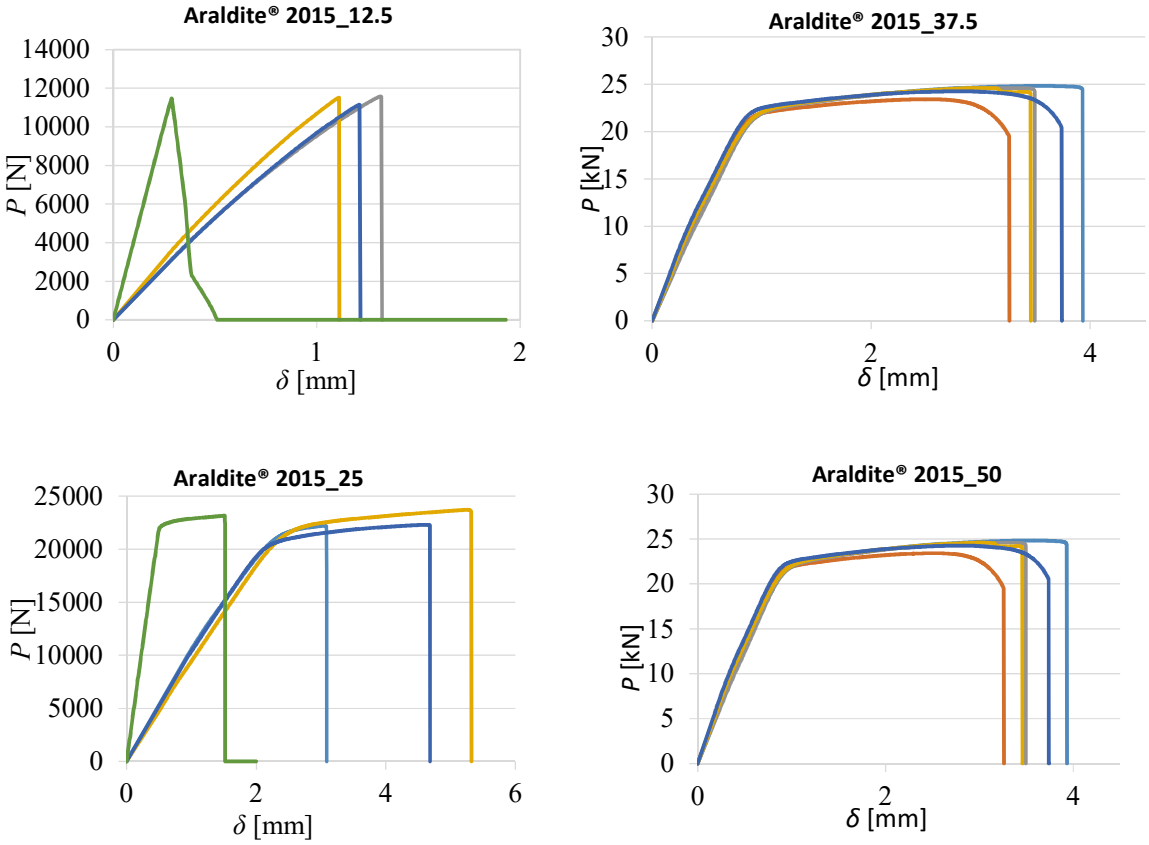

Figure 52 - P-δ curves for the double-lap joints bonded with the Araldite® 2015 and L_O=12.5, L_O= 25, L_O= 37.5, L_O= 50.

Table 15 - Pm and deviation for the double-lap joints bonded with the adhesive Sikaforce® 7752

L_O (mm)	12.5	25	37.5	50
P_m average (N)	3625.55	7175.51	10774.10	14383.65
Standard deviation	206.8	445.5	334.1	553.6
P_m increase (%)	-	97.9	50.2	33.5

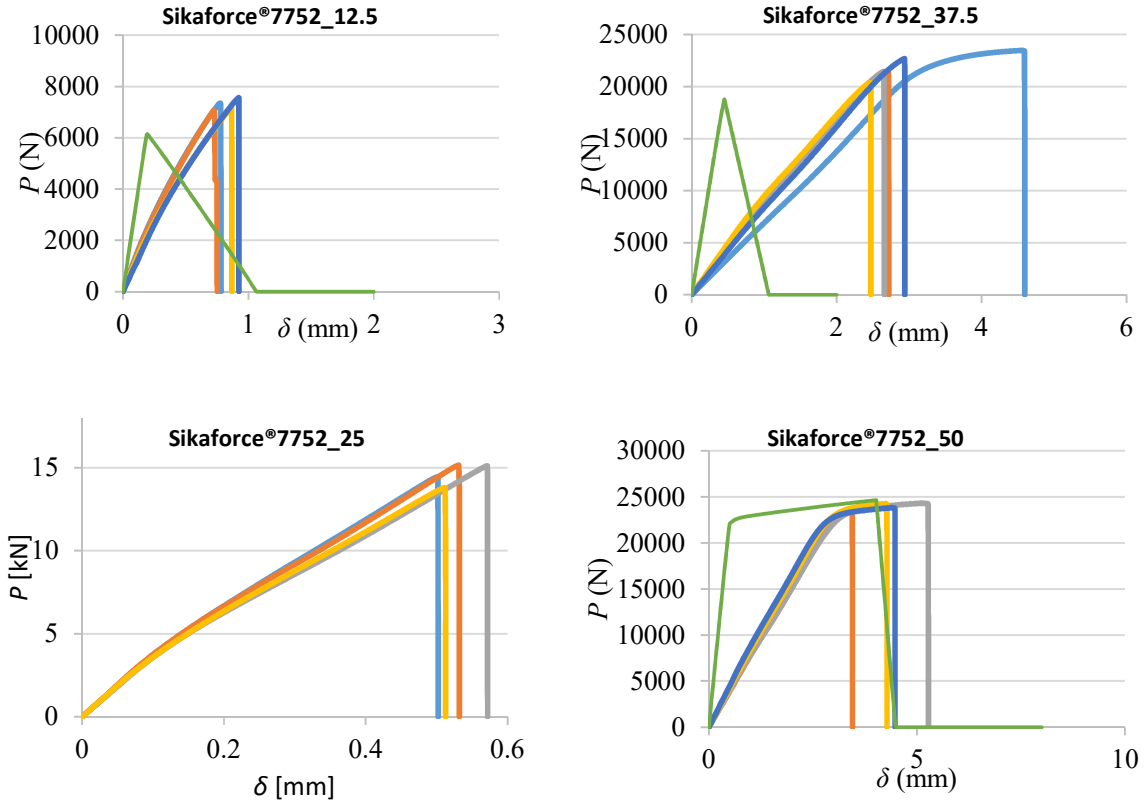

Figure 53 - P-δ curves for the double-lap joints bonded with the Sikaforce® 7752 and LO=12.5, LO= 25, LO= 37.5, LO= 50

3.1.5.2 Failure modes

3.1.5.2.1 Failure modes of Single-lap joints

The use of different adhesives and values of L_O may induce different failure modes. The failure modes of all joint configurations are presented in this subsection.

The failure modes of the specimens bonded with the adhesive Araldite® AV138 are presented in Figure 54 (a typical failure for each value of L_O is considered). All failures with this adhesive were cohesive in the adhesive layer. The obvious lack of adhesive at the bonded area is due to failure taking place nearby the interface between the adhesive layer and the adherend.

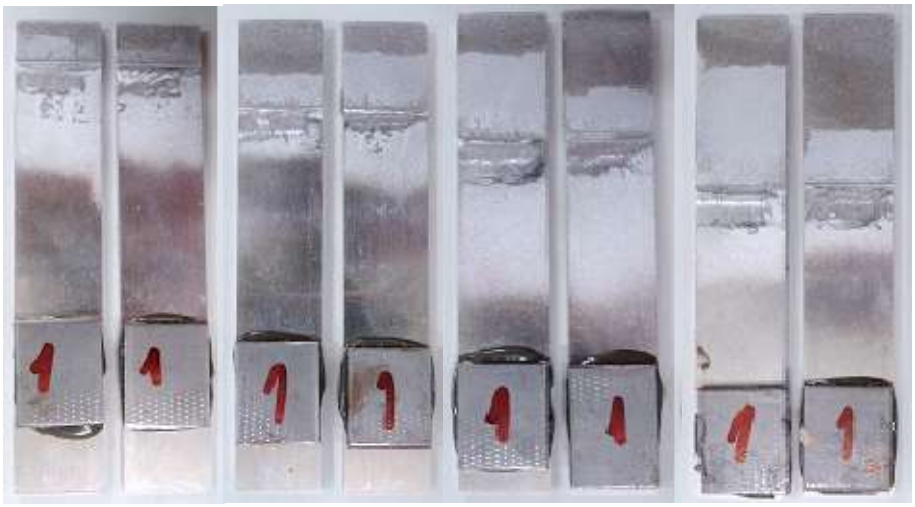

a) b) c) d)

Figure 54 - Failure modes of the specimens bonded with the adhesive Araldite ® AV138, and L_O=12.5 (a), 25 (b), 37.5 (c) and 50 mm (d)

The failure modes of the specimens bonded with the adhesive Araldite® 2015 are presented in Figure 55. A cohesive failure is seen for all specimens at the adhesive mid-thickness. This failure mode denotes an efficient bonding between the adherends and adhesive.

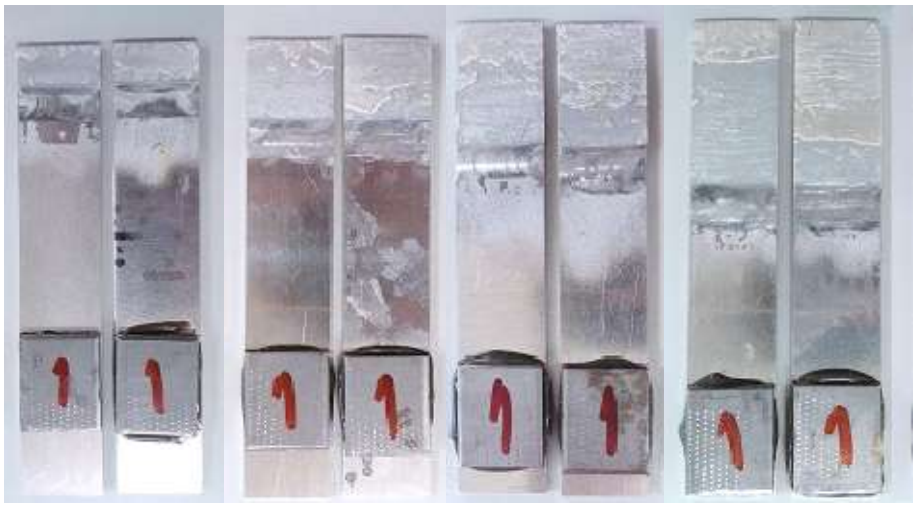

a) b) c) d)

Figure 55 - Failure modes of the specimens bonded with the adhesive Araldite ® 2015, and L_O=12.5 (a), 25 (b), 37.5 (c) and 50 mm (d)

Figure 56 shows the failure modes of the specimens bonded with the adhesive Sikaforce® 7752. The failures are adhesive; however, with careful inspection, adhesive can be found in both adherends, thus corresponding to a cohesive failure.

a) b) c) d)

Figure 56 - Failure modes of the specimens bonded with the adhesive Sikaforce®7752, and L_O=12.5 (a), 25 (b), 37.5 (c) and 50 mm (d)

3.1.5.2.2 Failure modes of Double-lap joints

In Figure 57 shows the fracture modes obtained for the DLJ tested with the Araldite® AV138 adhesive, for the various L_O values.

From Figure 57, which shows the rupture surfaces of a sample representative of each L_O value, it is seen that a cohesive break occurred in all, although the distribution of adhesive was not uniform on the surfaces between the substrates of each specimen, more noticeable adhesive distribution asymmetry at the joint with L_O = 50 mm. This is because the break occurred near the adhesive / substrate interface, leaving a thin film of adhesive on some of the joint surfaces and a thicker layer on the remaining ones.

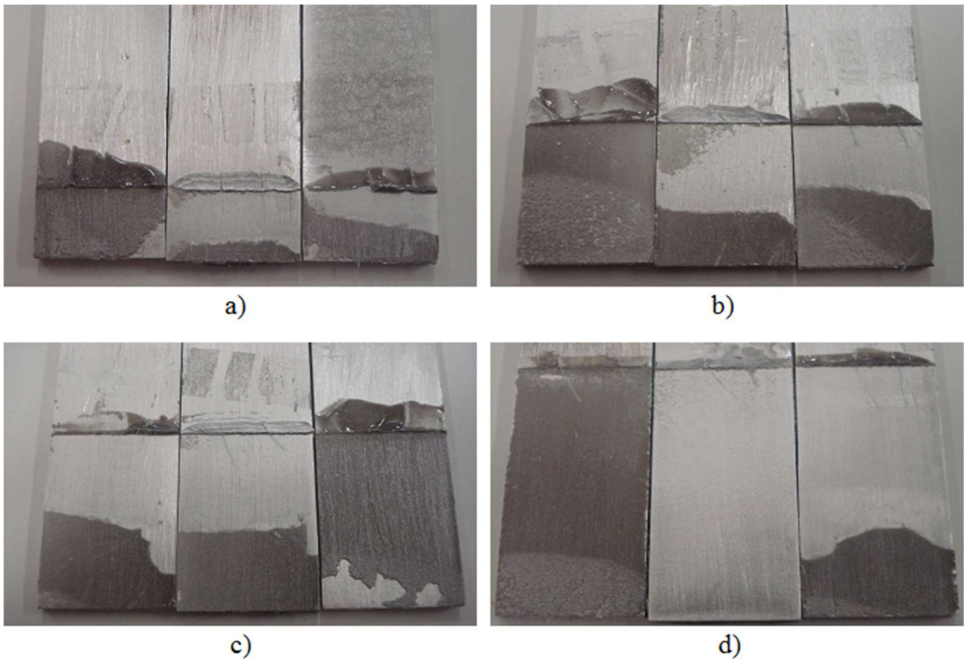

Figure 57 - Failure modes of DLJ specimens bonded with the adhesive Araldite ® AV138 : a) 12,5 mm, b) 25 mm, c) 37,5 mm and d) 50 mm.

From Figure 58 shows the fracture modes obtained for the DLJ's analyzed with the Araldite® 2015 adhesive, for the four L_O values.

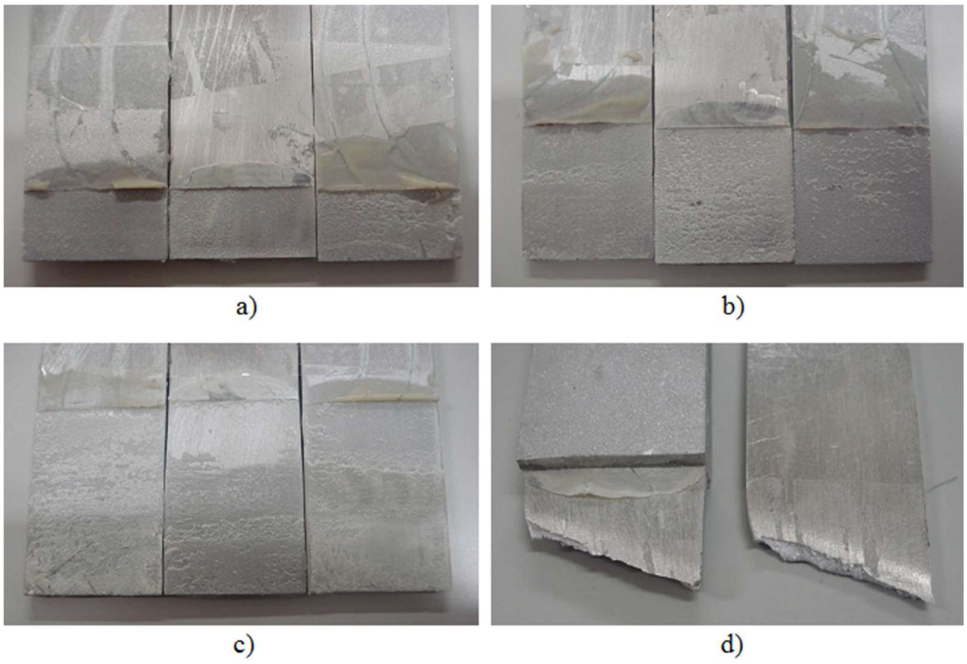

Figure 58 - Failure modes of DLJ specimens bonded with the adhesive Araldite ® 2015: a) 12,5 mm, b) 25 mm, c) 37,5 mm and d) 50 mm.

From Figure 58, which is a representative breaking surface of each L_O value, similarly to the DLJs tested with Araldite® AV138, uncoated cohesive breaks of the substrates for the L_O = 12.5 mm test pieces are recorded. In the case of joints with L_O = 25 mm and L_O = 37.5 mm, there was cohesive breakage of the adhesive, but with extensive adhesive in the substrates. On the other hand, in joints with L_O = 50 mm, the substrates were ruptured (Figure 58, d)). This happened because the adhesive strength was of greater size compared to the resistance of the substrate [13].

Figure 59 - Failure modes of DLJ specimens bonded with the adhesive Sikaforce®7752 L_O=12,5 mm.

Figure 60 - Failure modes of DLJ specimens bonded with the adhesive Sikaforce®7752 L_O=25 mm.

Figure 61 - Failure modes of DLJ specimens bonded with the adhesive Sikaforce®7752 L_O=37,5 mm.

Figure 62 - Failure modes of DLJ specimens bonded with the adhesive Sikaforce®7752 L_O=50 mm.

Analyzing Figure 59 to Figure 62, it can be seen that, like what happened with the DLJs tested with the two previous adhesives, all of the test pieces also suffered from cohesive breaks. In fact, there is also an equal adhesive remnant between the surfaces of the substrates of each specimen, as was the case with the DLJs tested with the Araldite® 2015 adhesive for L_O = 12.5 mm L_O = 25 mm and L_O = 37.5 mm. Nevertheless, there have been occasional cases of test pieces in which one of the surfaces of the substrates has only a thin film of adhesive, since the break occurs near the adhesive substrate interface. However, the good preparation of the surfaces during the manufacture of the DLJs led to excellent adhesion, which allowed cohesive breaks in all the test pieces.

3.1.5.3 Joint strength

In this subchapter, graphs and comparative tables are presented for each joint configuration and each adhesive, with mean P_{max} values as function of L_0.

3.1.5.3.1 Single-lap joints

In Table 16, the mean values of P_{max}, along with the respective standard deviations, are presented for SLJ for the three adhesives tested.

Table 16 - Mean values of Pmax [N] for the SLJ and for the different adhesives

L_0 (mm)	12.5	25	37.5	50
Araldite® AV138	5188.82	6950.853	8226.31	9656.433
Deviation	439.37	155.43	206.34	278.45
Araldite® 2015	5162.625	9405.209	12928.89	16073.56
Deviation	237.21	386.59	343.87	370.38
Sikaforce®7752	3121.777	6046.795	9070.123	12080.63
Deviation	206.80	445.45	334.10	553.55

In Figure 63 is shown a graphical representation of the values of the earlier table. Through the analysis of Table 16 of Figure 63, it is possible to verify that in all the adhesives there is an increase of the resistance with the increase of the L_0, although, that for the Araldite®AV138, this increase is the least pronounced due to the fragility of this adhesive. For Araldite®2015 and Sikaforce®7752, the increase is linear.

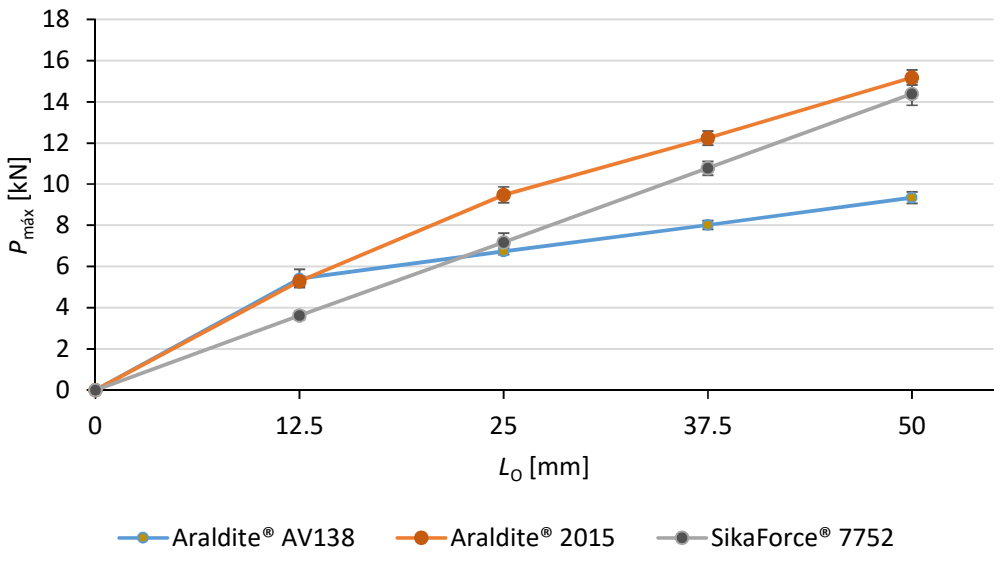

Figure 63 - Average values of P_{max} standard deviation for each value of L_O and adhesive type of SLJ

3.1.5.3.2 Double- lap joints

Table 17 shows the mean values of P_{max}, along with the respective standard deviations, for the DLJs for the three adhesives tested.

Table 17 - Mean values of Pmax [N] for the SLJ and for the different adhesives

L_0 (mm)	12.5	25	37.5	50
Araldite®AV138	12141.43	16116.50	16671.23	16980.78
Deviation	664.08	984.92	23.14	724.82
Araldite®2015	11405.35	22732.60	24052.43	24104.42
Deviation	234.49	836.52	438.38	188.60
Sikaforce®7752	7276.37	14622.80	21872.63	23973.37
Deviation	230.19	635.50	1210.06	387.80

Figure 64 shows a graphical representation of the values from the earlier table.

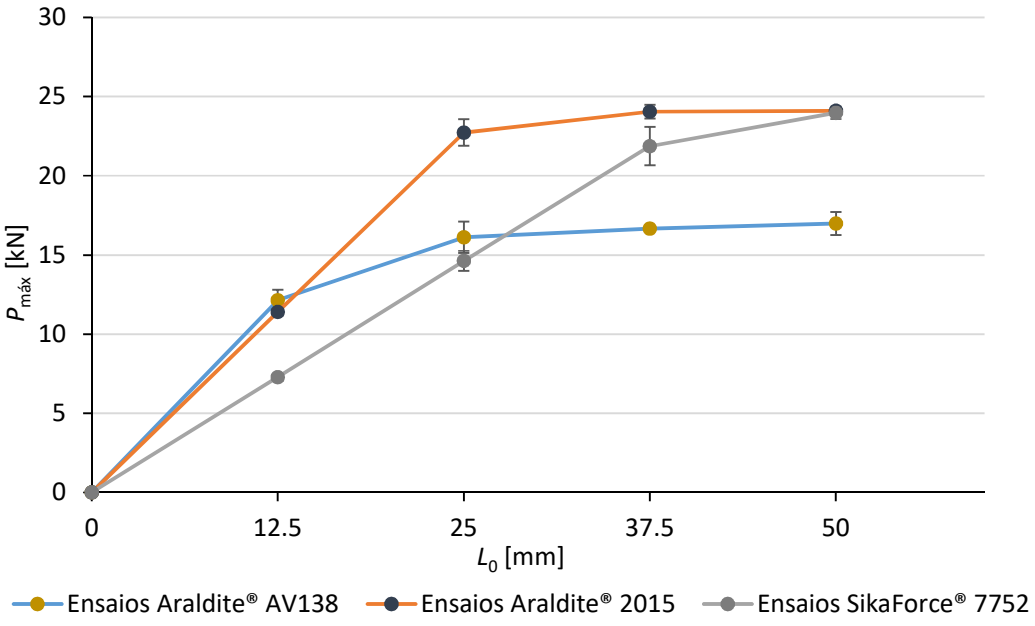

Figure 64 - Average values of Pm and standard deviation for each value of L_0 and adhesive type of DLJ

It can be seen from Figure 64 that, for Araldite®Av138, the increase in L_0 does not have a considerable influence on the increase of P_{max}, with the only increase of P_{max} in the range of L_0 = 12.5 mm for L_0 = 25 mm and from that point, the value still is at 16 kN. For

Araldite®2015, there is a linear increase of P_{max} at L_0 = 25 mm, but for L_0 = 37.5 mm and L_0 = 50 mm, the value stays at 24 kN. The Sikaforce®7752 is the one that has the best P_{max} increase L_0 function, being this perfectly linear up to L_0 = 37.5 mm, suffering a slight stagnation for L_0 = 50 mm.

3.1.5.4 Analysis the results obtained for single-lap joints and double-lap joints

After analyzing the data presented for the SLJ, it is possible to verify that P_{max} increases according to the value of L_0, and that increase varies from adhesive to adhesive, since it is more correct value and in some than in others. For L_0 = 12.5 mm, Araldite® AV138 and Araldite® 2015 have similar values of P_{max}, in the order of 5 kN, however, when increasing to L_0 = 25 mm, Araldite® AV138 only has one increase of 24.3% in P_{max}, while in Araldite® 2015 there was an increase of 79.3%. But the most significant increase occurred in Sikaforce® 7752, which for L_0 = 25 mm was 97.9%. For L_0 larger, there is a less pronounced increase, namely in Araldite® AV138 which, for L_0 = 50 mm, has an increase of 16.6% compared to the P_{max} obtained for L_0 = 37.5 mm. This happens in Araldite® AV138, because it is an adhesive considered fragile and has no plastification ability. In this way, when it approaches P_{max}, the joint breaks down. Araldite® 2015, which is considered a ductile adhesive, can plasticize and achieve higher P_{max} values. Sikaforce® 7752 is an adhesive that achieves a compromise between ductility and brittleness and, as such, has an intermediate behavior between Araldite® AV138 and Araldite® 2015, because, as shown in the results obtained, its P_{max} values are always situated between the values of the other two adhesives. For this joint configuration, the adhesive that stands out with the best results is Araldite® 2015, although Sikaforce® 7752 also obtained close values, for L_0 = 50 mm. Even so, Araldite® AV138 is a practical choice, depending on the application of the stresses to which the joint will be subjected. Regarding the values of the standard deviation, the three adhesives obtained low values. Regarding the maximum percentage standard deviation, Araldite® AV138, for L_0 = 12.5 mm, had a value of 8.1%, Araldite® 2015, for L_0 = 12.5 mm, obtained 4.5% and Sikaforce 7752, for L_0 = 25 mm, obtained 6.2%.

For the DLJ's, P_{max} also increases as a function of L_0, but in this configuration this increase is limited to the smaller overlapping lengths, with one exception, due to the plastification occurrence of the adhesives. In the case of Araldite® AV138, which for L_0 = 12.5 mm shows the highest P_{max} value, it suffers stagnation in L_0 = 25 mm (16.1 kN), and higher values of L_0 cannot reach more than one P_{max} in the order of 16 kN, that is, increases of 3.4 and 1.9% for L_0 of 37.5 mm and L_0 = 50 mm, respectively. For Araldite® 2015, slightly different results have already been obtained for the lower values of L_0. From L_0 = 12.5 mm for L_0 = 25 mm, P_{max} increased from 11.4 kN to 22.7 kN, that is, 99.3% (double). From L_0 = 25 mm for L_0 = 37.5 mm, the elastic limit of the adherends is exceeded, with only an increase of 5.8%. For L_0 = 50 mm the value of P_{max} stays practically the same. Sikaforce® 7752 also suffers an abrupt increase in P_{max} when it passes to L_0 = 25 (101%) and L_0 = 37.5 (49.6%). For L_0 = 50, P_{max} reaches a value like

Araldite® 2015. In conclusion, for DLJ joints with L_0 = 12.5 mm, both Araldite® AV138 and Araldite® 2015 are practical choices, since they reached values of P_{max} similar. For L_0 = 25 mm, the obvious choice is Araldite® 2015, which has the highest P_{max} value. For L_0 = 37.5 mm, again Araldite 2015 is the best choice, although the Sikaforce® 7752 is also a practical choice. Regarding the standard deviations, the values for Araldite® AV138 were reduced, with the highest value being 6.11% for L_0 = 25 mm. In the case of Araldite® 2015, the values were also relatively small, with only the highest of 3.68% being highlighted, for L_0 = 25 mm. For Sikaforce® 7752, the highest standard deviation was L_0 = 37.5 mm, with 5.53%.

3.2 Numerical work

This section addresses the numerical work of this thesis. The imposed numerical conditions and the XFEM formulation are initially presented. A stress analysis in the adhesive layer is further performed and discussed, as well as the joints strength prediction and it´s comparison with the experiments. Finally, a study on the influence of different conditions in the numerical analysis is performed.

3.2.1 Analysis conditions

The numerical analysis of the two types of joint was performed using ABAQUS® software. Based on the XFEM, in the choice of this software, it was also considered that it has integrated a Cohesive Damage Model, used to predict the resistance of the selected adhesive joints. In this software, the adhesives were modeled as elastoplastic solids and adhesives with CZM elements (see Figure 65). The joints were modeled in two dimensions, with solid elements of flat state of deformation for modeling the adherends. In the case of the CZM elements of the adhesive layer, it was only considered an element of the thickness of the adhesive, which follows a triangular tensile-separation law.

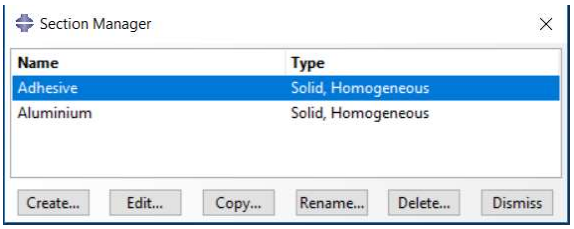

Figure 65 - ABAQUS® section manager used in the strength prediction

The fracture analysis by XFEM was performed considering non-geometric linearities. For the stress analysis models, the meshes are well refined, to obtain more exact results, especially in the overlap zone, because the mesh is more refined in this area and nearby, decreasing along the rest of the joint adhesive. The number of elements assigned and

the bias ratio (increasing refinement ratio along an edge of a model) depends on the length of the joint and the need to obtain more exact results.

As previously mentioned, the area of overlap and proximity of the joints were those that had the most refined mesh (see Figure 66, Figure 67), so the bias effect was applied from the central zone of the joint to the ends.

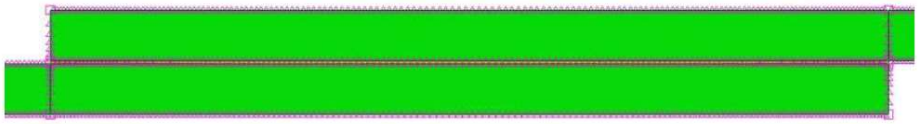

Figure 66 - bias effect in the overlap region of SLJ

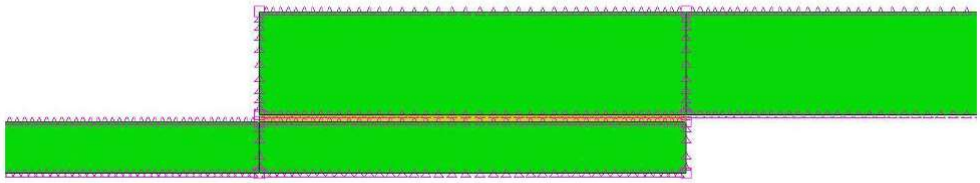

Figure 67 - bias effect in the overlap region of DLJ

With respect to the region of the joint that is not in contact with the adhesive, a bias effect was used, so that the mesh was more refined from the ends to the overlap zone (see Figure 68, Figure 69).

Figure 68 - Bias effect of the mesh in the unbound region of the adhesives for SLJ

Figure 69 - Bias effect of the mesh in the unbound region of the adhesives for DLJ

This variation of the number of elements and bias effect on the mesh of the different joint configurations has as main aim to decrease the processing ability needed for the simulations, and consequently the time of these, without compromising the precision of

the obtained results. In the case of simulation of the inner notch joint for α = 3.43°, this choice was crucial, since this was the joint configuration with greater weight at the processing and time level, with each simulation taking approximately 45 minutes.

To realistically simulate the experimental test conditions, the boundary conditions were defined so that one end of the joint was recessed, and the opposite end was subjected to a vertical constraint and a traction displacement. In Figure 70, Figure 71, it is possible to observe the boundary conditions for tests applied to the joints, using ABAQUS®.

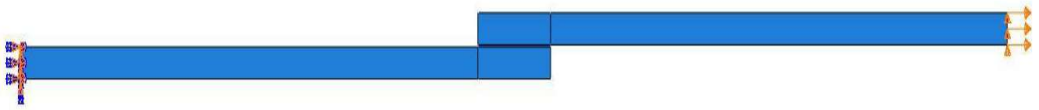

Figure 70 - Boundary conditions of SLJ

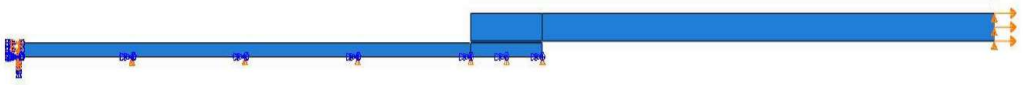

Figure 71 - Boundary conditions of DLJ

3.2.2 Cohesive zone models

3.2.2.1 Mixed-mode triangular CZM

CZM model the elastic loading, initiation of damage and further propagation due to local failure within a material. CZM are based on a relationship between stresses and relative displacements connecting initially superimposed nodes of the cohesive elements (Figure 72), to simulate the elastic behavior up to a peak load and subsequent softening, to model the gradual degradation of material properties up to complete failure.

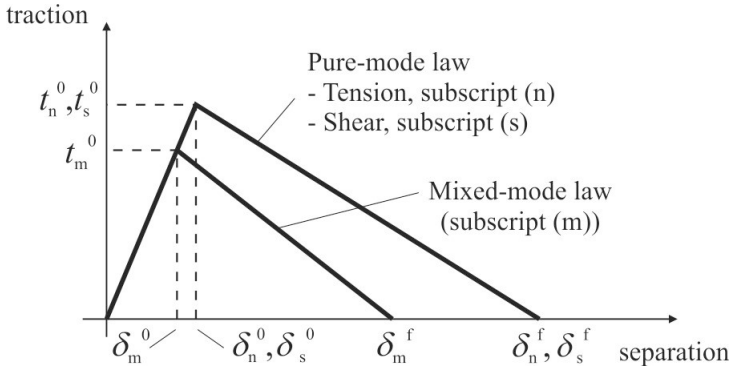

Figure 72 – Triangular traction-separation law (adapted from Abaqus® [74])

Generically speaking, the shape of the softening laws can be adjusted to conform to the behavior of the material or interface they are simulating [75, 76]. The areas under the

traction-separation laws in each mode of loading (tension and shear) are equaled to the respective fracture energy. Under pure mode, damage propagation occurs at a specific integration point when the stresses are released in the respective traction-separation law. Under mixed-mode, energetic criteria are often used to combine tension and shear [75], thus simulating the typical-mixed mode behavior inherent to bonded assemblies. In this work, a continuum-based approach, i.e. using the cohesive elements to model solids interfaces, was considered to model the finite thickness of the adhesive layer. The cohesive layer is assumed to be under one direct part of strain (through-thickness) and one transverse shear strain, which are computed directly from the element kinematics. The membrane strains are assumed as zero, which is right for thin and compliant layers between stiff adherends. The strength predictions of CZM modelling are expected to be mesh independent [55].

The traction-separation law assumes an initial linear elastic behavior followed by linear evolution of damage. Elasticity is defined by an elastic constitutive matrix relating stresses and strains across the interface [74]

$$\mathbf{t} = \begin{Bmatrix} t_n \\ t_s \end{Bmatrix} = \begin{bmatrix} K_{nn} & K_{ns} \\ K_{ns} & K_{ss} \end{bmatrix} . \begin{Bmatrix} \varepsilon_n \\ \varepsilon_s \end{Bmatrix} = \mathbf{K\varepsilon}. \tag{8}$$

The stiffness matrix (**K**) contains the stiffness parameters (K_{nn}, K_{ns}, K_{ss}) of the adhesive layer, given by the relevant elastic moduli. A suitable approximation for thin adhesive layers is provided with $K_{nn}= E$, $K_{ss}= G$, $K_{ns}=0$; E and G are the longitudinal and transverse elastic moduli [75]. Different criteria can specify damage initiation. In this work, the QUADS criterion was considered for the initiation of damage, already shown to give accurate results [77]. After the peak value in Figure 72 is reached, the material stiffness is degraded under different laws, depending on the material to be simulated. For brittle materials such as the Araldite® AV 138, a linear softening law is sufficiently appropriate, Figure 72 [78]. Complete separation is predicted by a linear power law form of the required energies for failure in the pure modes, with α=1.

3.2.3 Stress distributions

In this subchapter, the stresses in the elastic regime in the SLJ and DLJ are analyzed, comparing the σ_y and τ_{xy} stresses obtained numerically in the ABAQUS®. The analysis is performed at the adhesive thickness middle, for the several adhesives and L_O values. This analysis aims to understand the influence of each of the joint configurations on the stresses distribution and joint strength, helping to support the obtained P_{max} results. The stresses graphs presented in sub-chapters 3.2.3.1 and 3.2.3.2 were obtained through a stress normalization procedure, which consisted of dividing the σ_y and τ_{xy} stresses by the average stress (τ_{avg}) for each L_O value. The value of L_O has also been normalized to x/L_O (x is the distance from one of the overlapping ends), such that $0 \leq x/L_O \leq 1$.

3.2.3.1 Peeling stresses

Figure73, Figure74 and Figure75 show the σ_y stress distributions for the SLJ, as a function of L_O. The σ_y stresses have a lower magnitude than τ_{avg}, with the joint ends exception, because they constitute stress singularity zones due to the adherends rotation [79]. Because of this rotation, tensile stresses are generated in these regions, while in the innermost regions are generated compressive stresses. This is because the adherends deformation during loading causes the joint transverse deformation, which results in the traction of the adhesive bond ends and compression in the intermediate zone thereof. These joints strength is significantly affected by σ_y stresses, given their criticality for adhesive bonding, which may lead to early joint failure [80].

The L_O parametric study showed that the σ_y stresses peaks increased with the L_O increase. In the singularities vicinity it is observed σ_y compressive peaks which also tend to increase in intensity with the increase of L_O, while the compressive stresses in the interior direction of the adhesive bond tend to decrease. It should be noted that the increase of the σ_y stress peaks with the L_O increment tends to decrease the joint average strength in the bonding area, especially in the joints with fragile adhesives [81].

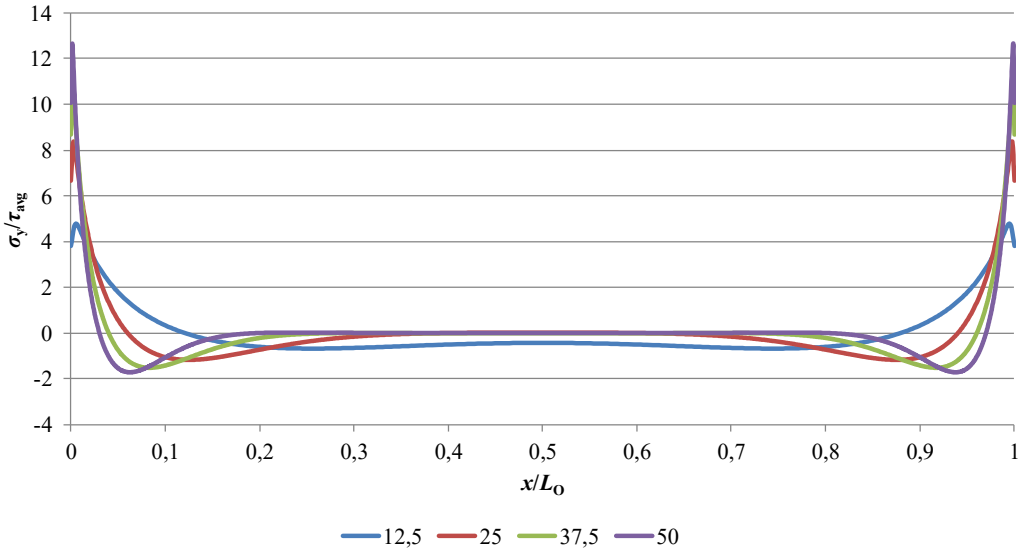

Figure73 – σ_y stress distribution in SLJ with the Araldite® AV138 adhesive, for the several L_O values.

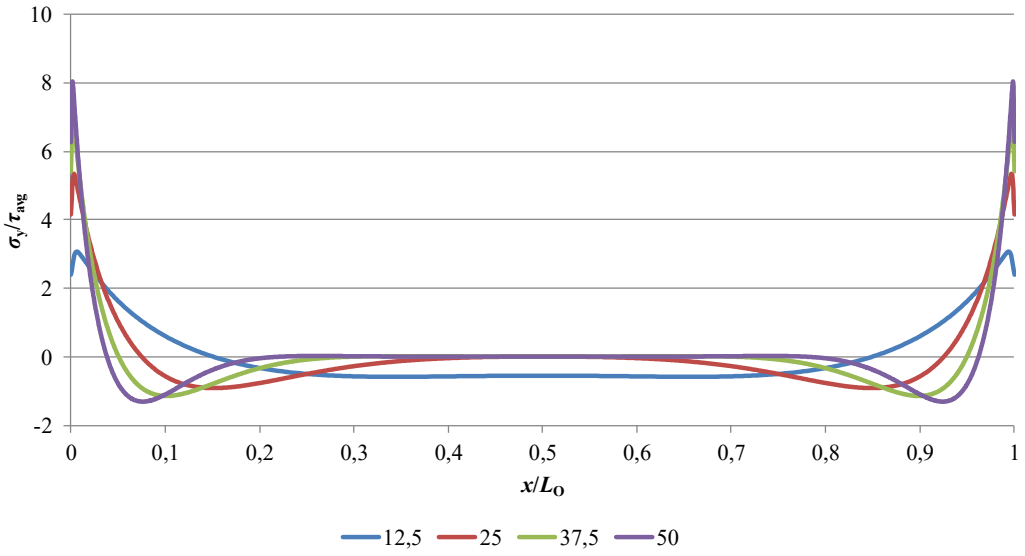

Figure74 – σ_y stress distribution in SLJ with the Araldite® 2015 adhesive, for the several L_O values.

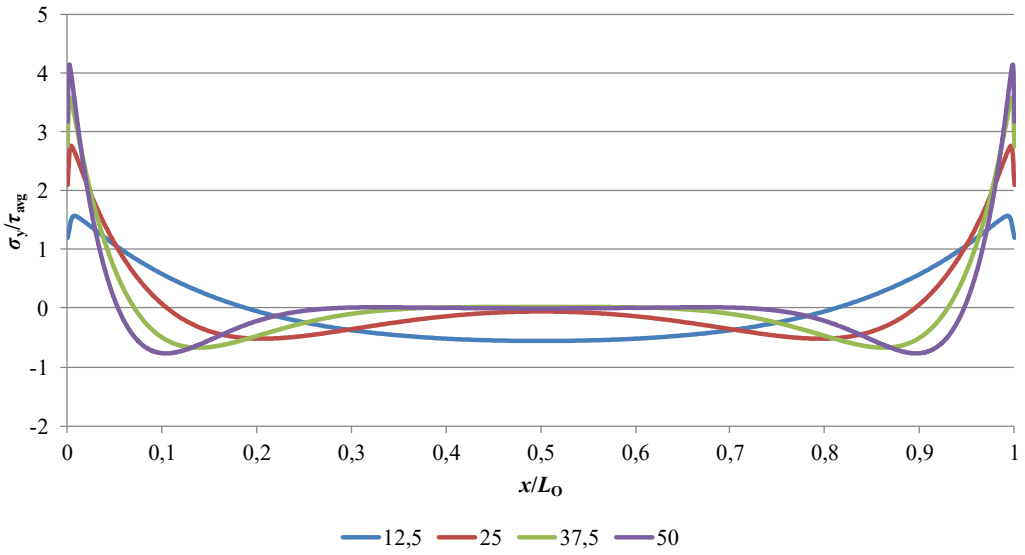

Figure75 – σ_y stress distribution in SLJ with the Sikaforce® 7752 adhesive, for the several L_O values.

It is observed that the Araldite® AV138 adhesive is the one that has the highest σ_y stress gradient for the several L_O values. This is justified by its superior stiffness, which influences the stresses distribution in the adhesive layer, and which can induce premature failure thereof. On the other hand, the Araldite® 2015 and Sikaforce® 7752 adhesives reveal more uniform stress distributions. Finally, in the σ_y stress analysis context, for the value of L_O=50 mm, the Araldite® AV138, Araldite® 2015 and Sikaforce® 7752 adhesives present σ_y stress peak values normalized in traction of 12.6, 8.0 and 4.1, respectively, which corresponds to the decreasing order of stiffness of the same ones.

Figure 76, Figure 77 and Figure 78, represent the σ_y stress distributions for the DLJ, for the several adhesives and L_O values. Similar to the SLJ, at this joints σ_y also has a lower magnitude than the τ_{avg} stresses, with the exception of the bonding ends due to the stress singularity zone [79]. However, the DLJ´s stress profile is not totally like that of the SLJ. At the DLJ left end, corresponding to the outer end of the overlap, occurred traction peaks [82], while at the inner end of the overlap are verified compression peaks [83]. These differences in stress profiles are mainly due to the fact that DLJ does not present transverse deflection of the inner adherend due to symmetrical loading [59]. This promotes a generalized reduction of σ_y peak stresses in the DLJ for all L_O values [84]. However, the σ_y stress values in the central region are approximately zero, with increasing gradients for the bond ends with the increment of L_O, like the SLJ. Thus, compressive stresses at the DLJ inner end, combined with lower σ_y peak stresses at the outer end in relation the SLJ, let predict significant benefits with respect to the joint´s strength for the same bond area [83].

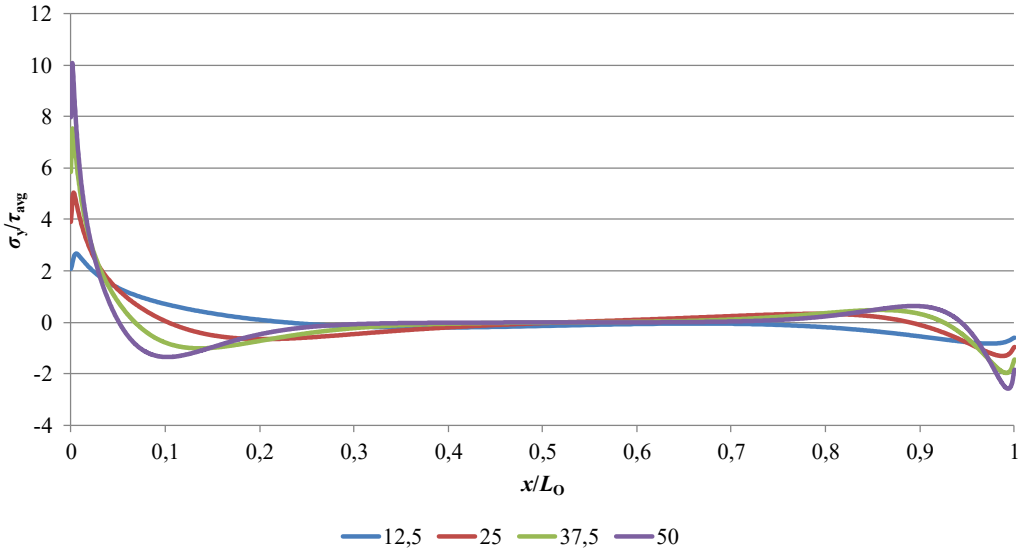

Figure 76 – Distribution of σ_y stresses in DLJ with the adhesive Araldite® AV138, for the several L_O values.

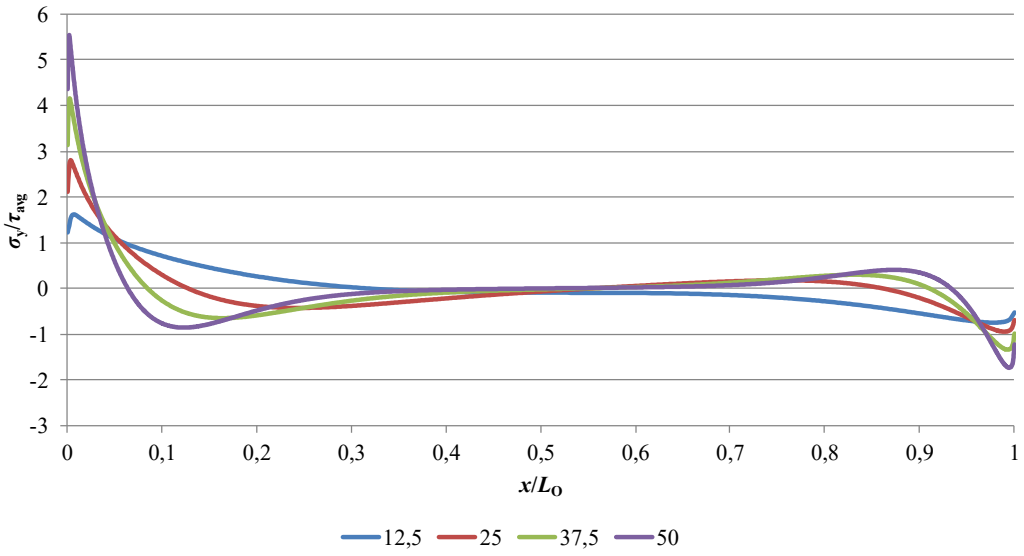

Figure 77 – Distribution of σ_y stresses in DLJ with the adhesive Araldite® 2015, for the several L_O values.

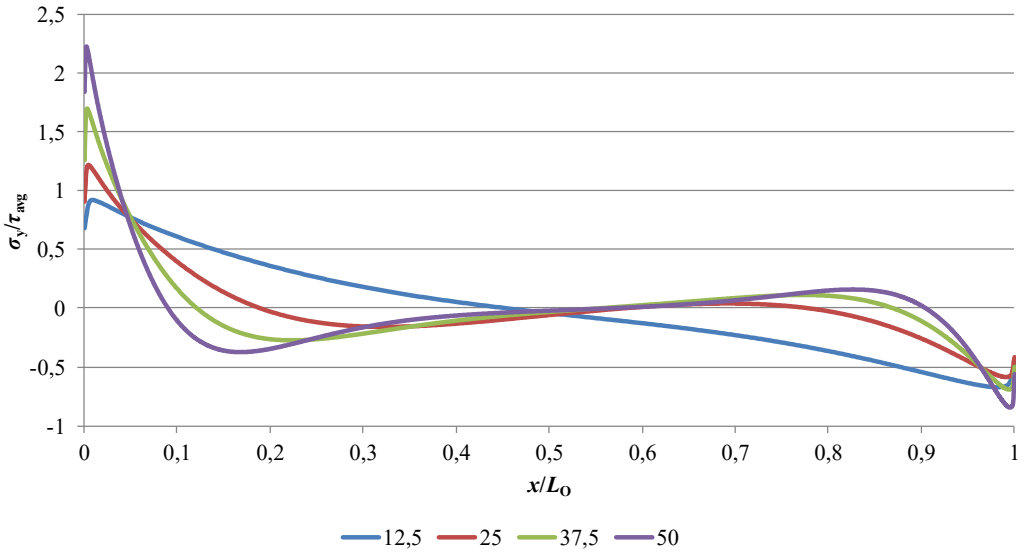

Figure 78 – Distribution of σ_y stresses in DLJ with the adhesive Sikaforce® 7752, for the several L_O values.

By making an analogy between the three tested DLJ adhesives, it is noted that the Araldite® AV138 adhesive is the one that presents the most pronounced σ_y stress peak values at the outer end. This is due to the adhesive´s high stiffness, which limits the stress distribution uniformity along the overlap. Furthermore, as previously referred for SLJs, a high stiffness may induce premature joint´s failure.

For the value of L_O=50 mm, the Araldite® AV138, Araldite® 2015 and Sikaforce® 7752 adhesives exhibit, respectively, σ_y stress peak values normalized in tensile of 10.0, 5.5 and 2.2, which matches the stiffness decreasing order of the same ones. The presented

σ_y stress peak values reveal a decrease, in relation to the homologues in SLJ, of 20.6%, 31.3% and 46.3%, respectively.

3.2.3.2 Shear stresses

In Figure 79, Figure 80 and Figure 81 its showed the τ_{xy} stress distributions for the several adhesives and L_O values (SLJ). In the inner zone of the overlap the τ_{xy} stresses have a lower magnitude than τ_{avg}, except at the ends of the overlap, which constitute stress concentration zones [23]. This behavior occurs due to the longitudinal differential deformation of each one of the adherends along the overlap, which is null at the free end thereof and increases until to the opposite end [85]. However, in the overlap central region, the referred effect is nullified, with the development of τ_{xy} stresses only due to the tensile load applied to the joint. It is also verified a progressive increase of τ_{xy} stress peaks with the L_O increasing. This tendency is due to the increasing gradient of longitudinal deformations of the adherends as the L_O value increase, which in turn is due to the increase of the bonding areas and transmitted loads [56]. Similarly to the σ_y stress gradients, it is verified that the τ_{xy} stress gradients are extremely damaging for the joints strength, especially if fragile adhesives are used, whose fracture occurs when τ_f is reached and by the almost null plasticization capacity of these adhesives [85]. This effect can be overcome by the use of ductile adhesives, since they allow adhesive plasticization and joint failure to τ_{avg} higher values [86]. This is verified because the plasticization capacity of these adhesives leads to a better stresses redistribution along the overlap, while the low stiffness contributes to a lower stresses gradient, which translates into a τ_{xy} stresses decrease at the overlap ends in relation to the fragile adhesives, and at the same time in a increase of referred stresses in the overlap internal region, which culminates in increased joint strength [87]. Thus, in a limit situation, the whole region of the overlap would be requested at the failure moment [86].

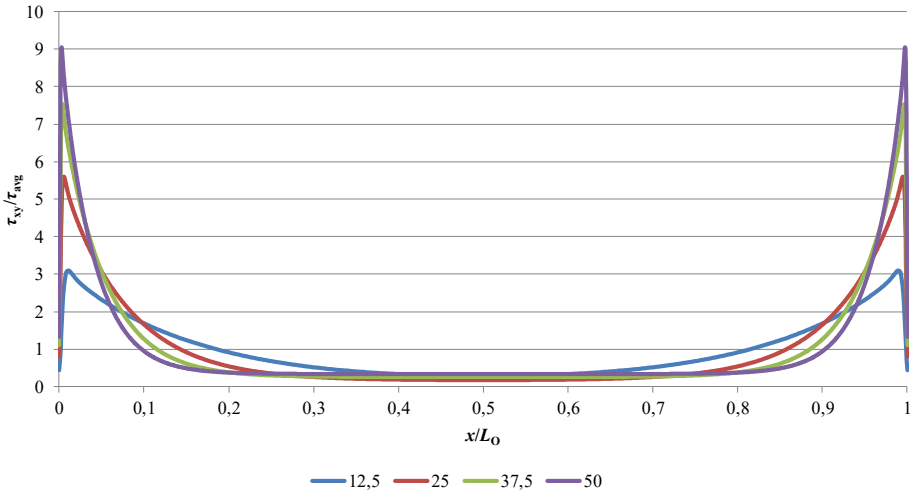

Figure 79 – Distribution of τ_{xy} stresses in SLJ with the adhesive Araldite® AV138, for the several L_O values.

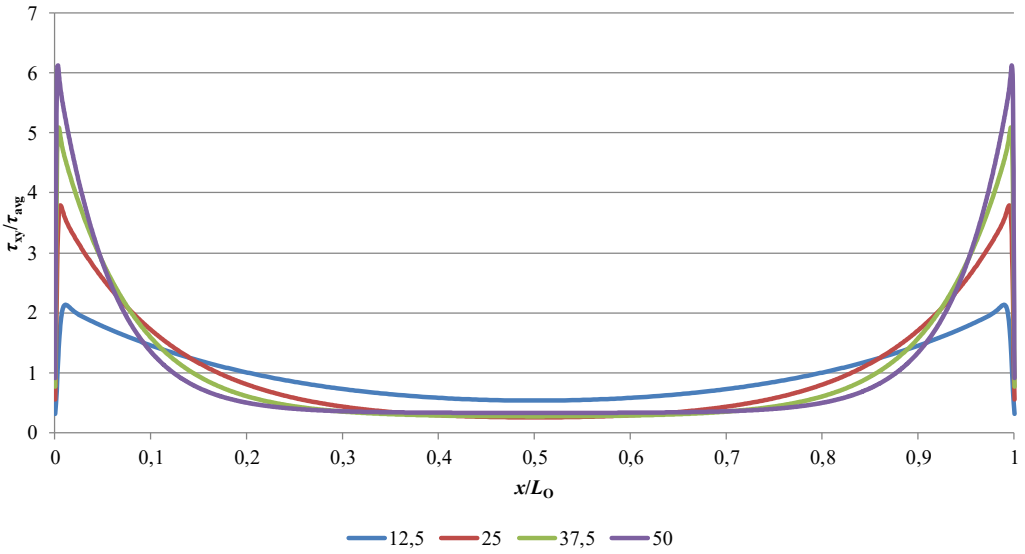

Figure 80 – Distribution of τ_{xy} stresses in SLJ with the adhesive Araldite® 2015, for the several L_O values.

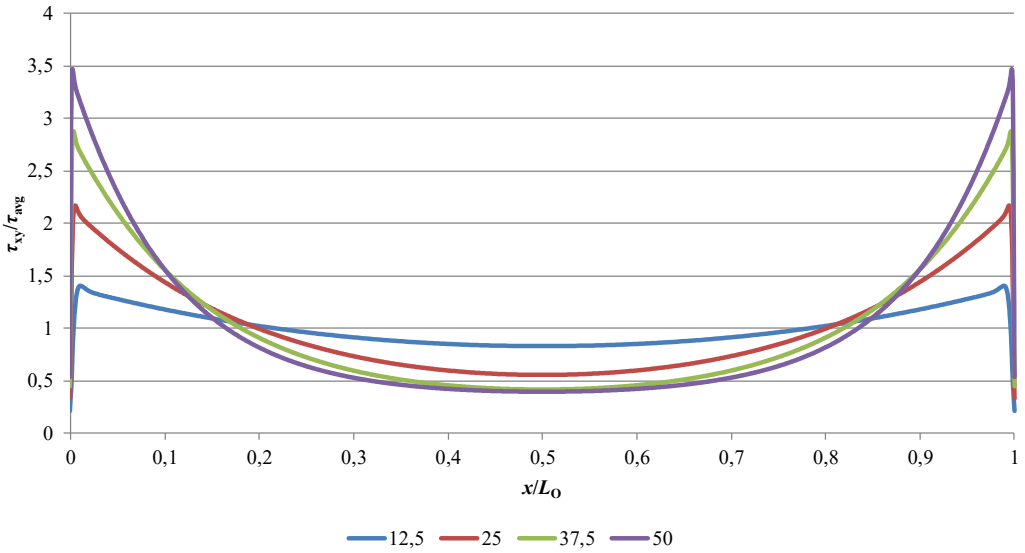

Figure 81 – Distribution of τ_{xy} stresses in SLJ with the adhesive Sikaforce® 7752, for the several L_O values.

By comparing τ_{xy} stresses on the adhesives used in SLJ, it is noted that the most brittle adhesive (Araldite® AV138) is the one with the highest stress peak values, which corresponds to higher stress gradients along the overlap. These facts are due to the high adhesive´s stiffness, which influences the stresses distribution in the adhesive layer. For L_O=50 mm, the Araldite® AV138, Araldite® 2015 and Sikaforce® 7752 adhesives present tensile τ_{xy} stress peak values of 9.04, 6.1 and 3.5, respectively, which matches with the stiffness decreasing order of the same ones.

In Figure 82, Figure 83 and Figure 84 are represented the τ_{xy} stress distributions for the DLJ, for the three tested adhesives and four L_O values. It is seen that the stress distribution is not symmetrical, contrary to the one registered in the SLJ. In fact, the outer end of the DLJ exhibits a size of τ_{xy} stresses above the opposite end, due to the solicitation to which the intermediate adherend is given, which translates into high loads in the vicinity of x/L_O=0. Comparing the τ_{xy} stress peaks with the equivalents in the SLJ, it is noted that in the inner overlapping end occurs a significant decrease in their size. At the outer end, there is also a decrease in the τ_{xy} stress peaks, although less significantly [88]. This difference is due to the lower variation of the longitudinal deformations between the two outer adherends and the inner adherend, which results in the differential deformation effect reduction of the same ones [83]. The changes in the τ_{xy} stresses profile of the DLJs, should be reflected in a joint strength greater than 2 times that of the SLJ, corresponding to the relationship between the bonded areas of both joint configurations [87]. Like what happened in SLJ, the P_{max} increase in the DLJs should also not be proportional to the L_O increase, since σ_y and τ_{xy} stress peaks suffer an increase with the L_O increase. This will be even more evident in the joints with fragile adhesives, since the adhesive will not allow plasticization when the limit stresses are reached [85].

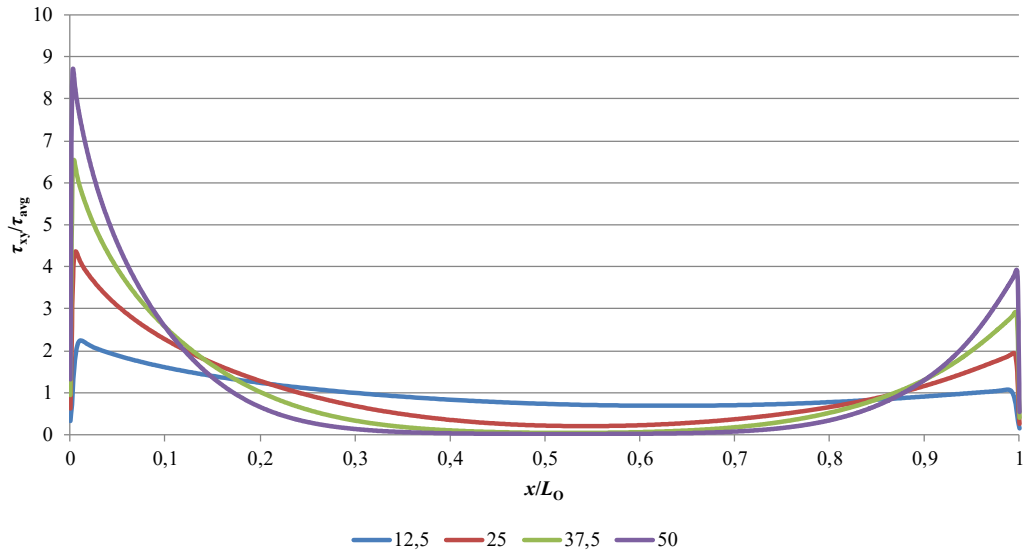

Figure 82 – Distribution of τ_{xy} stresses in DLJ with the adhesive Araldite® AV138, for the several L_O values.

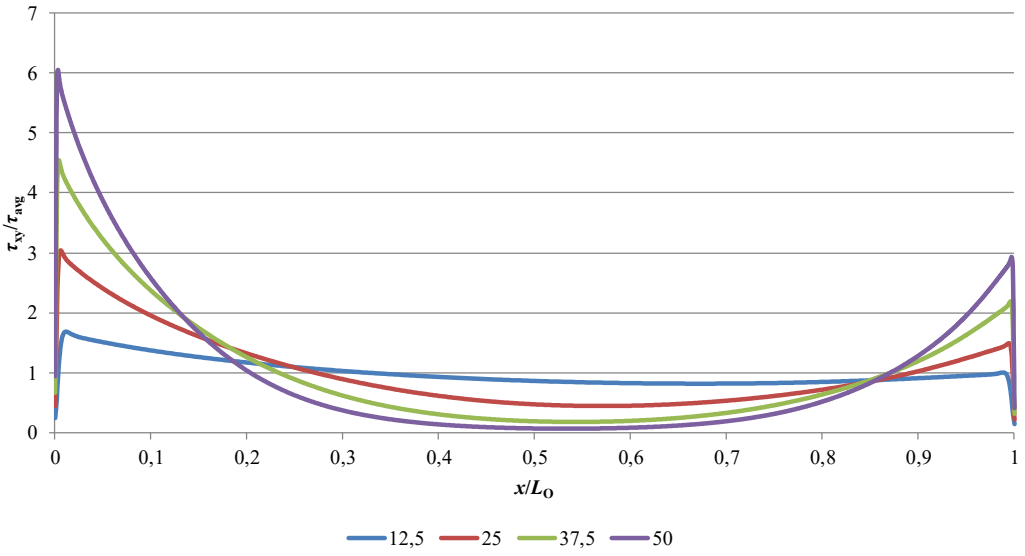

Figure 83 – Distribution of τ_{xy} stresses in DLJ with the adhesive Araldite® 2015, for the several L_O values.

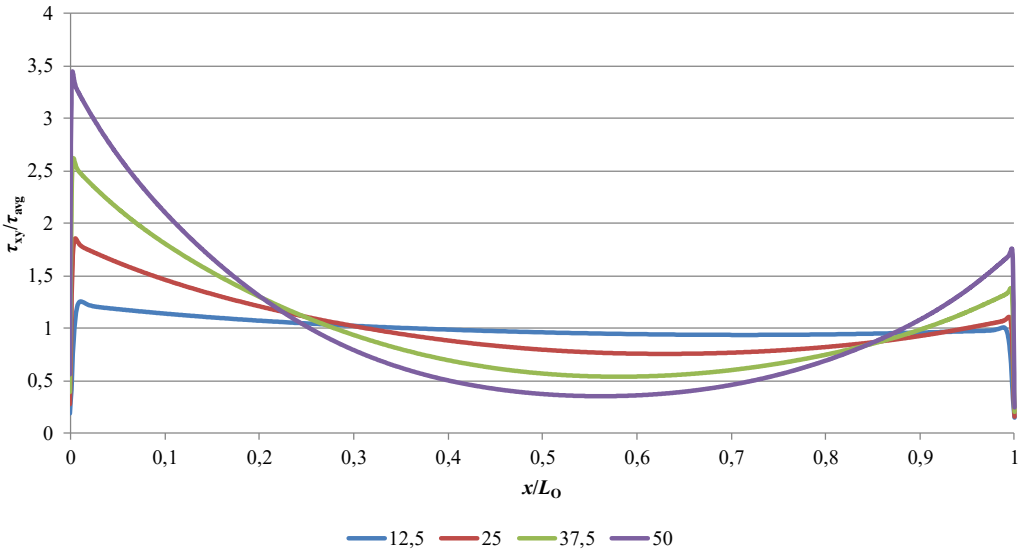

Figure 84 – Distribution of τ_{xy} stresses in DLJ with the adhesive Sikaforce® 7752, for the several L_O values.

Comparing the three tested adhesives, it is noted that the Araldite® AV138 adhesive, due to its brittleness, is the one that shows the highest τ_{xy} stresses gradient due to its rigidity. In addition, it denotes preponderance with respect to the τ_{xy} peak stresses at the bond ends.

Quantifying the τ_{xy} stresses peak normalized at the DLJ ends, for the Araldite® AV138, Araldite® 2015 and Sikaforce® 7752 adhesives, and L_O=50 mm, values of 8.72, 6.0 and 3.44 were obtained, respectively. This variation agrees with the adhesive's stiffness decreasing order, similar to what happened in the SLJ. Comparing the τ_{xy} stresses values

presented under the same conditions with respect to the SLJ, it is verified a percentage decrease of the referred τ_{xy} peak stresses of 3.7%, 2.17% and 0.9%, respectively. This decrease should handle an increase in the DLJ strength in relation to the SLJ with an equal L_O value, greater than 2 times (ratio of bonded areas).

3.2.4 Joint strength

3.2.4.1 Joint strength of single-lap joints

Analyzing the figure, for the Araldite® AV138 adhesive, the numerical P_{max} values coincide with the experimental P_{max} values, being contained in the calculated standard deviation. Regarding Araldite® 2015, the numerical P_{max} values are coincident with the experimental ones, but this only happens up to L_0 = 25 mm (inclusive). For L_0 = 37.5 mm, there is a small lag, with the numerical P_{max} being at the threshold of the upper standard deviation of the experimental result. For L_0 = 50 mm, the same behavior is seen, but more pronounced, since the numerical P_{max} value is outside the upper value of the standard deviation of the experimental result. About Sikaforce® 7752, the mismatch between numerical and experimental P_{max} values starts at L_0 = 12.5 mm, with experimental P_{max} being greater than QUADS value and lies in a close margin with other criteria values.

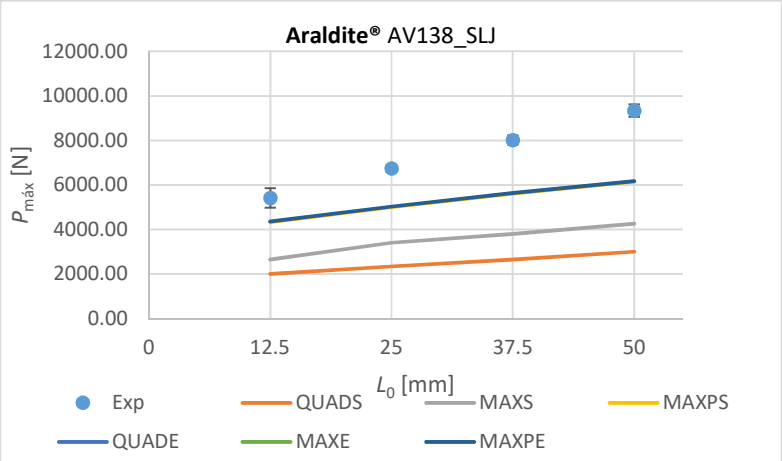

Figure 85 - Comparison of numerical P_{max} values with experimental values of SLJ Araldite® AV138

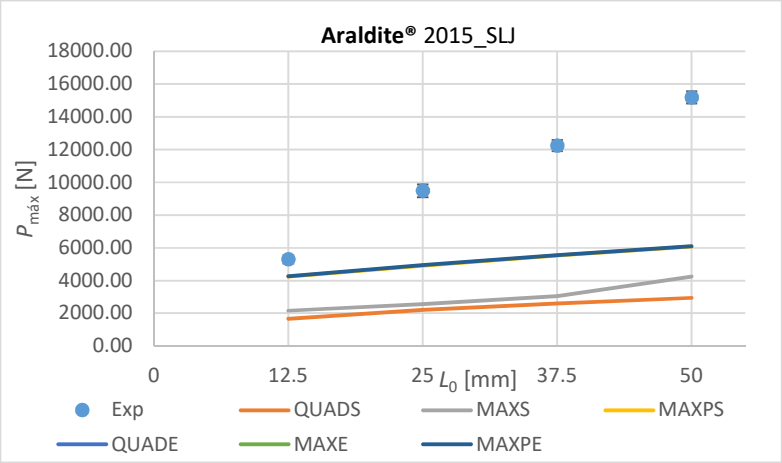

Figure 86 - Comparison of numerical P_{max} values with experimental values of SLJ Araldite® 2015

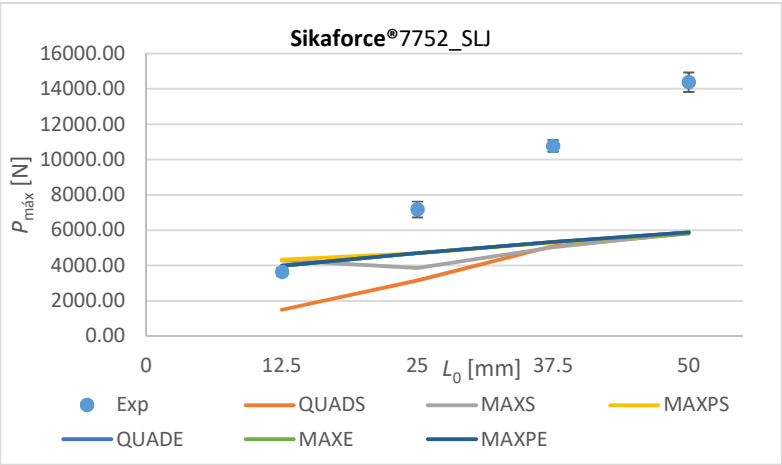

Figure 87 - Comparison of numerical P_{max} values with experimental values of SLJ Sikaforce® 7752

This discrepancy between numerical and experimental P_{max} values for Araldite® 2015 adhesives and Sikaforce® 7752 (more ductile adhesive), is that in the simulations a triangular law is used, and that due to the ductility of the adhesives, it would be more suitable to use a trapezoidal law [67]. In the case of Araldite® AV138 (fragile adhesive), the triangular law is quite adequate, considering that there is no lag between numerical and experimental values. At the quantitative level, as in the experimental values, the Araldite® 2015 is the adhesive that achieves better performance throughout the L_0. In the case of numerical values, there is a greater discrepancy between the P_{max} values for Araldite® 2015 and Sikaforce® 7552 than for the experimental results.

3.2.4.2 Joint strength of double-lap joints

In Figure 125, a comparison between the numerical P_{max} values and the experimental values of the DLJs is presented. For Araldite® AV138, it is possible to verify the repetition of the same behavior already observed in the SLJ, that is, the numerical and

experimental P_{max} values, coincide perfectly. This, as already mentioned in the earlier subchapter, Due to the fragility of the adhesive and the use of a triangular law in the simulation of joints. In the case of Araldite® 2015, a difference in behavior regarding SLJ is already noted, since in this case the numerical and experimental P_{max} values are quite similar throughout L_0. In Sikaforce® 7752, there is still a slight difference between numerical and experimental P_{max} values, although this time this difference passes through all L_0, except for L_0 = 50 mm, where the numerical and experimental values are equivalent.

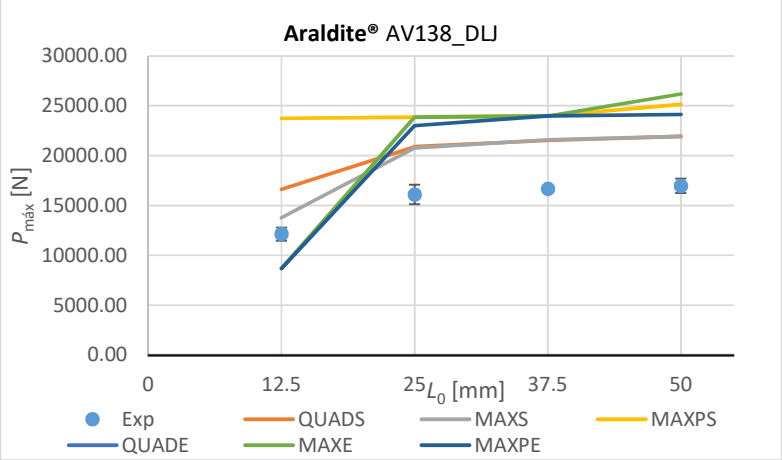

Figure 88 - Joint strength of double-lap joint with the adhesive Araldite® AV138

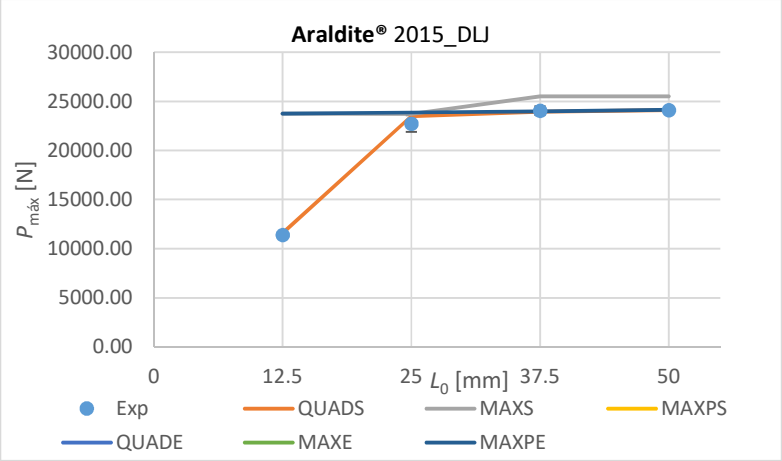

Figure 89 - Joint strength of double-lap joint with the adhesive Araldite® 2015

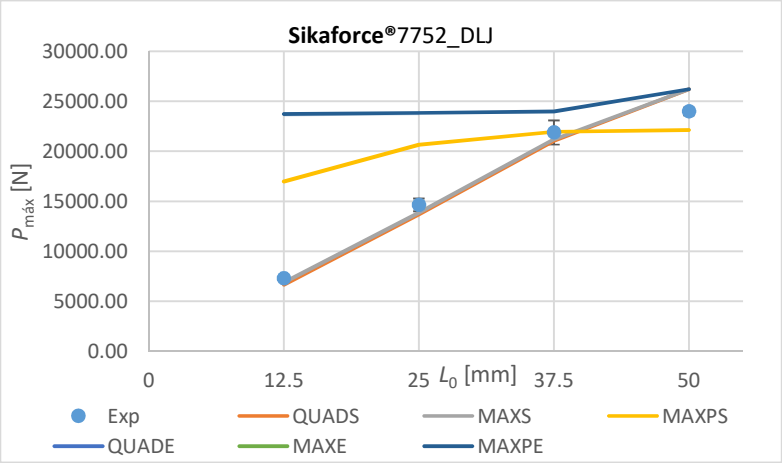

Figure 90 - Joint strength of double-lap joint with the adhesive Sikaforce® 7752

As in the experimental P_{max} results, numerical Araldite® 2015 and Sikaforce® 7752 adhesives have similar P_{max} values for L_0 = 50 mm, with a sharp difference of L_0 = 25 mm.

3.2.5 Strength prediction

3.2.5.1 Strength prediction of the Effect of damage criterion

Analyze the strength prediction by using the law of exponential propagation was necessary to change some parameters in the ABAQUS® models. The softening, called softening, in Figure 91 was changed from Linear (law of propagation triangular) for Exponential. It can also be seen in the figure that the parameter Power differs. In the triangular propagation law, Power = 1 is used while applying the exponential propagation law, the Power parameter assumes the values 0.5, 1 or 2 of test different criteria. Figure 91 compares the parameters that differ in the study of the effect of propagation law.

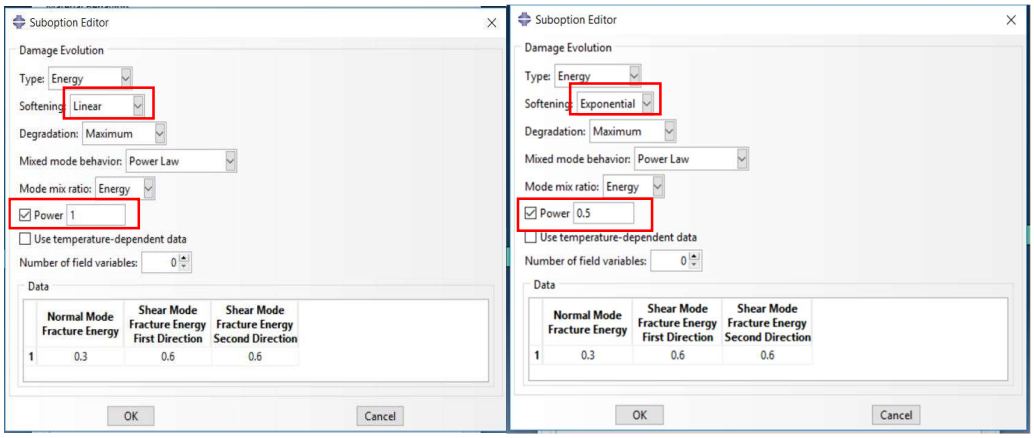

Figure 91 - Comparison of the parameters between the linear and exponential law.

A huge variation between the experimental and numerical value is found since in ABAQUS XFEM simulation for single lap joints the maximum load is considered as the crack initiation load, due to the impossibility to model crack propagation along the adhesive layer because of the significant joint rotations.

3.2.5.2 Damage initiation criteria of Single-lap joints

The damage initiation criteria of the three adhesives explained using upcoming graphs.

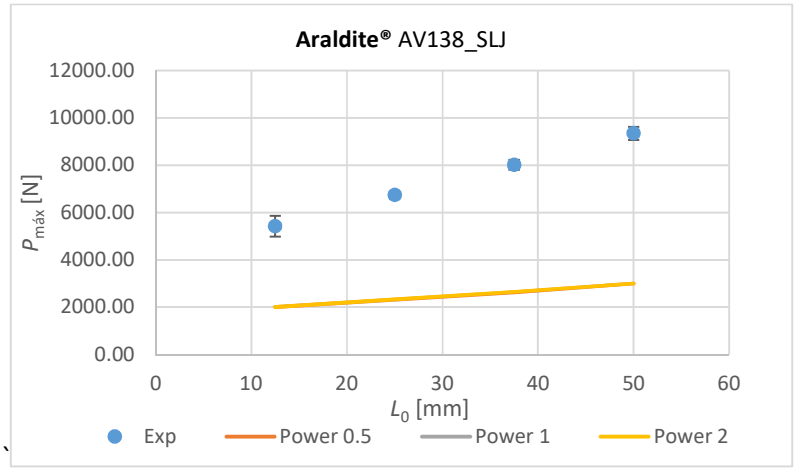

Figure 92 - Damage initiation criteria of SLJ Araldite® AV138

For adhesive Araldite® AV138 at 12.5 mm width of adhesive the maximum load attained during numerical simulation is 2 kN whereas the obtained experimental value is 5.42 kN likewise for 25 mm width the values are 2.31 kN and 6.73 kN for 37.5 mm width the respective values are 2.62 kN and 8.01 kN and for 50 mm width the values are 3 kN and 9.34 kN. From these values the adhesive length is proportional to the maximum load carried by the joint before failure.

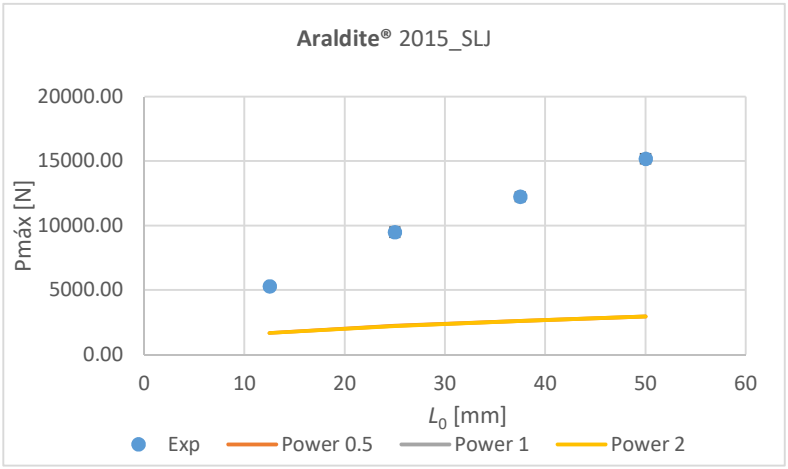

Figure 93 - Damage initiation criteria of SLJ Araldite®2015

For adhesive Araldite® 2015 at 12.5 mm width of adhesive the maximum load attained during numerical simulation is 1.67 kN whereas the obtained experimental value is 5.28 kN likewise for 25 mm width the values are 2.22 kN and 9.48 kN for 37.5 mm width the respective values are 2.58 kN and 12.23 kN and for 50 mm width the values are 2.94 kN and 15.18 kN, from these values the adhesive length is proportional to the maximum load carried by the joint before failure.

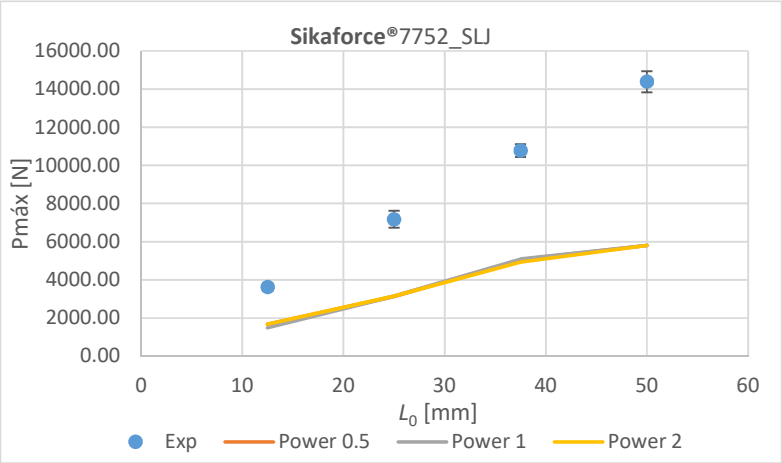

Figure 94 - Damage initiation criteria of SLJ Sikaforce® 7752

For adhesive Sikaforce® 7752 at 12.5 mm width of adhesive the maximum load attained during numerical simulation is 1.68 kN whereas the obtained experimental value is 3.62 kN likewise for 25 mm width the values are 3.161 kN and 7.17 kN for 37.5 mm width the respective values are 5.05 kN and 10.77 kN and for 50 mm width the values are 5.80 kN and 14.38 kN. From these values the adhesive length is proportional to the maximum load carried by the joint before failure.

3.2.5.3 Damage initiation criterion of double-lap joints

For adhesive Araldite®AV138 of power 0.5 at L_O=12.5 mm width of adhesive the maximum load attained during numerical simulation is 13.13 kN whereas the obtained experimental value is 12.14 kN likewise for L_O=25 mm width the values are 15 kN and 16.11 kN for L_O=37.5 mm width the respective values are 15.26 kN and 16.67 kN and for L_O=50 mm width the values are 16.47 kN and 16.98 kN, From these values the adhesive length is proportional to the maximum load carried by the joint before failure of L_O=25 mm and L_O=37.5. mm. For power-1 and L_O=12.5 mm the maximum load attained during numerical simulation is 16.63 kN whereas the obtained experimental value is 12.14 kN likewise for L_O=25 mm the values are 20.94 kN and 16.11 kN, for L_O=37.5 mm the respective values are 21.54 kN and 16.67 kN, and for L_O=50 mm the values are 21.93 kN and 16.98 kN. For power-2 L_O=12.5 mm width of adhesive the maximum load attained during numerical simulation is 17.70 kN whereas the obtained experimental value is 12.14 kN likewise for L_O=25 mm the values are 23.12 kN and 16.11 kN for L_O=37.5 mm

width the respective values are 23.29 kN and 16.67 kN, and for L_O=50 mm width the values are 23.33 kN and 16.98 kN. From these values the adhesive length is proportional to the maximum load carried by the joint failure.

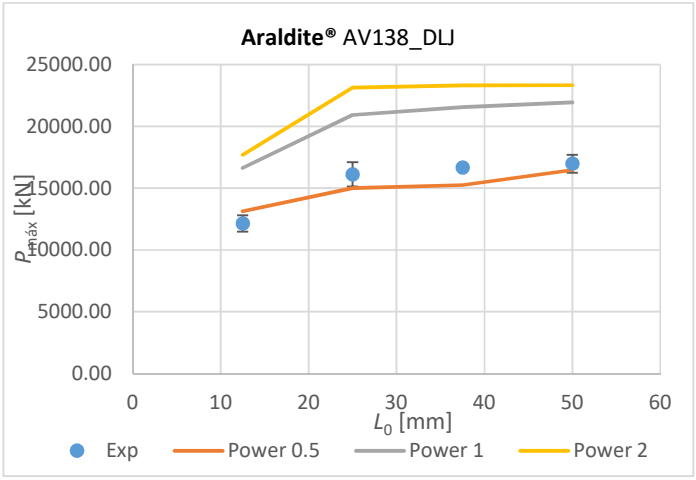

Figure 95 - Damage initiation criteria of DLJ Araldite® AV138

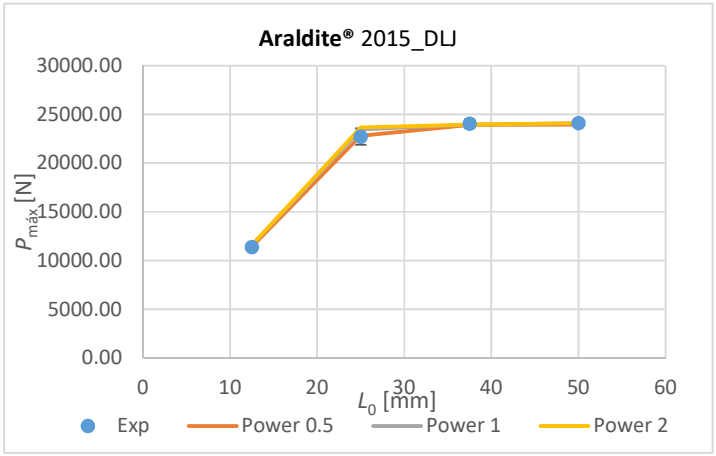

Figure 96 - Damage initiation criteria of DLJ Araldite®2015

For adhesive Araldite® 2015 at 12.5 mm width of adhesive the maximum load attained during numerical simulation is 11.40 kN whereas the obtained experimental value is 11.40 kN likewise for 25 mm width the values are 22.80 kN and 22.73 kN for 37.5 mm width the respective values are 23.92 kN and 24.05 kN and for 50 mm width the values are 23.93 kN and 24.10 kN From these values the adhesive length is proportional to the maximum load carried by the joint similar to the failure.

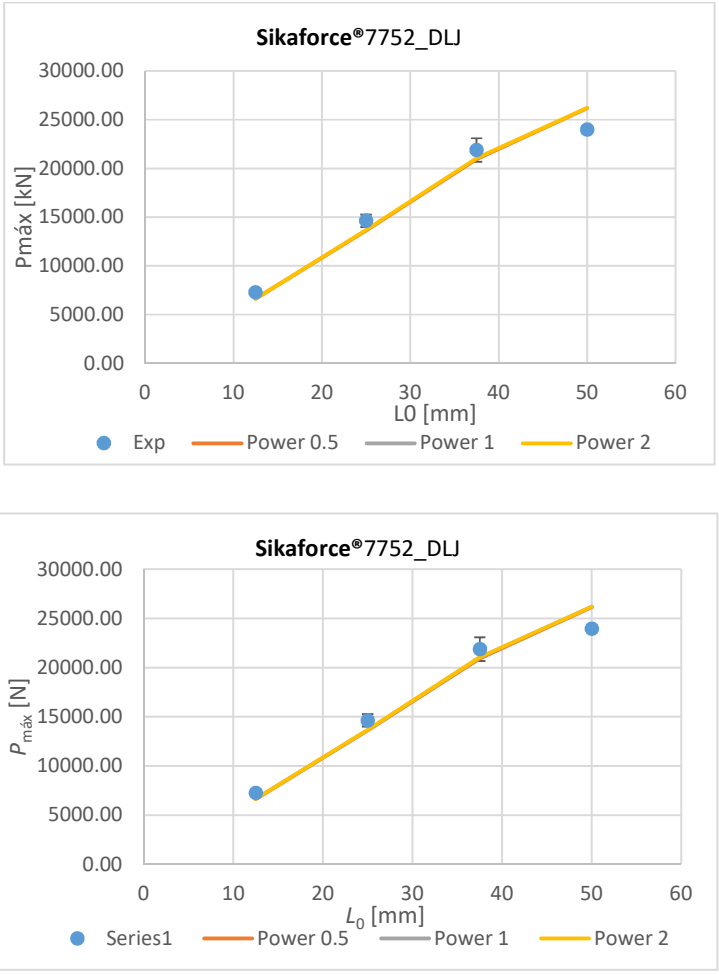

Figure 97 - Damage initiation criteria of DLJ Sikaforce® 7752

For adhesive Sikaforce® 7752 at 12.5 mm width of adhesive the maximum load attained during numerical simulation is 6.62 kN whereas the obtained experimental value is 7.27 kN likewise for 25 mm width the values are 13.61 kN and 14.62 kN for 37.5 mm width the respective values are 20.92 kN and 21.87 kN and for 50 mm width the values are 26.15 kN and 23.97 kN From these values the adhesive length is proportional to the maximum load carried by the joint failure.

For adhesive Araldite® AV138 and Araldite® 2015 L_o and the power value dose not influence on the maximum load attained, whereas Sikaforce® 7752 the maximum load attain varies exponentially with respective L_o and the power value.

3.2.6 Strength prediction: effect of the damage growth criterion

3.2.6.1 Damage growth criterion of Single-lap joints

The damage growth criteria of the three adhesives explained using upcoming graphs.

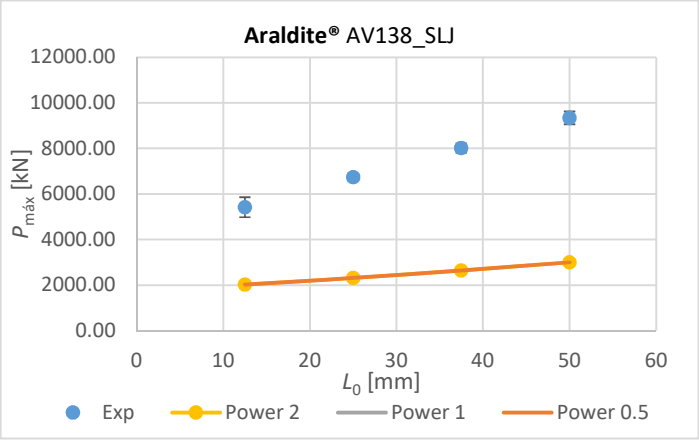

Figure 98 - Damage growth criteria of SLJ Araldite®AV138

For adhesive Araldite® AV138 at 12.5 mm width of adhesive the maximum load attained during numerical simulation is 2.02 kN whereas the obtained experimental value is 5.42 kN likewise for 25 mm width the values are 2.31 kN and 6.73 kN for 37.5 mm width the respective values are 2.64 kN and 8.01 kN and for 50 mm width the values are 3 kN and 9.34 kN. From these values the adhesive length is proportional to the maximum load carried by the joint before failure. Since the exponential value of the Power, Pw-0.5,1,2 lays in the same region.

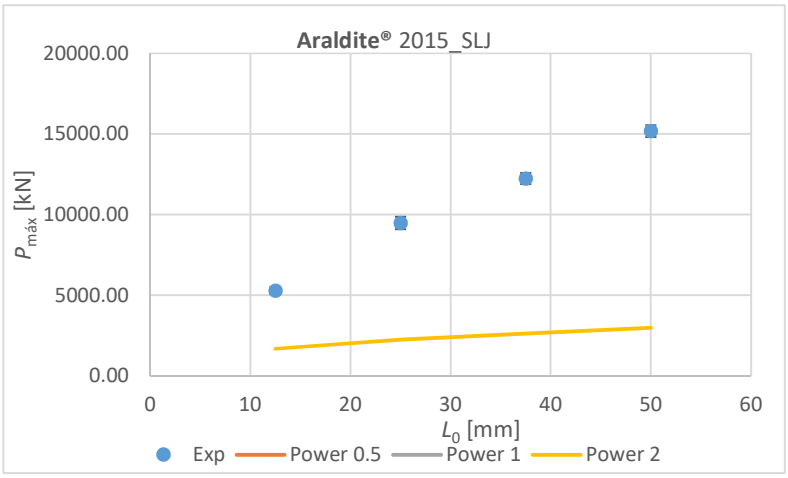

Figure 99 - Damage growth criteria of SLJ Araldite®2015

For adhesive Araldite® 2015 at 12.5 mm width of adhesive the maximum load attained during numerical simulation is 1.67 kN whereas the obtained experimental value is 5.28 kN likewise for 25 mm width the values are 2.23 kN and 9.48 kN for 37.5 mm width the respective values are 2.61 kN and 12.23 kN and for 50 mm width the values are 2.97 kN and 15.18 kN From these values the adhesive length is proportional to the maximum load carried by the joint before failure.

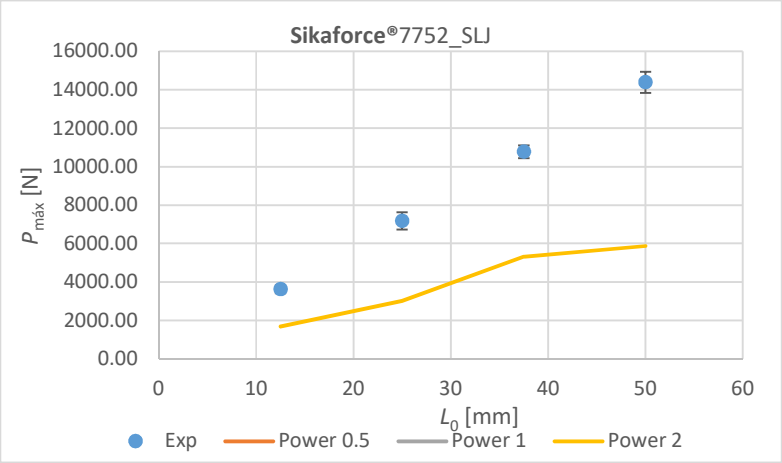

Figure 100 - Damage growth criteria of SLJ Sikaforce® 7752

For adhesive Sikaforce® 7752 at 12.5 mm width of adhesive the maximum load attained during numerical simulation is 1.68 kN whereas the obtained experimental value is 3.62 kN likewise for 25 mm width the values are 3.02 kN and 7.17 kN for 37.5 mm width the respective values are 5.31 kN and 10.77 kN and for 50 mm width the values are 5.87 kN and 14.38 kN. From these values the adhesive length is proportional to the maximum load carried by the joint before failure.

3.2.6.2 Damage growth criterion of double-lap joints

For adhesive Araldite® AV138 at 12.5 mm width of adhesive the maximum load attained during numerical simulation is 23.75 kN whereas the obtained experimental value is 12.14 kN likewise for 25 mm width the values are 23.86 kN and 16.11 kN for 37.5 mm width the respective values are 23.99 kN and 16.67 kN and for 50 mm width the values are 26.19 kN and 16.98 kN From these values the adhesive length is proportional to the maximum load carried by the joint similar to the failure.

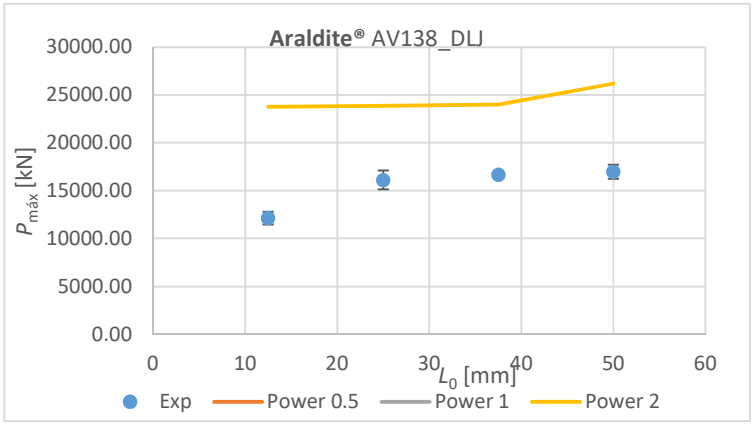

Figure 101 - Damage growth criteria of DLJ Araldite® AV138

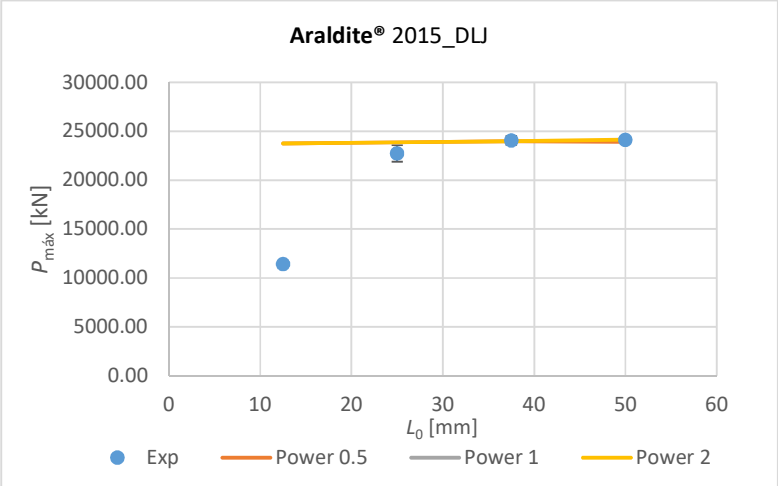

Figure 102 - Damage growth criteria of DLJ Araldite®2015

For adhesive Araldite® 2015 at 12.5 mm width of adhesive the maximum load attained during numerical simulation is 23.75 kN whereas the obtained experimental value is 11.40 kN likewise for 25 mm width the values are 22.86 kN and 22.73 kN for 37.5 mm width the respective values are 23.98 kN and 24.05 kN and for 50 mm width the values are 23.93 kN and 24.10 kN From these values the adhesive length is proportional to the maximum load carried by the joint similar to the failure.

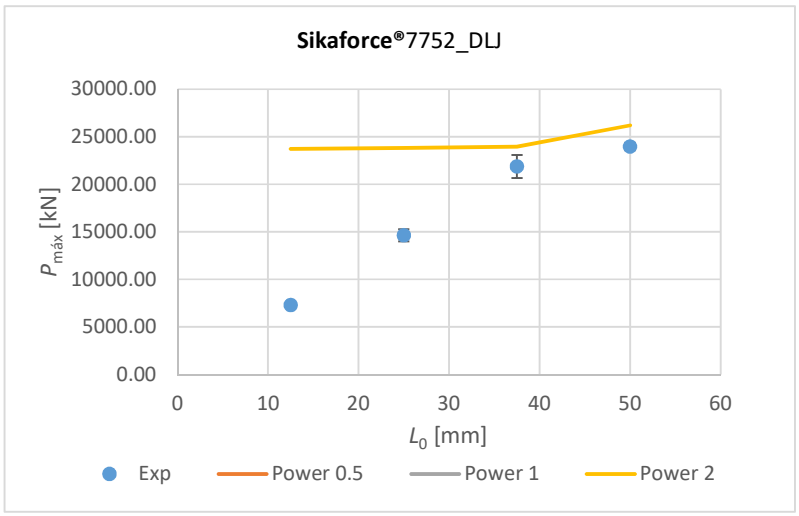

Figure 103 - Damage growth criteria of DLJ Sikaforce® 7752

For adhesive Sikaforce® 7752 at 12.5 mm width of adhesive the maximum load attained during numerical simulation is 23.72 kN whereas the obtained experimental value is 7.27 kN likewise for 25 mm width the values are 23.84 kN and 14.62 kN for 37.5 mm width the respective values are 23.96 kN and 21.87 kN and for 50 mm width the values are 26.19 kN and 23.97 kN From these values the adhesive length is proportional to the maximum load carried by the joint failure.

The power value does not influence the growth criteria as we can see the maximum load attain at all the Lo values are equal. But that the variation between the experimental and the numerical value is marginally high.

3.2.7 Comparison with CZM

In order to evaluate the ability and precision of the XFEM strength prediction of joints the results obtained numerical analysis using the XFEM were compared with the numerical results using the CZM obtained in a work previous. Figure 104 and Figure 105 show the comparison between the results using the QUADS initiation criterion and the Triangular propagation, CZM and experimental results of the joints bonded with the Araldite® AV138, Araldite® 2015 and Sikaforce® 7752 adhesives, respectively. To evaluate the XFEM's ability and accuracy in predicting joint resistance

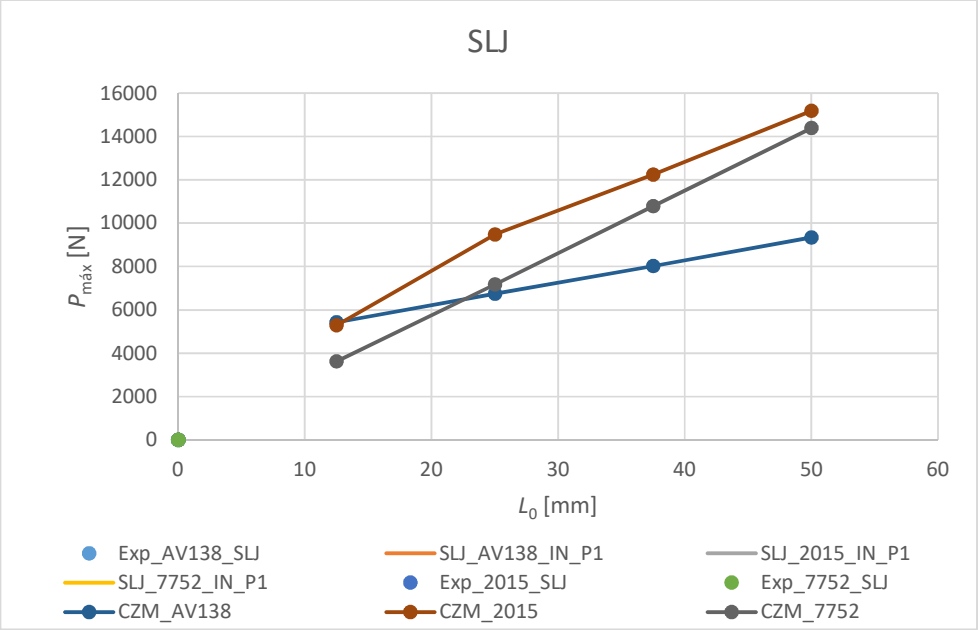

Figure 104 - Experimental/CZM/XFEM P_{max} comparison for the SLJ

As can be seen in Figure 104, for joints bonded with the adhesive Araldite® AV138, Araldite® 2015, Sikaforce® 7752 the XFEM slightly overestimates the P_m value compared to the CZM value and experimental value of single-lap joints with QUADS power-1. Considering these results, it is verified that XFEM is capable to predict the resistance quite closely with respect to the CZM. Since CZM is a linear function the value of CZM is similar to the experimental values. Thus, it is suggested that CZM function can be used to get exact results closer to experimental value.

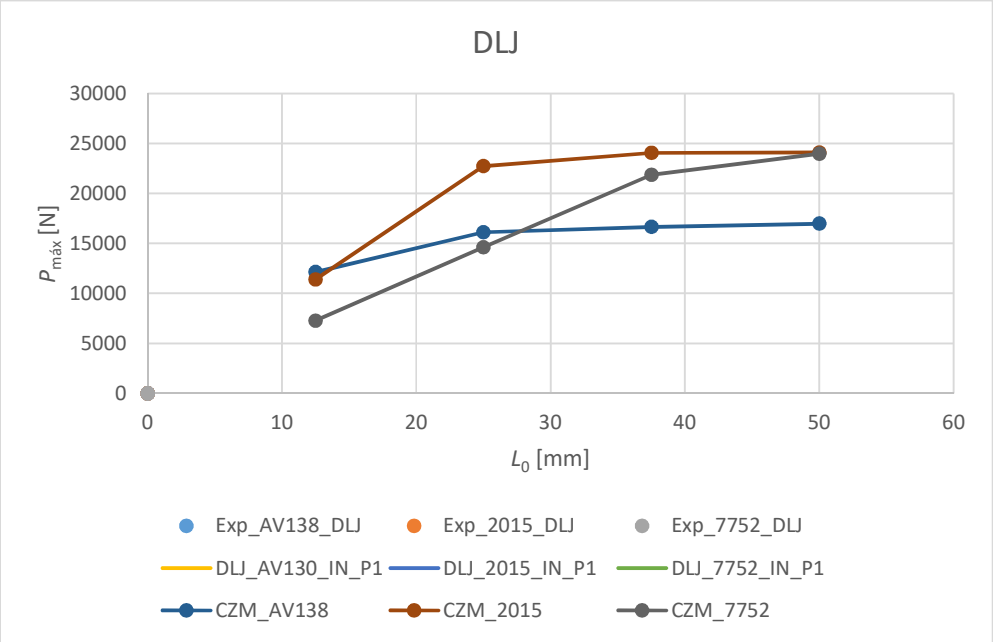

Figure 105- Experimental/CZM/XFEM P_{max} comparison for the DLJ

As can be seen in Figure 105, for joints bonded with the adhesive Araldite® AV138, Araldite® 2015, Sikaforce® 7752 the XFEM slightly overestimates the P_m value compared to the CZM value and experimental value of double-lap joints with QUADS power-1. Considering these results, it is verified that XFEM is capable to predict the resistance quite closely with respect to the CZM. Since CZM is a linear function the value of CZM is similar to the experimental values. Thus, it is suggested that CZM function can be used to get exact results closer to experimental value.

CONCLUSIONS

4 CONCLUSIONS AND PROPOSALS OF FUTURE WORKS

In this work, an experimental and numerical comparison was made by eXtended finite element method of several types of adhesive joints for three adhesives.

The main purpose of this thesis was to evaluate different simulation conditions in the XFEM analysis for a correct strength prediction of a thin adhesive layer in SLJ and DLJ, after validation of the methodology with experiments. Different L_O values and XFEM features were considered: the elastic stiffness of the damage law, the percentile variation of the damage parameters and the assessment of different initiation and propagation criteria. This study is important and essential for the complete understanding the correct application of these adhesives. With this purpose, an aluminum alloy (AW6082-T651) was bonded using three different adhesives: the brittle adhesive Araldite® AV138, the moderately ductile adhesive Araldite® 2015 and the ductile Sikaforce® 7752.

The numerical work performed with the software ABAQUS® began with the presentation of the simulation's conditions, i.e., adhesives and adherends characterization, mesh design, the boundary conditions XFEM Criteria's and the CZM formulation (mixed-mode triangular law, damage initiation and growth criteria). For a better understanding of the joints' behavior, a stress analysis in the adhesive layer was initially performed. The parametric study on L_O showed for all adhesives that both σ_y and τ_{xy} stresses peak at the overlap edges and concentrated in smaller normalized regions with the increase of L_O. The adhesive Araldite® AV138 attained the highest peaks of σ_y and τ_{xy} stresses, due to higher stiffness, promoting therefore higher stress gradients, which resulted on reduced overall joint strength. On the other hand, the adhesive Sikaforce® 7752 presents, for all values of L_O, peak σ_y and τ_{xy} stresses of lower magnitude than the adhesives Araldite® AV 138 and Araldite® 2015, mainly due to its flexibility. Moreover, owing to its plasticization ability, the adhesive layer was put under load gradually when the adhesive at the overlap edges started to plasticize. This promoted a significant improvement of P_m with the increase of L_O. The adhesive Araldite® 2015, due to its' moderate flexibility, presented intermediate gradients of σ_y and τ_{xy} stresses compared with the other two adhesives.

From the experimentally obtained results, it is possible to conclude that the performance of the joints is very influenced by the choice of the adhesive. For Araldite® AV138, the lower overlapping values, the DLJ was the joint that best behaved, doubling SLJ values. This is due to the fact that the overlap area of the DLJ is double, for the same L_0. However, the rigidity of Araldite® AV138 is its weak point, as it does not allow

plastification, which means that the increase of L_0 does not have much effect on the improvement of P_{max}. For Araldite® 2015, which is a more ductile adhesive, it has been found that DLJ is the joint that performs best for this adhesive. This is due to its greater ductility, allied to the greater area of overlap of the DLJ. But this joint only approaches the P_{max} value of the DLJ, for L_0 higher. It is also possible to verify that the value of P_{max} for the DLJ does not suffer significant improvements with the increase of L_0, from a certain point (L_0 = 37.5 mm), because it reaches the plastification limit of the adherend, would verify that the values of the joint was further reduced, failing to pass above 25 kN of P_{max}. With regard to Sikaforce® 7752 (more ductile adhesive), it is possible to once again note that DLJ is the geometry with the best performance. It is also verified that the value of DLJ for Araldite® 2015 and for Sikaforce® 7752, for L_0 = 50 mm, is practically the same. This is as already mentioned, to the fact that the adhesion plastification limit is reached. The remaining seam settings have P_{max} values well below the DLJ. Again, this is due to the fact that this joint geometry has a greater overlap area, for a given L_0

The realization of this dissertation allows to conclude that the Sikaforce® 7752 adhesive is the suitable for SLJ and DLJ adhesive joints since it allows to distribute the load over a larger area in the adhesive layer resulting in greater joint strength. The parameters that most influence the strength of the joints are the value of L_O and the type of adhesive used.

As proposals for future works, the following ideas are suggested:

- Validate de XFEM in more types of joints;
- Develop more sophisticated techniques for the SLJ;
- Consider adhesives with different properties;
- Consider the XFEM for dynamic loadings.

REFERENCES AND OTHER SOURCES OF INFORMATION

5 REFERENCES AND OTHER SOURCES OF INFORMATION

1. Da Silva, L.F., A. Öchsner, and R.D. Adams, *Handbook of adhesion technology*. 2011: Springer Science & Business Media.
2. de Sousa, C.C.R.G., *Comparação de técnicas analíticas e numéricas para previsão da resistência de juntas adesivas de sobreposição simples*. 2016, Tese de Mestrado em Engenharia Mecânica - Ramo Construções Mecânicas. Instituto Superior de Engenharia do Porto: Porto.
3. Carvalho, U.T.F., *Modelação de juntas adesivas por modelos de dano coesivo utilizando o método direto*. 2016.
4. Brockmann, W., et al., *Adhesive Bonding as a Joining Technique.* Adhesive Bonding: Materials, Applications and Technology, 2009: p. 1-3.
5. da Silva, L.F.M., A.G. de Magalhaes, and M.F.S. de Moura, *Juntas adesivas estruturais*. 2007: Publindústria.
6. Campilho, R.D.S.G., et al., *Modelling of Single-Lap Joints Using Cohesive Zone Models: Effect of the Cohesive Parameters on the Output of the Simulations.* The Journal of Adhesion, 2012. **88**(4-6): p. 513-533.
7. Ebnesajjad, S. and A.H. Landrock, *Adhesives technology handbook*. 2014: William Andrew.
8. Lee, L.-H., *Adhesive bonding*. 2013: Springer Science & Business Media.
9. Carlberger, T. and U. Stigh, *An explicit FE-model of impact fracture in an adhesive joint.* Engineering fracture mechanics, 2007. **74**(14): p. 2247-2262.
10. Packham, D., *The mechanical theory of adhesion*. 2003: CRC Press.
11. Lee, L.-H., *Fundamentals of adhesion*. 2013: Springer Science & Business Media.
12. Good, R.J., *Contact angle, wetting, and adhesion: a critical review.* Journal of adhesion science and technology, 1992. **6**(12): p. 1269-1302.
13. Baldan, A., *Adhesively-bonded joints and repairs in metallic alloys, polymers and composite materials: adhesives, adhesion theories and surface pretreatment.* Journal of materials science, 2004. **39**(1): p. 1-49.
14. Molitor, P., V. Barron, and T. Young, *Surface treatment of titanium for adhesive bonding to polymer composites: a review.* International Journal of Adhesion and Adhesives, 2001. **21**(2): p. 129-136.
15. Cagle, C.V., H. Lee, and K. Neville, *Handbook of adhesive bonding/edited by Charles V. Cagle, Henry Lee and Kris Neville.* 1973.
16. Adams, R.D., *Adhesive bonding: science, technology and applications*. 2005: Elsevier.
17. Mittal, K.L. and A. Pizzi, *Handbook of sealant technology*. 2009: CRC Press.
18. Bennett, S.J., *Adhesive fracture in viscoelastic materials*. 1973, Department of Mechnical Engineering, University of Utah.

19. DeVries, K., M. Williams, and M. Chang, *Adhesive fracture of a lap shear joint.* Experimental Mechanics, 1974. **14**(3): p. 89-97.

20. Petrie, E.W., *Handbook of adhesives and sealants*. 2nd ed ed. 1999, New York: McGraw-Hill.

21. Kinloch, A., *Adhesion and Adhesives, Science and Technology, Chapman and Hall.* New York, 1987.

22. Dvorak, G.J., J. Zhang, and O. Canyurt, *Adhesive tongue-and-groove joints for thick composite laminates.* Composites science and technology, 2001. **61**(8): p. 1123-1142.

23. Taib, A.A., et al., *Bonded joints with composite adherends. Part II. Finite element analysis of joggle lap joints.* International Journal of Adhesion and Adhesives, 2006. **26**(4): p. 237-248.

24. Cognard, P., *Technical characteristics and testing methods for adhesives and sealants*, in *Handbook of Adhesives and Sealants*. 2005, Elsevier. p. 21-99.

25. Gacoin, A., et al., *Comparison between experimental and numerical study of the adhesively bonded scarf joint and double scarf joint: Influence of internal singularity created by geometry of the double scarf joint on the damage evolution.* International Journal of Adhesion and Adhesives, 2009. **29**(5): p. 572-579.

26. Volkersen, O., *Die Nietkraftverteilung in zugbeanspruchten Nietverbindungen mit konstanten Laschenquerschnitten.* Luftfahrtfor schung, 1938. **15**: p. 41-47.

27. Fernandes, T.A., et al., *Adhesive selection for single lap bonded joints: experimentation and advanced techniques for strength prediction.* The Journal of Adhesion, 2015. **91**(10-11): p. 841-862.

28. Adams, R. and N. Peppiatt, *Stress analysis of adhesive-bonded lap joints.* Journal of strain analysis, 1974. **9**(3): p. 185-196.

29. Harris, J. and R. Adams, *Strength prediction of bonded single lap joints by non-linear finite element methods.* International Journal of Adhesion and Adhesives, 1984. **4**(2): p. 65-78.

30. Sosa, J.C. and N. Karapurath, *Delamination modelling of GLARE using the extended finite element method.* Composites Science and Technology, 2012. **72**(7): p. 788-791.

31. Goland, M., *The stresses in cemented joints.* J. Applied Mechanics, Trans. ASME, 1944. **66**: p. A-17-A-27.

32. Panigrahi, S. and B. Pradhan, *Three dimensional failure analysis and damage propagation behavior of adhesively bonded single lap joints in laminated FRP composites.* Journal of Reinforced plastics and Composites, 2007. **26**(2): p. 183-201.

33. Hart-Smith, L., *Stress analysis- A continuum mechanics approach(in adhesive bonded joints).* Developments in adhesives- 2.(A 82-28576 13-39) London, Applied Science Publishers, 1981, 1981: p. 1-44.

34. Penado, F.E., *Analysis of singular regions in bonded joints.* International journal of fracture, 2000. **105**(1): p. 1-25.

35. Williams, M., *The stresses around a fault or crack in dissimilar media.* Bulletin of the seismological society of America, 1959. **49**(2): p. 199-204.

36. Fernlund, G. and J. Spelt, *Failure load prediction of structural adhesive joints: Part 1: Analytical method.* International Journal of Adhesion and Adhesives, 1991. **11**(4): p. 213-220.

37. Barenblatt, G.I., *The formation of equilibrium cracks during brittle fracture. General ideas and hypotheses. Axially-symmetric cracks.* Journal of Applied Mathematics and Mechanics, 1959. **23**(3): p. 622-636.

38. Feraren, P. and H.M. Jensen, *Cohesive zone modelling of interface fracture near flaws in adhesive joints.* Engineering Fracture Mechanics, 2004. **71**(15): p. 2125-2142.

39. Ji, G., et al., *Effects of adhesive thickness on global and local Mode-I interfacial fracture of bonded joints.* International Journal of Solids and Structures, 2010. **47**(18-19): p. 2445-2458.

40. Yang, Q. and M.D. Thouless, *Mixed-mode fracture analyses of plastically-deforming adhesive joints.* International Journal of Fracture, 2001. **110**(2): p. 175-187.

41. Khoramishad, H., et al., *Predicting fatigue damage in adhesively bonded joints using a cohesive zone model.* International Journal of fatigue, 2010. **32**(7): p. 1146-1158.

42. Daudeville, L. and P. Ladeveze, *A damage mechanics tool for laminate delamination.* Composite Structures, 1993. **25**(1-4): p. 547-555.

43. Pepel, V., et al., *Crack growth through low-cycle fatigue loading of material ARMOX 500T.* Metalurgija, 2016. **55**(4): p. 691-693.

44. Shenoy, V., et al., *Fracture mechanics and damage mechanics based fatigue lifetime prediction of adhesively bonded joints subjected to variable amplitude fatigue.* Engineering Fracture Mechanics, 2010. **77**(7): p. 1073-1090.

45. Mohammadi, S., *Extended finite element method: for fracture analysis of structures*. 2008: John Wiley & Sons.

46. Belytschko, T. and T. Black, *Elastic crack growth in finite elements with minimal remeshing.* International journal for numerical methods in engineering, 1999. **45**(5): p. 601-620.

47. Moës, N., J. Dolbow, and T. Belytschko, *A finite element method for crack growth without remeshing.* International journal for numerical methods in engineering, 1999. **46**(1): p. 131-150.

48. Abaqus, A., *6.13 analysis user's manual.* SIMULIA, Providence, IR, 2013.

49. Sukumar, N. and J.-H. Prévost, *Modeling quasi-static crack growth with the extended finite element method Part I: Computer implementation.* International journal of solids and structures, 2003. **40**(26): p. 7513-7537.

50. Vatén, A., et al., *Callose biosynthesis regulates symplastic trafficking during root development.* Developmental cell, 2011. **21**(6): p. 1144-1155.

51. Stuparu, F., et al., *A Combined Cohesive Elements—XFEM Approach for Analyzing Crack Propagation in Bonded Joints.* The Journal of Adhesion, 2016. **92**(7-9): p. 535-552.

52. Melenk, J.M. and I. Babuska, *Seminar fur Angewandte Mathematik, Eidgenos-sische Technische Hochschule*. null. Vol. null. 1996. null.

53. Campilho, R.D.S.G., et al., Comput. Mater. Sci, 2011. **50**(null): p. 1543.

54. Campilho, R.D., M. De Moura, and J. Domingues, *Using a cohesive damage model to predict the tensile behaviour of CFRP single-strap repairs.* International Journal of Solids and Structures, 2008. **45**(5): p. 1497-1512.

55. Campilho, R.D.S.G., et al., *Strength prediction of single- and double-lap joints by standard and extended finite element modelling.* International Journal of Adhesion and Adhesives, 2011. **31**(5): p. 363-372.

56. Campilho, R.D.S.G., et al., Int. J. Adhes. Adhes, 2011. **31**(null): p. 363.

57. Stuparu, F.A., et al., *Cohesive and XFEM evaluation of adhesive failure for dissimilar single-lap joints.* Procedia Structural Integrity, 2016. **2**: p. 316-325.

58. Santos, T. and R. Campilho, *Numerical modelling of adhesively-bonded double-lap joints by the eXtended Finite Element Method.* Finite Elements in Analysis and Design, 2017. **133**: p. 1-9.

59. Zhao, B., Z.-H. Lu, and Y.-N. Lu, *Two-dimensional analytical solution of elastic stresses for balanced single-lap joints—Variational method.* International Journal of Adhesion and Adhesives, 2014. **49**: p. 115-126.

60. da Silva, L.F., et al., *Analytical models of adhesively bonded joints—Part I: Literature survey.* International Journal of Adhesion and Adhesives, 2009. **29**(3): p. 319-330.

61. Shishesaz, M. and N. Bavi, *Shear stress distribution in adhesive layers of a double-lap joint with void or bond separation.* Journal of Adhesion Science and Technology, 2013. **27**(11): p. 1197-1225.

62. Liao, L., T. Sawa, and C. Huang, *Numerical analysis on load-bearing capacity and damage of double scarf adhesive joints subjected to combined loadings of tension and bending.* International Journal of Adhesion and Adhesives, 2014. **53**: p. 65-71.

63. Liljedahl, C., et al., *Damage modelling of adhesively bonded joints.* International journal of fracture, 2006. **141**(1-2): p. 147-161.

64. Moreira, R. and R. Campilho, *Strength improvement of adhesively-bonded scarf repairs in aluminium structures with external reinforcements.* Engineering Structures, 2015. **101**: p. 99-110.

65. Carvalho, U.T.F., *Modelação de juntas adesivas de sobreposição simples e dupla por modelos de dano coesivo com obtenção das leis coesivas pelo método direto*. 2016, Tese de Mestrado de Engenharia Mecânica - Ramo Contruções Mecânicas. Instituto Superior de Engenharia do Porto: Porto.

66. Moreira, P.M.G.P., et al., *Fatigue crack growth in friction stir welds of 6082-T6 and 6061-T6 aluminium alloys: A comparison.* Theoretical and Applied Fracture Mechanics, 2008. **50**(2): p. 81-91.

67. Campilho, R.D.S.G., et al., *Fracture toughness determination of adhesive and co-cured joints in natural fibre composites.* Composites Part B: Engineering, 2013. **50**: p. 120-126.

68. Neto, J.A.B.P., R.D.S.G. Campilho, and L.F.M. da Silva, *Parametric study of adhesive joints with composites.* International Journal of Adhesion and Adhesives, 2012. **37**: p. 96-101.

69. Campilho, R.D.S.G., et al., *Modelling adhesive joints with cohesive zone models: effect of the cohesive law shape of the adhesive layer.* International Journal of Adhesion and Adhesives, 2013. **44**: p. 48-56.

70. Faneco, T.M.S., *Caraterização das propriedades mecânicas de um adesivo estrutural de alta ductilidade*. 2014, Tese de Mestrado em Engenharia Mecânica - Ramo Materias e Tecnologias de Fabrico. Instituto Superior de Engenharia do Porto: Porto.

71. Campilho, R.D., et al., *Strength prediction of single-and double-lap joints by standard and extended finite element modelling.* International Journal of Adhesion and Adhesives, 2011. **31**(5): p. 363-372.

72. McGeorge, D., *Inelastic fracture of adhesively bonded overlap joints.* Engineering Fracture Mechanics, 2010. **77**(1): p. 1-21.

73. Adams, R.D., et al., *Structural adhesive joints in engineering*. 1997: Springer Science & Business Media.

74. ABAQUS® Documentation. 2009, Dassault Systèmes: Vélizy-Villacoublay.

75. Campilho, R.D.S.G., M.F.S.F. de Moura, and J.J.M.S. Domingues, *Using a cohesive damage model to predict the tensile behaviour of CFRP single-strap repairs.* International Journal of Solids and Structures, 2008. **45**(5): p. 1497-1512.

76. Campilho, R.D.S.G., M.F.S.F. de Moura, and J.J.M.S. Domingues, *Numerical prediction on the tensile residual strength of repaired CFRP under different geometric changes.* International Journal of Adhesion and Adhesives, 2009. **29**(2): p. 195-205.

77. Campilho, R.D.S.G., et al., *Modelling the tensile fracture behaviour of CFRP scarf repairs.* Composites Part B: Engineering, 2009. **40**(2): p. 149-157.

78. Alfano, G., *On the influence of the shape of the interface law on the application of cohesive-zone models.* Composites Science and Technology, 2006. **66**(6): p. 723-730.

79. Radice, J. and J. Vinson, *On the use of quasi-dynamic modeling for composite material structures: analysis of adhesively bonded joints with midplane asymmetry and transverse shear deformation.* Composites science and technology, 2006. **66**(14): p. 2528-2547.

80. Campilho, R.D.S.G., M.F.S.F. de Moura, and J.J.M.S. Domingues, *Modelling single and double-lap repairs on composite materials.* Composites Science and Technology, 2005. **65**(13): p. 1948-1958.

81. Reis, P.N.B., F.J.V. Antunes, and J.A.M. Ferreira, *Influence of superposition length on mechanical resistance of single-lap adhesive joints.* Composite Structures, 2005. **67**(1): p. 125-133.

82. Jiang, W. and P. Qiao, *An improved four-parameter model with consideration of Poisson's effect on stress analysis of adhesive joints.* Engineering Structures, 2015. **88**: p. 203-215.

83. Campilho, R.D.S.G., et al., *Computational Modelling of the Residual Strength of Repaired Composite Laminates Using a Cohesive Damage Model.* Journal of Adhesion Science and Technology, 2008. **22**(13): p. 1565-1591.

84. Shin, K.C. and J.J. Lee, *Bond parameters to improve tensile load bearing capacities of co-cured single and double lap joints with steel and carbon fiber-epoxy composite adherends.* Journal of composite materials, 2003. **37**(5): p. 401-420.

85. Grant, L.D.R., R.D. Adams, and L.F.M. da Silva, *Experimental and numerical analysis of single-lap joints for the automotive industry.* International Journal of Adhesion and Adhesives, 2009. **29**(4): p. 405-413.

86. da Silva, L.F.M., et al., *Effect of material, geometry, surface treatment and environment on the shear strength of single lap joints.* International Journal of Adhesion and Adhesives, 2009. **29**(6): p. 621-632.

87. Davis, M. and D. Bond, *Principles and practices of adhesive bonded structural joints and repairs.* International Journal of Adhesion and Adhesives, 1999. **19**(2–3): p. 91-105.

88. Vallée, T., J.R. Correia, and T. Keller, *Probabilistic strength prediction for double lap joints composed of pultruded GFRP profiles part I: Experimental and numerical investigations.* Composites Science and Technology, 2006. **66**(13): p. 1903-1914.